university of groningen / faculty of science and engineering

PHILIPS

Industrial Engineering and Management
Master design project

Flexible end of arm tool (EOAT) for the automation of lacquering part (un)loading at Philips Drachten

Author	Supervisors (RuG)	Supervisor (Philips)
Prajwal Ambekar (S3473694)	**Mehran Mohebbi, MSc.** Lecturer, Industrial Engineering systems **prof. dr. ir. Bayu Jayawardhana** Professor, Mechatronics and Control of Nonlinear Systems	**ir. Eric Sloot** Senior Architect Production Systems

Table of Contents

Abstract v

List of abbreviations and symbols vi

List of tables vii

List of figures ix

1. Introduction 1

1.1. Industry 4.0 1

1.2. Flexible Automation 2

1.3. Philips Drachten 3

1.4. Report outline 3

2. Problem analysis 4

2.1. Lacquering 4

2.2. System description 6

2.3. Stakeholder analysis 6

2.4. Conceptual model 7

2.5. Problem statement 8

2.6. Goal statement 8

2.7. Research question 8

3. EOAT design elements 9

3.1. Gripper classification 9

3.2. Gripper selection 12

3.3. Gripper design guidelines 13

3.4. Grasping flexibility 13

3.5. Grasp synthesis 14

3.6. Prehension strategy 16

4. Methods and tools 18

4.1. Strategy 18

4.2. Part and process study 19

4.3. Gripper selection 20

4.4. Grasp synthesis and analysis 22

4.5. Prehension strategy 26
4.6. Flexible EOAT design 29
4.7. Validation 34
5. Results 39
5.1. Grasp stability 39
5.2. Visual check 40
5.3. Cross-cut test 40
5.4. Part alignment 41
5.5. Simulation study 42
5.6. Cost and time 43
6. Conclusion 45
Limitations and future work 46
7. Bibliography 47
8. Appendices 53
Appendix A: PA-12 material datasheet 53
Appendix B: Agilus 30 material datasheet 54
Appendix C: HP MultiJet fusion 3D printer specifications 55
Appendix D: Stratasys J750 digital anatomy 3D printer specifications 56
Appendix E: Universal robots UR5 specifications 57
Appendix F: Mechanical properties of the lacquering parts 58
Appendix H: Robotiq Hand-e gripper specifications 60
Appendix I: Festo DGSL-4-20-PA mini slide pneumatic cylinder specifications 61
Appendix J: Festo MEH-5/2-1/8-P-B solenoid valve 62
Appendix K: Fixturing assembly 63
Appendix L: Part-alignment distance measurement images 64
Appendix M: Tevema D12680 compression spring specifications 67
Appendix M: Force calibration readings 68
Appendix N: CAPEX breakdown 70
Appendix O: Allowable positional inaccuracy measurement images 71
Appendix P: Positional variation measurements 74

Abstract

This thesis presents the proof-of-concept of a flexible end-of-arm-tool (EOAT) for the automation of loading and unloading of 8+ parts in the lacquering line at Philips Drachten. While multi-purpose universal EOATs are expensive to implement in a flexible manufacturing line, part-specific EOATs require a change-over when switching between parts, and hence do not meet the cycle time requirements. The EOAT presented integrates multiple grasp configurations with spring elements and flexible jaws to obtain the required flexibility. The design was experimentally validated against the functional requirements of grasp stability, part alignment and (dis)mounting success, along with a FEM stress and displacement study, and a fatigue analysis simulation. The financial and temporal validation of the design was achieved through a comparison of the estimated CAPEX and payback period for the flexible EOAT against a standard part-specific EOAT, as well as the current manual (un)loading. The flexible EOAT has an estimated €900k CAPEX (savings of about €900k relative to a part-specific EOAT) with a payback period of 1.75 years.

List of abbreviations and symbols

k = thousand
M = million euros
BEP = break-even period = pay-back period
CAD = Computer aided design
DTN = Philips Drachten facility
EOAT = End of arm tool = gripper = end effector
FCP = Factory cost price
FMS = Flexible manufacturing system
FTE = Full time equivalent
HQ = Headquarters = Philips Amsterdam (here)
I4 = Industry 4.0 = (transition to) the fourth industrial revolution
IGM = Integral gross margin
IPD = Initial problem description
IRAM = Industrial robotic arm manipulator
NPV = Net present value
OECD = The Organization for Economic Co-operation and Development
RDP = Research design plan
ROI = Return on investment

List of tables

Table 1. Stakeholder requirements classified into quality, cost and time aspects..... 6
Table 2. 5W2H analysis for the flexible EOAT design problem 7
Table 3. Grasping method selection matrix based on the feasibility of grasping each part. 20
Table 4. Gripper type selection matrix based on the feasibility of grasping each part. 21
Table 5. Grasp configurations for each of the parts for part-picking from the tray and (dis)mounting..... 25
Table 6. Robot-arm program for the loading function with part-specific waypoints 27
Table 7. Robot-arm program for the unloading function with part-specific waypoints 27
Table 8. Approach clearance in terms of the part and tray dimensions (in mm)..... 28
Table 9. Constraints posed by the approach clearance on the dimensions of the fingers and jaws for (a). Vertical grasp and (b). Horizontal grasp 29
Table 10. Components of the flexible EOAT for vertical and horizontal grasp configurations. 30
Table 11. Distance and angle between the gripping points defined for the 6 representative parts. 33
Table 12. Specifications of the 3D printed components..... 33
Table 13. Parameters and tests for each validation function 34
Table 14. Grasp stability (API – TPV) for each part 39
Table 15. Allowable positional inaccuracy (API) for the 6 parts..... 39
Table 16. Visual check results showing the number of samples checked for each part and the number of parts that successfully prevented part damage (pre-and post- lacquer), mounted on the jig, and dismounted from the jig. 40
Table 17. Part-alignment results measured as a success if all the markers are visible after alignment. 41
Table 18. Force calibration results: Force (in N) for every 5% increase in Force% displayed in the UR5 42
Table 19. Robot arm parameters of speed and acceleration of the joint for MovJ and tool for MovL..... 43
Table 20. CAPEX estimate of the automation components for a flexible EOAT compared to that of part-specific EOAT 44
Table 21. Net Present Value particulars for the 3 alternatives. 44
Table 22. Validation of the flexible EOAT design against the functional requirements, along with the tests used for validation and their results. 45
Table 23. PA-12 MJF printing properties and material datasheet (GetDocument.aspx (hp.com)) 53
Table 24. Agilus30 material datasheet (Agilus 30: A Flexible Photopolymer 3D Printing Material | Stratasys) 54
Table 25. HP MJF 3D printer specifications (GetDocument.aspx (hp.com)) 55
Table 26. Stratasys j750 3D printer specifications (J750 Digital Anatomy 3D Printer for Lifelike Medical Models | Stratasys)..... 56
Table 27. UR5 robot arm specifications (ur5_en.pdf (universal-robots.com))..... 57
Table 28. Mechanical properties of the lacquering parts (Philips) 58
Table 29. Robotiq hand-e gripper specifications (Specifications (robotiq.com)) 60
Table 30. Festo pneumatic cylinder specifications (Mini slide DGSL-4-20-PA (festo.com)) 61

Table 31. Festo solenoid valve specifications (Solenoid valve MEH-5/2-1/8-P-B (festo.com)) 62
Table 32. Compression spring specifications (Tevema D12680) 67
Table 33. Spring 1 force calibration readings 68
Table 34. Spring 1 force calibration readings 68
Table 35. CAPEX breakdown comparison between part-specific and flexible EOAT for the automated (un)loading process components and their quantities to meet the cycle-time requirements. 70
Table 36. Positional variation readings for Part 1 74
Table 37. Positional variation readings for Part 2 74
Table 38. Positional variation readings for Part 3 74
Table 39. Positional variation readings for Part 4 75
Table 40. Positional variation readings for Part 5 75
Table 41. Positional variation readings for Part 6 75

List of figures

Figure 1. The technological innovations and phase transitions through the industrial revolutions (Farahhanis, 2021) and the role of automation (self-behavior) and flexibility (and adaptability) characteristics of the smart manufacturing technologies in the transition towards Industry 4.0 (Frank, Dalenogare and Ayala, 2019).....1
Figure 2. Conventional parts of a robot arm manipulator including the end of arm tool (EOAT) depicted using an example image of a UR5e Universal robot (2021). 2
Figure 3. Representation of the components of the jig assembly on which the lacquering parts are mounted. 4
Figure 4. Robotic lacquering in the spray-painting chamber at Philips Drachten (Philips, 2021). 4
Figure 5. Schematic representation of the lacquering line showing the sequential activities and performers, with the project scope shown in the green dashed box. 5
Figure 6. High-level system diagram depicting the sequential phases of the lacquering functions. 6
Figure 7. Low-level system diagram depicting the sequential sub-functions of the loading and unloading functions. 6
Figure 8. Schematic representation of the 5-tier hierarchical structure of stakeholders. 7
Figure 9. What-Why analysis of the EOAT design problem (Annamalai et. al., 2013). 8
Figure 10. (a) Schematic representation of impactive gripper forcing the object into prehension. 9
Figure 11. Schematic representation of form, force, and combined methods of gripper closure (Bajd et al., 2010). 9
Figure 12. Schematic representation of opening and closing of angular and parallel jaw grippers (Omega, 2021). 10
Figure 13. Schematic representation of external and internal gripper using a parallel jaw gripper example (Omega, 2021). 10
Figure 14. (a) Schematic representation of ingressive gripper forcing the object into prehension. 11
Figure 15. (a) Schematic representation of astrictive gripper forcing the object into prehension. 11
Figure 16. (a) Schematic representation of contigutive gripper forcing the object into prehension. 11
Figure 17. Gripper selection framework developed by Fantoni et al. (2014). 12
Figure 18. Schematic representation of a universal (jamming) gripper developed by Amend et al., (2012) showing three different operational modes for handling objects of varying geometrical properties. 13
Figure 19. The dynamic relationship between the EOAT specificity and expenses incurred to meet cycle-time and positional accuracy requirements. 14
Figure 20. Complex contacts and their primitive equivalents Nguyen (1987). 15
Figure 21. Fingertip profile selection rules developed by Pedrazzoli, P., Rinaldi, R. and Boer, C.R., (2001)15
Figure 22. Handling zones of a workpiece (Monkman, G.J., et. al., 2007): 16
Figure 23. EOAT design strategy based on the components of finger-design flowchart by Honarpardaz et al. (2017) and the gripper selection framework by Fantoni et al. (2014), depicting the sequential chain of events leading to the proof of concept. 18

Figure 24. The design iteration for gripper components not available readily in the maket. 18
Figure 25. Pictorial representation of the list of all the parts that are currently lacquered in the lacquering line at DTN with the similarly shaped parts considered equivalent for grasping and their material properties.....19
Figure 26. Pictorial representation of the (dis)mounting mechanism for Part 2 (example) showing the place (pivot) and click (snap-fit cantilever beam) features of the part and the jig.....19
Figure 27. Pictorial representation of the handling zones depicting the prehension zones for Part 1 (Hera s1000 front panel) and the gripping points selected within the prehension zones. 22
Figure 28. Pictorial representation of the handling zones depicting the prehension zones for Part 2 (Hera s3000 front panel) and the gripping points selected within the prehension zones. 23
Figure 29. Pictorial representation of the handling zones depicting the prehension zones for Part 3 (Poseidon s7000 front panel) and the gripping points selected within the prehension zones. The part positioning in the tray causing potential collision during part picking is circled in red, and the part-picking sequence which solves the problem shown alongside. 23
Figure 30. Pictorial representation of the handling zones depicting the prehension zones for Part 4 (Atlas chest shown in picture) and the gripping points selected within the prehension zones. The tray hole used for part placement and the smooth curvature of the bottom surface of the part are circled in red. 24
Figure 31. Pictorial representation of the handling zones depicting the prehension zones for the Hera s3000 deco panel and the gripping points selected within the prehension zones. 24
Figure 32. Pictorial representation of the handling zones depicting the prehension zones for the Hera s3000 on/off button and the gripping points selected within the prehension zones. 25
Figure 33. Pictorial representation of grasp configurations: vertical, horizontal, and distal, along the part length, width, and height, respectively, with the gripper fingers. 25
Figure 34. Dimensional legend for Table 8 depicting the length (y), width (x), height (z), distance between the neighboring objects (x_p and y_p), and the distance between the tray boundaries (x_t and y_t) of Part 1 (example) 28
Figure 35. Constraints posed by the approach clearance on the dimensions of the fingers and jaws for (a). Vertical grasp and (b). Horizontal grasp 29
Figure 36. Schematic representation of (a) Vertical finger and jaw assembly mounted onto a Robotiq gripper (b) vertical finger features including mounting base with 4 screw-clearance holes, offset column for alignment of parallel fingers, and a spring-element at the jaw-mount (c) Rack and pinion mechanism of the Robotiq hand-e gripper with mounting holes on the racks. 30
Figure 37. Schematic representation of the (a) horizontal finger (b) pneumatic mechanism for collision protection and actuation of horizontal fingers (c) extended cylinders for CPS in the top image and for the fingers in the bottom image. 31
Figure 38. Flexible EOAT assembly design depicting the vertical and horizontal fingers, and their drive and mounting components. 32

Figure 39. Pictorial representation of the angular compliance introduced by the spring element in the vertical jaw. 33
Figure 40. Experimental setup at the ICD robotics lab at Philips, Drachten. 34
Figure 41. (a) Tool movement between 3 waypoints (b) Tool re-orientation through rotation of the 3 wrist joints 35
Figure 42. Pictorial representation of the allowable positional inaccuracy (API) measurement for Part 2 (example) depicting the distances measured between the part and jig features at jig chamfers. 35
Figure 43. Pictorial representation of the part-alignment test for Part 3 depicting (a) the potential extreme positions of the part where the 4 markers are not visible and (b) the aligned part with the 4 markers visible. 36
Figure 44. SOLIDWORKS simulation parameters for the linear static study of the vertical finger and jaw depicting the material, contact sets, fixtures, and external loads assigned to the study. 37
Figure 45. S-N curves for (a) PA-12 (Van Hooreweder et. al., 2013) and (b) rubber material (Luo, R.K. et. al., 2003) 37
Figure 46. Pictorial representation of the Robotiq hand-e gripper force calibration using Tevema D12680 compression spring with a spring rate of 6.68N/mm. 38
Figure 47. Force calibration test graph depicting the relationship between the force % displayed on the UR5 and the actual force exerted by the fingers. 42
Figure 48. SolidWorks simulation results depicting (a) von Mises stress and (b) static displacement 42
Figure 49. Fatigue plots showing the fatigue (a)life and (b)damage of the finger-jaw assembly locations. 43
Figure 50. Cumulative NPV for the period 2023 Q1 until 2028 Q1 with the manual (un)loading as reference. 44
Figure 51. The fixturing assembly depicting how the 6-folded cross is held in place for the experimental validation. 63
Figure 52. Top, front, and bottom views of the adapter (a) shaft and (b) base. 63
Figure 53. Images showing the visibility of markers (a) before and (b) after the horizontal alignment of Part 1 64
Figure 54. Images showing the visibility of markers (a) before and (b) after the horizontal alignment of Part 2 64
Figure 55. Images showing the visibility of markers (a) before and (b) after the horizontal alignment of the Poseidon chest. 65
Figure 56. Images showing the visibility of markers (a) before and (b) after the horizontal alignment of the Atlas chest. 65
Figure 57. Images showing the visibility of markers (a) before and (b) after the horizontal alignment of Part 5. 66
Figure 58. Distances measured for the API calculation for Part 1 71
Figure 59. Distances measured for the API calculation for Part 2 71
Figure 60. Distances measured for the API calculation for Part 3 72

Figure 61. Distances measured for the API calculation for Part 4 72
Figure 62. Distances measured for the API calculation for Part 5 73
Figure 63. Distances measured for the API calculation for Part 6 73

1. Introduction

1.1. Industry 4.0

The global economy is undergoing a massive phase transition to the fourth industrial revolution (I4) led by new socio-economic formation caused by technological innovations (Melnyk et al., 2019). The essential characteristics for transitioning to I4 - considered as the integration of modern technologies to achieve higher industrial performance (Dalenogare et al., 2018; Frank et al., 2019) - include the following:

1. Self-behavior (Oztemel and Tekez, 2009): Further minimization of human intervention to generate automated manufacturing systems using intelligent and collaborative robots.
2. Adaptability and flexibility (Popkova et al., 2019): Improving the responsiveness of the system to adapt to quick changes in specialization and the introduction of new product types (speed), and the flexibility of the production processes to adjust to variation in product types and volumes (scope) to generate flexible manufacturing systems.

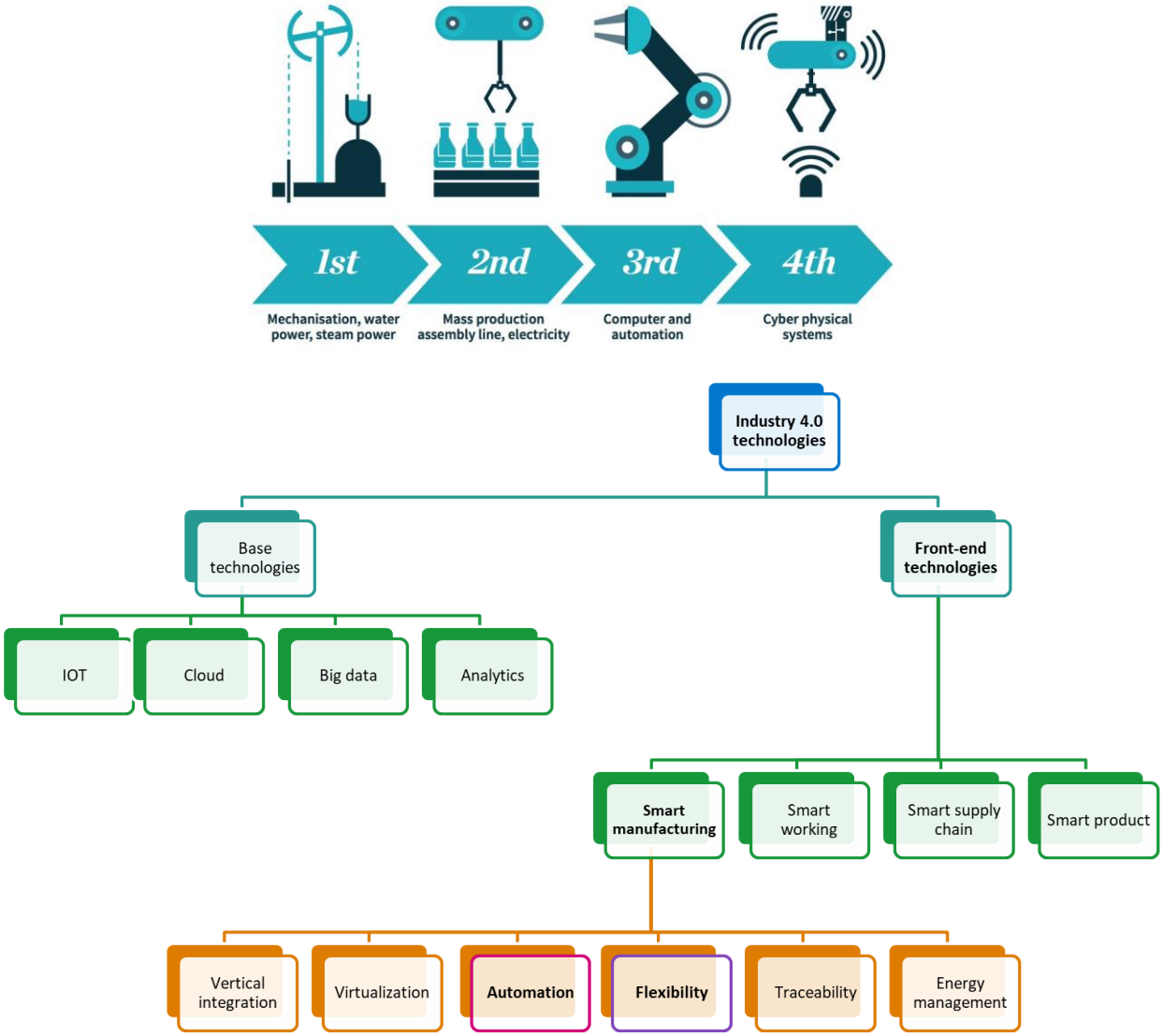

Figure 1. The technological innovations and phase transitions through the industrial revolutions (Farahhanis, 2021) and the role of automation (self-behavior) and flexibility (and adaptability) characteristics of the smart manufacturing technologies in the transition towards Industry 4.0 (Frank, Dalenogare and Ayala, 2019)

1.2. Flexible Automation

Automation improves the consistency of product quality while eliminating human ergonomic constraints and other health and safety issues, saving time, and avoiding wasted human potential which can otherwise be utilized for creative work and strategic thinking tasks (Bouchard, 2018). Automation in manufacturing systems is generally classified into 3 types based on the flexibility of the system to handle the speed and scope of products (Custodio and Machado, 2020):

1. Fixed automation: fixed and hard to change program of instructions used in extensive production of the same product with little or no flexibility to accommodate product variety type.
2. Programmable automation: time consuming changeability of program of instructions to allow flexibility at the cost of lower production rates.
3. Flexible automation: cost-effective response to changes in volume and product-mix requirements.

Flexible automation directly improves the industrial performance with immediate beneficial effects on internal efficiency measures like machine utilization and defect rate, and their reflections in the performance indicators of growth in sales and ROI (Parthasarthy and Sethi, 1992).

Automation of manufacturing tasks generally involve industrial robot arm manipulators (IRAMs) with application-specific end of arm tools (EOATs) which attach to the end of the IRAM (as seen in Figure 2) and perform the required function. While the function of the arm is to bring the tool to the required location and orientation without colliding with external objects, the function of the tool depends on the manufacturing operation like machine (un)loading, part inspection, bin picking, (dis)assembly (Löfving et al., 2018).

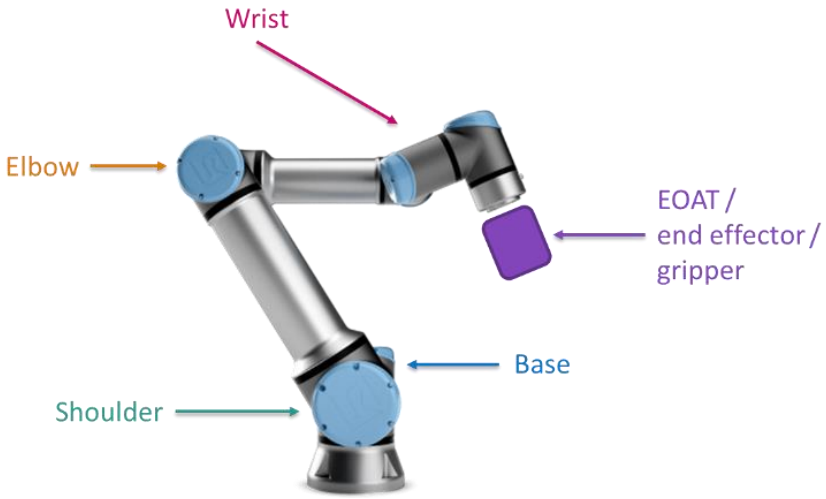

Figure 2. Conventional parts of a robot arm manipulator including the end of arm tool (EOAT) depicted using an example image of a UR5e Universal robot (2021).

Several studies have been conducted on EOAT problems in flexible automation contexts such as car body component assembly, hose insertion (Landuré, J. et al., 2021), batteries (Schumacher and Jouaneh, 2013), and (semi-)destructive electronic components disassembly (Feldmann, K. et al., 1998). EOAT for the flexible automation of non-destructive snap-fit assembly/disassembly of fragile parts has a wide range of applications from reuse/recycle of end-of-life (EOL) products in circular economy business models to Industry 4.0 transition (Blunck and Werthmann, 2017), to which this study aims to contribute.

1.3. Philips Drachten

Royal Philips is an industry leading health technology company headquartered in Amsterdam, focused on improving people's health through innovative products including grooming, diagnostic and monitoring, and other healthcare products. Philips-Drachten (DTN) is the development, industrialization, and production center of Philips shavers located in the north of the Netherlands. DTN focuses on future product development and state-of-the-art production processes including the I4 technologies of additive manufacturing and intelligent robotics, with system architects and process engineers working on embedding these technologies (Philips, 2021).

With the electric shaver market forecasted to grow significantly (about 4.6%) in the next decade (NMSC, 2021), DTN plans to utilize this growth to increase the market share by competing strongly, both internally (with other Philips production sites in China and Indonesia) as well as externally (with rival shaver manufacturers). Market share goals are primarily decided by product pricing which in turn are affected by production costs and labor costs. Netherlands has one of the highest unit labor costs (average cost of labor per unit of output produced) - considered a measure of price competitiveness - in the OECD countries (OECD, 2021) with an increasing trend in the unit labor costs, which is in stark contrast to Asian countries like China and Indonesia, which have a significantly lower unit labor cost with a decreasing trend (Trading economics, 2021).

Shaver manufacturing at DTN follows the sequence of 1. injection molding -> 2. lacquering -> 3. assembly -> 4. customization, of which 1 and 2 are largely automated, while 3 and 4 are still heavily dependent on Labor (Philips, 2021). Recent internal investigations found an opportunity to automate the lacquering line, which currently employs 5 operators working across 3 shifts, earning about €50,000 per year incurring labor costs of about €750k per year. This led to the beginning of a new project to automate the lacquering line using I4 technologies, led by production system architects and process engineers.

1.4. Report outline

This report is split into:

1. Problem analysis: The problem is introduced through system diagrams and analysis models to then arrive at the problem statement. The research question, goals, and stakeholder requirements are also briefed here.
2. EOAT design elements: The design considerations for an EOAT are detailed through literature review.
3. Methods and tools: The functional requirements of the flexible EOAT are defined, and the methods and tools used to design the flexible EOAT and validate it against those requirements are elaborated.
4. Results: The results of the validation tests described in the previous section along with their interpretation.
5. Conclusion: The methods and results are summarized in the context of the problem, along with the limitations and their potential solutions.

2. Problem analysis

2.1. Lacquering

Lacquering is the process of applying lacquer (paint) onto a part, for aesthetic (color and texture) as well as protective (stain/dust resistance) reasons. The visible surfaces of components of fully assembled Philips shavers are lacquered using spray-painting to get the required properties. The sequential steps in the lacquering line can be summarized into four primary functions:

1. Loading: The parts to be lacquered - arriving in trays from the previous production step - are collected and mounted - by 2 operators - onto jigs (Figure 3), which in turn are mounted onto spindles fixed on a conveyor line.

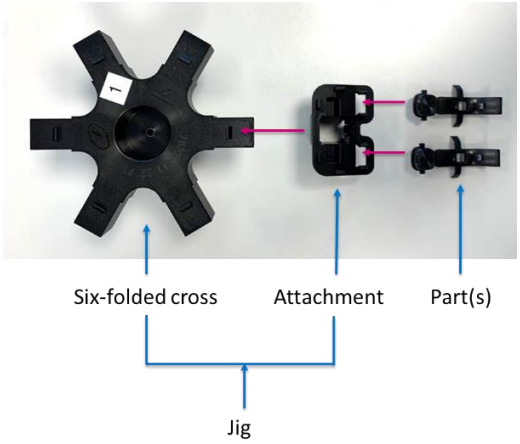

Figure 3. Representation of the components of the jig assembly on which the lacquering parts are mounted.

2. Lacquering: The lacquering function includes dust removal step to remove contaminants from the part surface followed by multiple layers of spray-painting (Figure 4), followed by heat treatment to bond the lacquer to the parts. The conveyor belt is designed to rotate the spindles at specific positions in the spray-painting chambers, where a robot sprays the required lacquer.

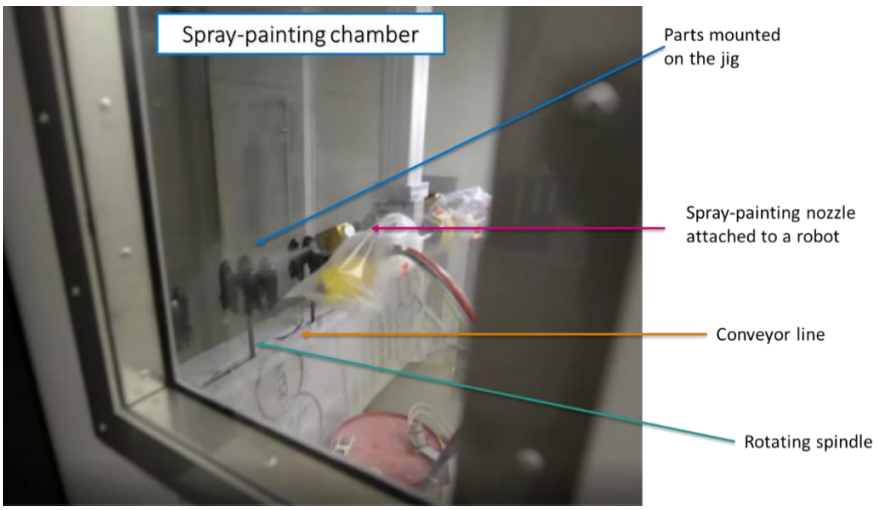

Figure 4. Robotic lacquering in the spray-painting chamber at Philips Drachten (Philips, 2021).

3. Unloading: The lacquered parts are manually dismounted from the jig by 2 operators.
4. Visual inspecting: The lacquered parts are visually inspected by 1 operator to check for the quality and consistency of lacquer.

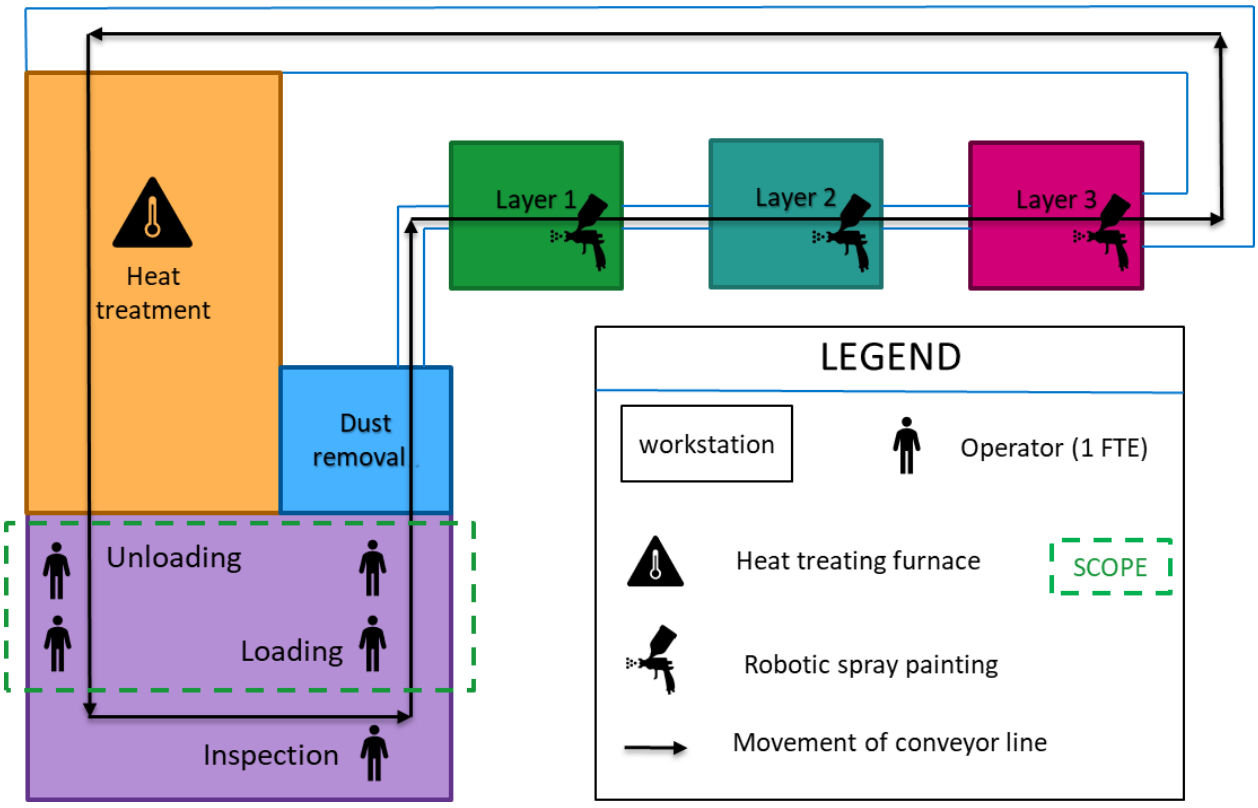

Figure 5. Schematic representation of the lacquering line showing the sequential activities and performers, with the project scope shown in the green dashed box.

Due to the functional difference in the manual steps of loading/unloading and the visual inspection, the lacquering automation project was split into two investigations:

1. Inspection automation led by the senior process engineer, who is investigating a laser-based droplet detection system to replace the post-lacquer check requiring 1 FTE.
2. Loading and unloading automation led by the senior architect of the production systems.

The loading and unloading steps are considered labor intensive due to the following reasons:

1. Part variation: 8 different parts varying in their geometrical and material properties, are currently processed in the lacquering line with more variations to be potentially added in the future.
2. Part fragility: The plastic parts are decorative sub-assembly components prone to damage and have critical-to-quality features visible to the end consumer.
3. Complexity of part loading and unloading: The part loading involves identification, collection, and movement of the part, followed by mounting of the part onto a work-holding device.

2.2. System description

The lacquering line receives injection molded parts in trays fed by the tray-feeder. The part-specific jig is selected and mounted onto the spindle before loading the parts. The parts then go through the lacquering steps and then unloaded and inspected before being sent to the assembly line.

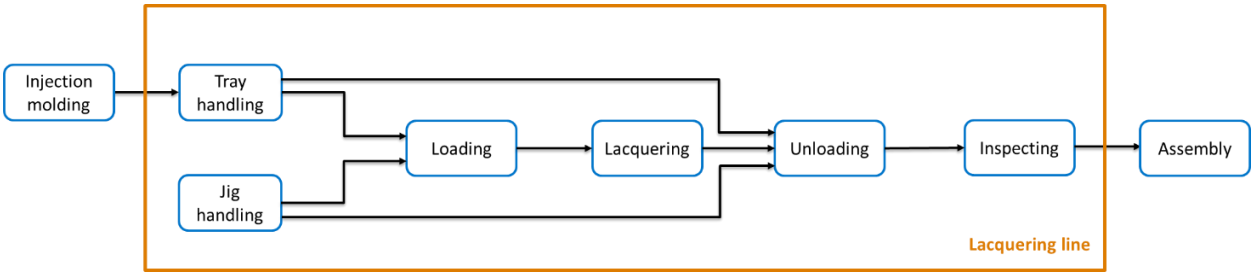

Figure 6. High-level system diagram depicting the sequential phases of the lacquering functions.

The loading and unloading functions begin with the operators picking the parts from the trays and mounting them to the jigs, which is split into 4 functions for the automated setup: part alignment to achieve repeatable grasping, part grasping and releasing, part movement between the tray and the jig, and (dis)mounting of the part. The robot arm does the part movement while the rest of the functions are done by the EOAT.

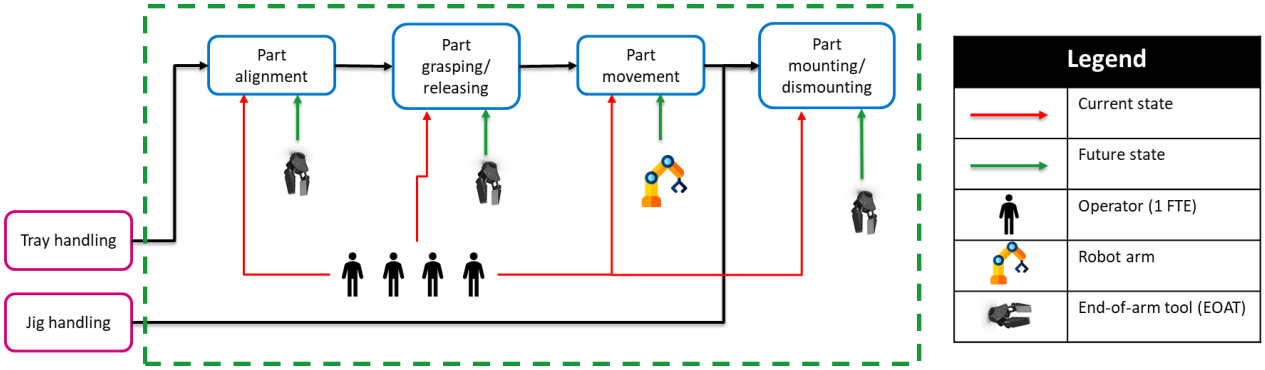

Figure 7. Low-level system diagram depicting the sequential sub-functions of the loading and unloading functions.

2.3. Stakeholder analysis

The various stakeholders affecting (or affected by) this research along with the qualitative comparison of their power is shown in the Figure 8. The problem owner: Eric Sloot, Senior production systems architect, along with the lacquering line process engineer and cost engineer, decide the primary constraints and requirements of the project, listed in Table 1.

Table 1. Stakeholder requirements classified into quality, cost and time aspects

Aspect	Requirement
Quality	Process repeatability
	Part Safety
Cost	Budget = €1.2M (2 years or lesser payback time)
Time	CT requirement = 2 seconds / part

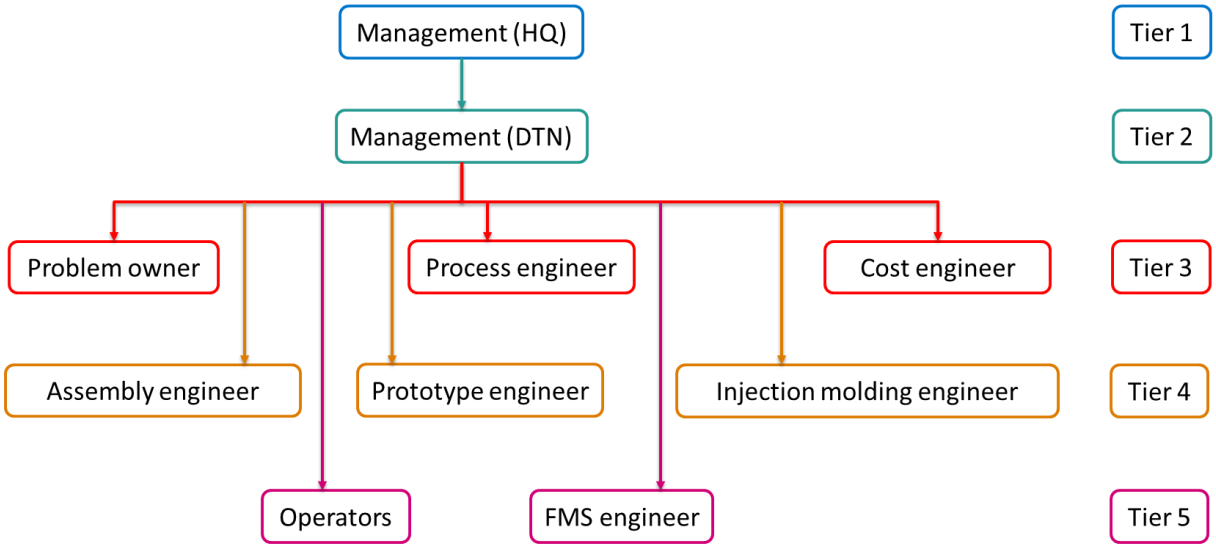

Figure 8. Schematic representation of the 5-tier hierarchical structure of stakeholders.

2.4. Conceptual model

2.4.1. 5W2H

The 5W2H analysis asks questions to quantify the project specifications, as seen in the table below:

Table 2. 5W2H analysis for the flexible EOAT design problem

What?	EOAT setup for flexible automation of part loading/unloading
Why?	Economically automate labor intensive steps to reduce labor costs
Who?	Eric Sloot, Senior production systems architect -> Problem owner
Where?	Lacquering line
When?	Proof of concept by end of December 2021; to be implemented in a few years
How?	Propose solutions, critique for constraint satisfaction, modify to meet design goals
How much?	~€1.7M budget with a break-even-period of 2 years

2.4.2. What-why

Next, the problem is analyzed through what-why analysis model developed by Annamalai et. al., (2013) to understand the causal relationships between interlinking problems. The original problem of the automation of lacquering part (un)loading arises due to high labor costs which in turn increase the factory cost price (FCP). This leads to a decrease in the integral gross margin which has 2 potential outcomes: 1. The non-competitive product pricing could force the management to replace the process or 2. The increased FCP could force the management at headquarters (HQ) to move the production to a lower FCP facility like Batam, Indonesia, or look for alternative manufacturing processes to reduce the FCP.

The automation of lacquering part (un)loading is an issue due to the expensive implementation of part-specific EOAT (due to change-over times) and inaccuracies of a universal EOAT, elaborated in Section 3.4.

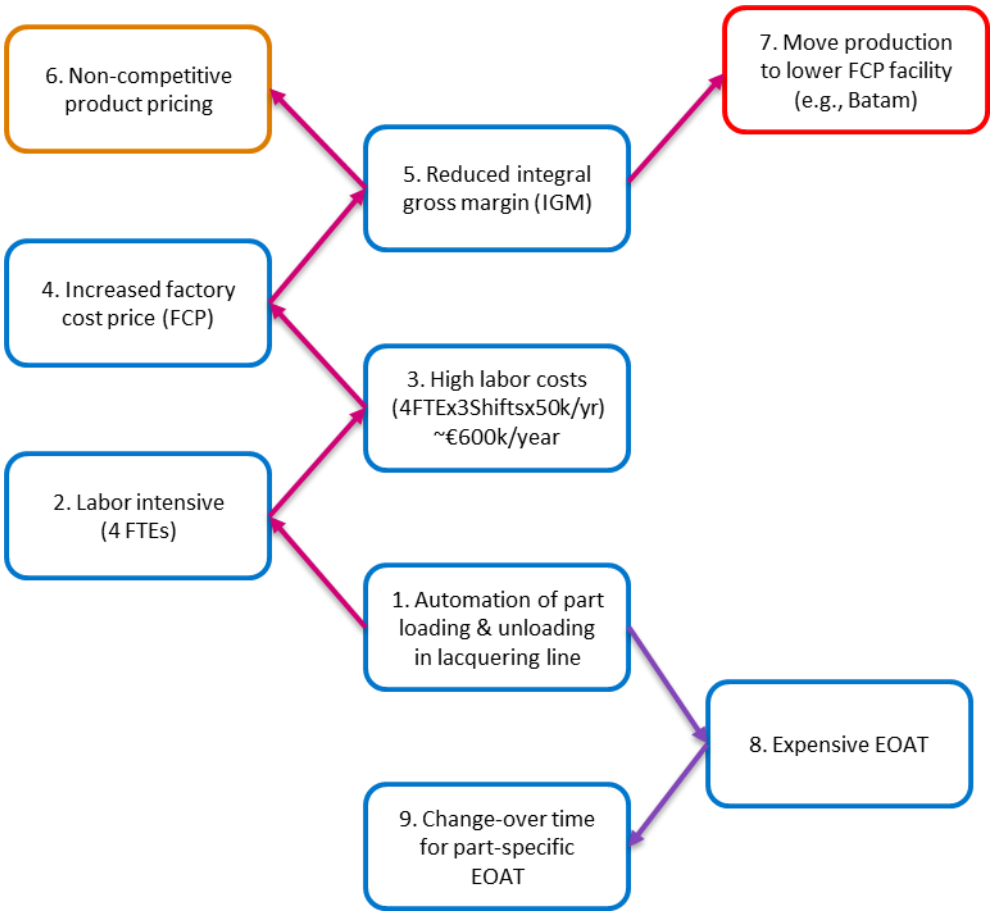

Figure 9. What-Why analysis of the EOAT design problem (Annamalai et. al., 2013).

2.5. Problem statement

Increasing labor costs in the Netherlands has made the production line at Philips Drachten uncompetitive, causing the management to investigate automation opportunities. The flexible automation of labor-intensive steps in the lacquering line has been expensive due to high costs of end-of-arm-tools (EOATs).

2.6. Goal statement

To develop a proof of concept of a flexible EOAT - by the end of December - capable of grasping 8+ (to be) lacquered parts without damaging them - while fulfilling financial constraints (to meet cycle time requirements) - to economically automate the loading/unloading steps of the lacquering line.

2.7. Research question

How can a flexible EOAT be designed for pick and place, and non-destructive snap-fit (dis)assembly of fragile parts varying in geometry while meeting cycle time and financial requirements?

3. EOAT design elements

In this section, the EOAT design parameters are explained through a literature review of types of end-of-arm tools and their selection, prehension strategy defining the robot and EOAT movement, and grasp synthesis to determine the contact points and their analysis.

3.1. Gripper classification

Monkman et al., (2007) classified grippers (generic term for pick and place EOATs) based on the grasping methods into the following types:

1. Impactive: also called mechanical gripper since it uses impact forces against the object surface, examples of which include jaws, tongs, or clamps.

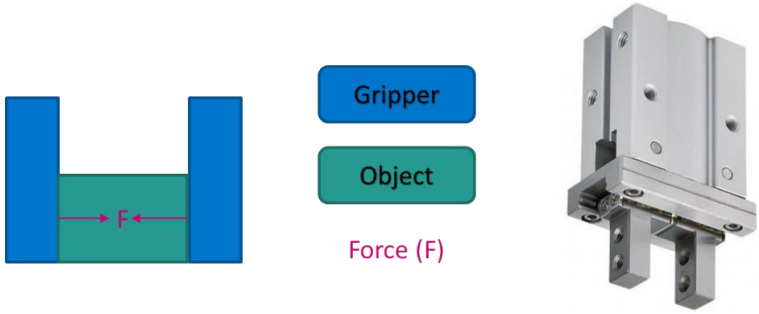

Figure 10. (a) Schematic representation of impactive gripper forcing the object into prehension.

(b) Example of an impactive friction jaw gripper (Tameson, 2021).

Impactive grippers are further classified based on

a. Object enclosure:
   i. Form closure: object is fully restrained through the shape of the set of contacts irrespective of the force magnitude.
   ii. Force closure: any motion of the object is resisted by the forces exerted by the set of contacts.
   iii. Combined closure: both the shape of the fingers and the forces exerted by them are used to resist external force/torque.

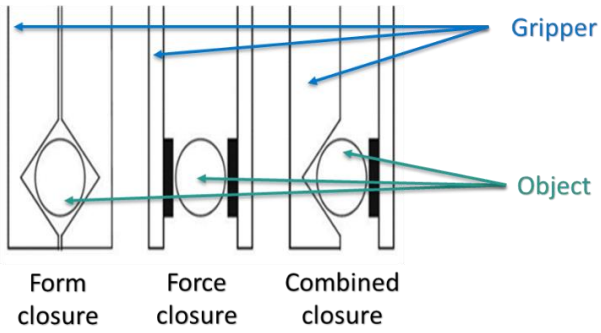

Figure 11. Schematic representation of form, force, and combined methods of gripper closure (Bajd et al., 2010).

Form closure is generally used for grasping heavy (relative to the gripper mass and robot payload) objects and/or when the object being grasped has delicate surfaces, while force closure allows secure grasping, especially when the object needs to be re-oriented for the next operational step.

b. Finger movement relative to the gripper axis
    i. Angular: The jaws pivot about the gripper normal axis to open/close the fingers.
    ii. Parallel: The jaws move parallel to each other to open/close the gripper fingers.

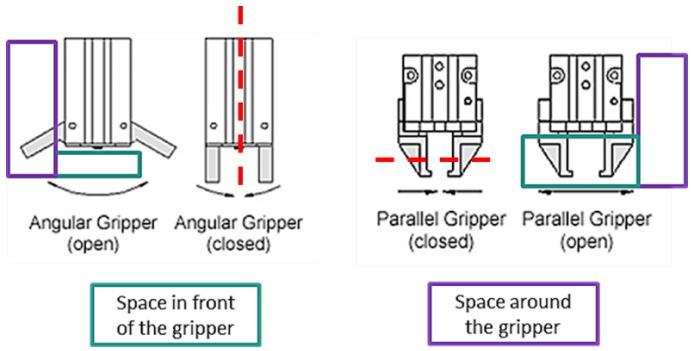

Figure 12. Schematic representation of opening and closing of angular and parallel jaw grippers (Omega, 2021).

Angular jaws are preferred when the operation requires clearance in front of the gripper, while parallel grippers are preferred when the operation requires the space around the grippers to be empty.

c. Finger movement relative to the object:
    i. Internal: The gripper finger jaws grasp the object surface by opening against internal edges of object surfaces like holes. The grasping is achieved by opening of the gripper fingers i.e., the fingers moving away from each other.
    ii. External: The gripper finger jaws grasp the object by closing against the external surfaces of the object. The grasping is achieved by closing of the gripper fingers i.e., the fingers moving towards each other.

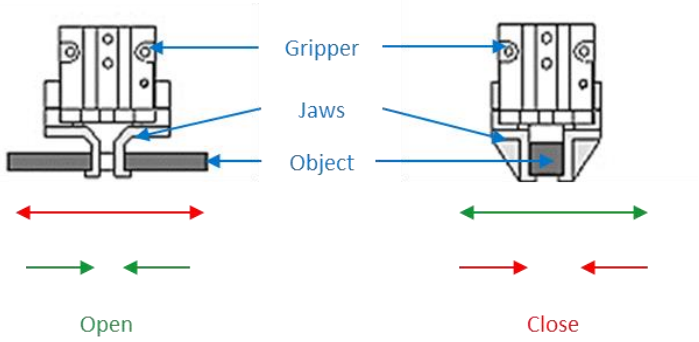

Figure 13. Schematic representation of external and internal gripper using a parallel jaw gripper example (Omega, 2021).

The selection of internal/external type of gripper depends on the availability of holes in the object and the location of grasp-feasible surfaces on the object.

2. Ingressive: permeates the object surface by
    a. intrusion of sharp features (intrusive)
    b. hooking to loops within the object surface (non-intrusive)

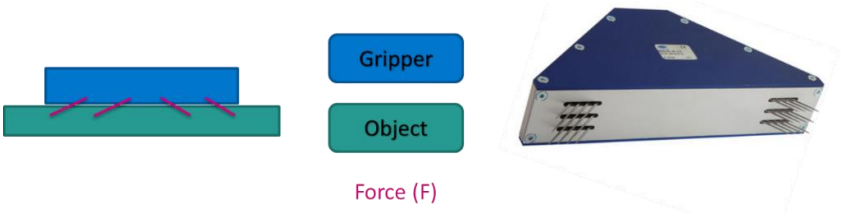

Figure 14. (a) Schematic representation of ingressive gripper forcing the object into prehension.

(b) Example of an ingressive needle gripper (Schmalz, 2021).

Ingressive grippers are preferred to grasp objects like fabrics stacked on top of each other.

3. Astrictive: requires the use of binding forces (vacuum suction/magneto adhesion/electro adhesion) produced by a field to grasp the object.

Figure 15. (a) Schematic representation of astrictive gripper forcing the object into prehension.

(b) Example of a vacuum suction gripper (Schmalz, 2021)

(c) Example of a magnetic gripper (OnRobot, 2021).

Astrictive grippers are used to grasp objects with non-porous, flat surfaces.

4. Contigutive: makes direct contact with the object surface to achieve prehension.

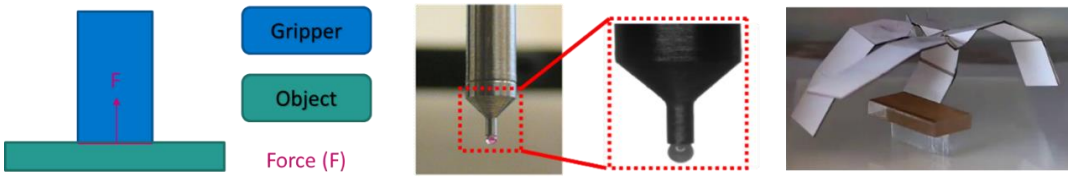

Figure 16. (a) Schematic representation of contigutive gripper forcing the object into prehension.

(b) Example of a fluid (capillary action) gripper (Arai, Chaillet and Martel, 2021; Lenders, C. et al, 2008)

(c) Example of a thermal (shape-changing) gripper (NC state, 2019).

Contigutive grippers are used to grasp objects capable of reacting with the gripper to allow prehension, such as objects which change properties upon the application of heat or chemicals (active), fluids which allow the gripper to use the capillary or surface tension properties of the fluid for prehension.

3.2. Gripper selection

Fantoni G. et. al. (2014) developed a system for the selection of robot grippers based on grasp rules defined by stakeholder requirements and parameters describing the problem:

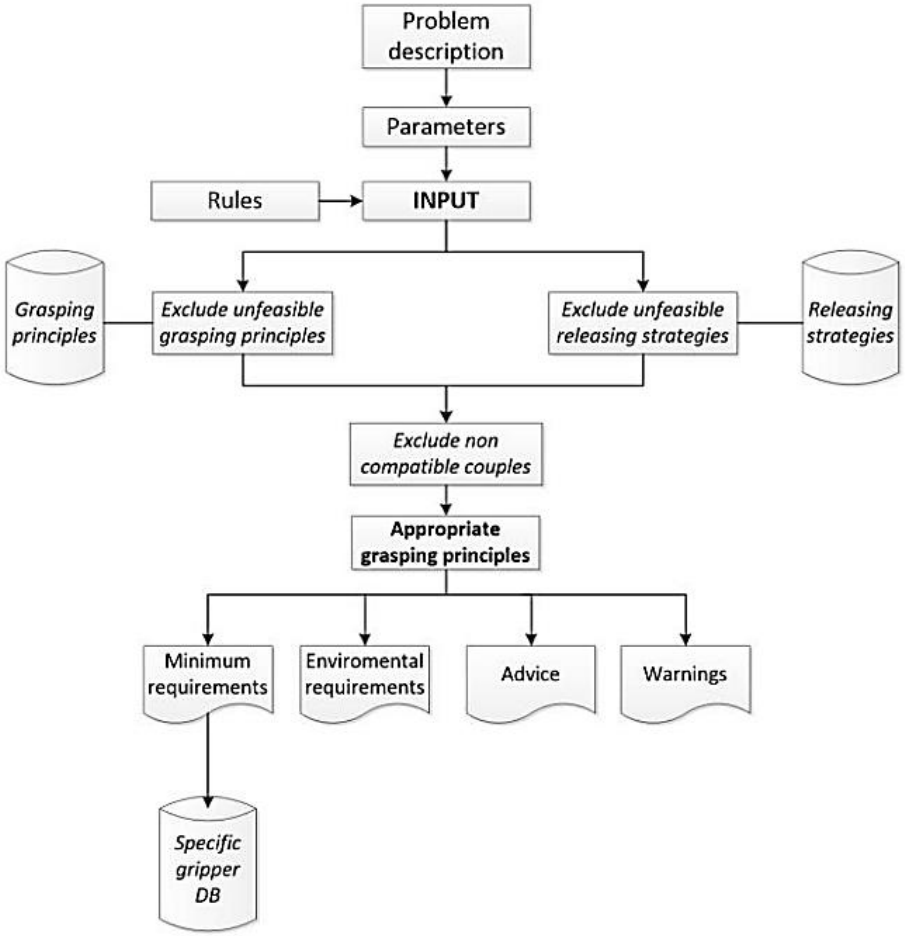

Figure 17. Gripper selection framework developed by Fantoni et al. (2014).

The authors classified the parameters into

1. Object parameters: physical and geometrical properties of the workpiece to be handled.
2. Operation (process) parameters: properties of the pick and place, as well as any additional functions required to be performed by the gripper, listed below:
    a. Feeding: Events leading up to the pick function.
    b. Handling: Events after the pick function, including moving to the place location, reorientation of the object, and additional functions.
    c. Placing: Events leading to the place function.

Similar gripper selection strategies, rules and frameworks are also found in the works of Pham and Yeo, 1988 and 1991; Pedrazzoli, Rinaldi and Boer, 2001.

3.3. Gripper design guidelines

Causey and Quinn (1998) described design guidelines for grippers to improve system throughput and reliability of modular manufacturing work cells, summarized below:

1. Minimize gripper footprint: The minimum empty (obstruction-less) 3-dimensional space around the gripper to satisfy the approach clearance constraint - collision-free approach and grasp of the part located in the part-feeder – is called the gripper footprint (Causey and Quinn, 1998).
2. Chamfer finger exterior: This helps the gripper to approach the part without crashing into a misaligned part or a neighboring part not satisfying the approach clearance.
3. Align grasped parts using fingers: The gripper should have an additional functionality of aligning the parts before or during grasping, to repeatably grasp irregular shaped parts.
4. Grasp securely: The gripper should ensure that the grasped part is not dropped, or its orientation is not changed during high-speed robot movements.
5. Grasp safely: The gripper should not damage (defined based on the object and operation parameters) the part during grasping.
6. Avoid tool changes: Changing the grippers while switching from a particular object (or operation) to a different one increases the change-over time, irrespective of whether the tool changing is manual (stoppage time) or automatic (additional robot movements). Alternative ways of handling a range of different parts without compromising on the cycle time include:
    a. Multiple grippers on a single wrist: Object or operation specific tools could be mounted on the same wrist by compromising on the accuracy of high-speed robot movements by ensuring the total weight still falls below the robot payload capacity, and the gripper footprint still allows sufficient approach clearance.
    b. Multi-functional grippers: The other alternative is to design the gripper fingers such that they can handle multiple parts or perform multiple operations.
7. Minimize finger length: Longer gripper fingers are generally not preferred due to deflections during grasping, which can destabilize the grasp, and reduce the life of the fingers.

3.4. Grasping flexibility

Based on the range of parts that can be grasped, grippers can be classified into

1. Specific grippers: custom designed to handle specific objects with a small degree of variability.
2. Universal grippers: wide clamping ranges designed to handle diverse object shapes.

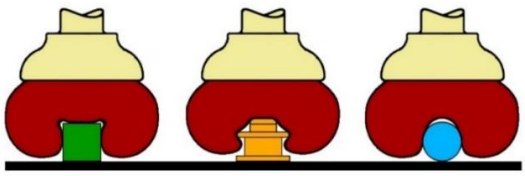

Figure 18. Schematic representation of a universal (jamming) gripper developed by Amend et al., (2012) showing three different operational modes for handling objects of varying geometrical properties.

Although specific grippers are customized to handle each part and hence have a high accuracy, multiple grippers to handle multiple parts not only increases the cost of EOAT, but also that of robots, since additional robots would be required to mitigate the gripper changeover time. On the other hand, Universal grippers are expensive to begin with and have a low accuracy to accommodate a range of different parts, requiring additional sensors and feedback systems to increase the accuracy, further increasing the expenses. The dynamic relationship between the part specificity and the expenses of automation, is shown in Figure 19.

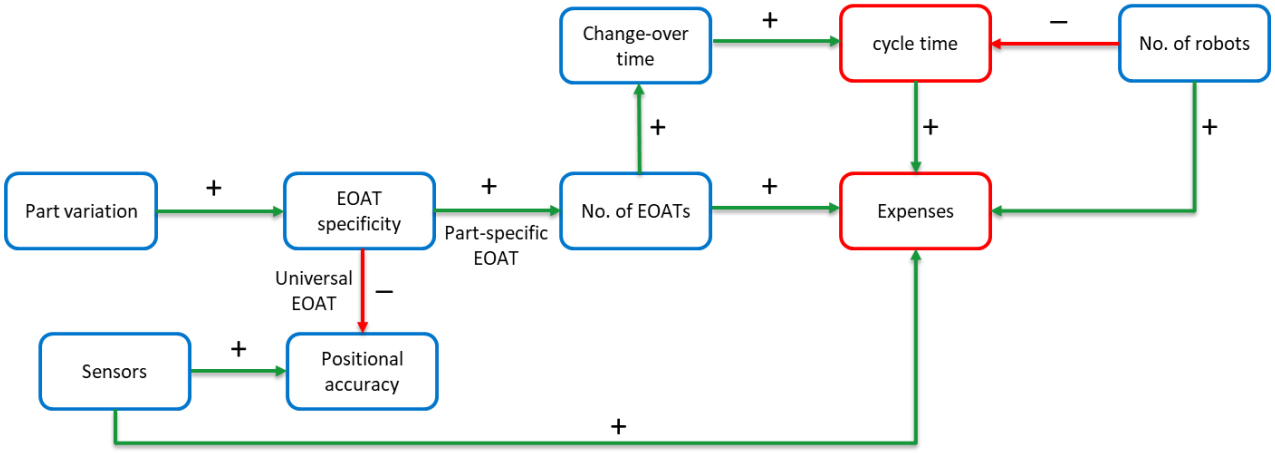

Figure 19. The dynamic relationship between the EOAT specificity and expenses incurred to meet cycle-time and positional accuracy requirements.

3.5. Grasp synthesis

Grasp synthesis is the determination of finger parameters including grasping contacts and the fingertip profile for required properties (Shimoga, 1996).

3.5.1. Grasping contacts

Nguyen, (1987) presented algorithms for stable force closure grasp-synthesis based on the object shape and the friction cones at the points of contact. The friction cone for force closure contacts is the cone formed by the normal force at the center of the cone and the lateral surface area formed by the components of the normal force along the friction angle. Frictional fingers are classified into the following types based on their ability to constrain the object displacements and/or rotation:

1. Hard finger: can constrain the normal and tangential displacements of the object.
2. Soft finger: can constrain normal rotation as well as the normal and tangential displacements.

For a 2-jaw soft finger gripper, a stable grasp is achieved when the angles between the planes of contact is less than the angle of friction cone i.e., twice the friction angle (Nguyen, 1987; Pham and Yeo, 1988). This in turn can be achieved by lowering the angle between the planes of contact by choosing appropriate surfaces, or by increasing the angle of friction by choosing a gripper material with a higher static coefficient of friction.

The author also described the relationship between the points of contact and their friction cones, and how complex (line, area, or surface) contacts can be described as the sum of primitive point contacts, as seen in Figure 20. Due to the large friction cones formed at the sharp corners and edges, the surfaces of the object having those features are preferred for stable grasping.

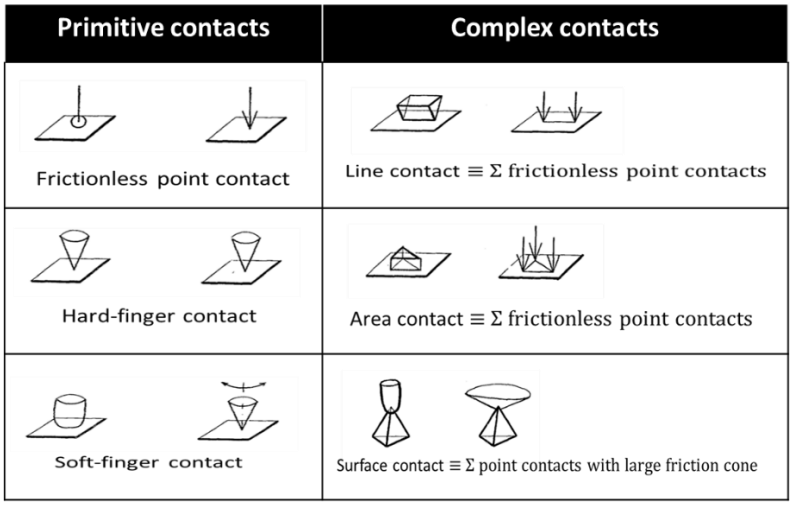

Figure 20. Complex contacts and their primitive equivalents Nguyen (1987).

3.5.2. Fingertip (jaw) profile

Pedrazzoli, Rinaldi and Boer, (2001) developed a rule-based fingertip type determination framework (Figure 21) which categorized fingertip profiles into flat, V, C, and non-standard types and their selection rules based on the surface of the object being grasped (grip site). The C fingertip profile provides the most contact surface of the standard profiles resulting in a larger discharging surface and lower surface pressure and is hence preferred over the V-profile for delicate materials.

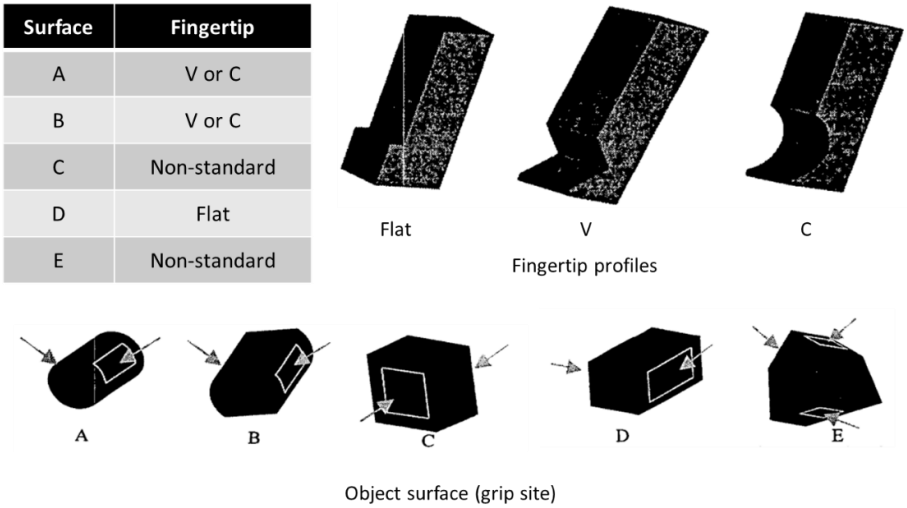

Figure 21. Fingertip profile selection rules developed by Pedrazzoli, P., Rinaldi, R. and Boer, C.R., (2001)

While Nguyen (1987) explained the selection of gripping point for a stable force-closure grasp based on the object material and shape, Pedrazzoli, Rinaldi and Boer, (2001) explained the shaping of the finger-tip profiles based on the surfaces of the object being grasped.

3.6. Prehension strategy

Once the gripper components are selected, a gripping procedure must be strategized to program the autonomous implementation of prehension as described by Monkman et al. (2007):

1. Preparation for contact: Aligning the spatial orientation of the gripper with that of the object to repeatably grasp the object at the gripping point with the required positional accuracy using sensor systems like robot vision to match the gripper orientation with that of the object, or by using the gripper or an external device to re-align the object orientation to match that of the gripper.
2. Prehension: Establishing contact between the gripper and the object surfaces to achieve autonomous implementation of prehension based on the programmed prehension strategy:
    a. Gripping point (pick location): The location of the feeder from which the object is grasped:
        i. Fixed: Static feeder location.
        ii. Moving: Pre-determined feeder movement such as conveyor feed.
        iii. Unknown: Variable feeder and object location determined by sensors.
    b. Location of prehension: The surfaces of the object which could potentially be used for grasping constrained by the accessibility of the location, and the object parameters. The authors defined object handling zones to arrive at the prehension location:
        i. Forbidden zones: Surfaces of the object which are constrained by object parameters such as fragility or sensitivity of the object toward prehension.
        ii. Reserved zones: Surfaces of the object which are already held by other operational devices.
        iii. Support zones: Surfaces of the object which are partially or completely in contact with the pick or place location.
        iv. Prehension zones: All the surfaces not overlapping with the other zones.

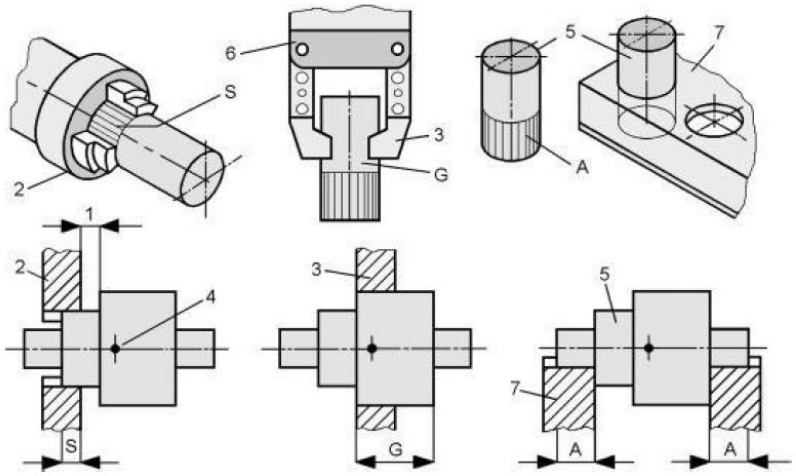

Figure 22. Handling zones of a workpiece (Monkman, G.J., et. al., 2007):

1. Safety margin, 2. Chuck, 3. Gripper jaw, 4. Centre of gravity, 5. Workpiece,

6. Gripper, 7. Magazine, A. Support zone, G. Prehension zone, S. Reserved zone

   c. Gripping force: The force required to ensure that the grasped object does not reorient due to their weight or inertia. The effective gripping force depends on the object parameters, grasping method, active surfaces, and jaw profiles.
   d. Active surfaces: The number of contact points or surfaces between the object and the gripper jaw(s). The effective gripping force can be reduced by increasing the active surfaces through the increase of number of jaws, or the increase in the contact area of jaw profile.
   e. Jaw profile: the shape and contour of the jaw surface that come in contact with the object. The extent of matching between the jaw and object profile is directly proportional to the grasp stability.
3. Retention: Maintaining the grasp on the object through the robot movement from/to the pick, place, and additional (if any) locations.
4. Release: When the object is moved to its destination, the grasping forces need to be decreased to release the object.

4. Methods and tools

4.1. Strategy

Based on the gripper selection framework by Fantoni et al. (2014) and finger-design flowchart by Honarpardaz et al. (2017), a design strategy was formulated (Figure 23). Object and operation parameters obtained from the part and process study; functional requirements defined from the stakeholder analysis formed the constraints around which the EOAT was designed. Literature review, market study, and interviews with relevant people at Philips, were used to determine off-the-shelf components suited for the application. Components which were not readily available in the market were designed, iterated, and prototyped to validate against the functional requirements to obtain the proof of concept.

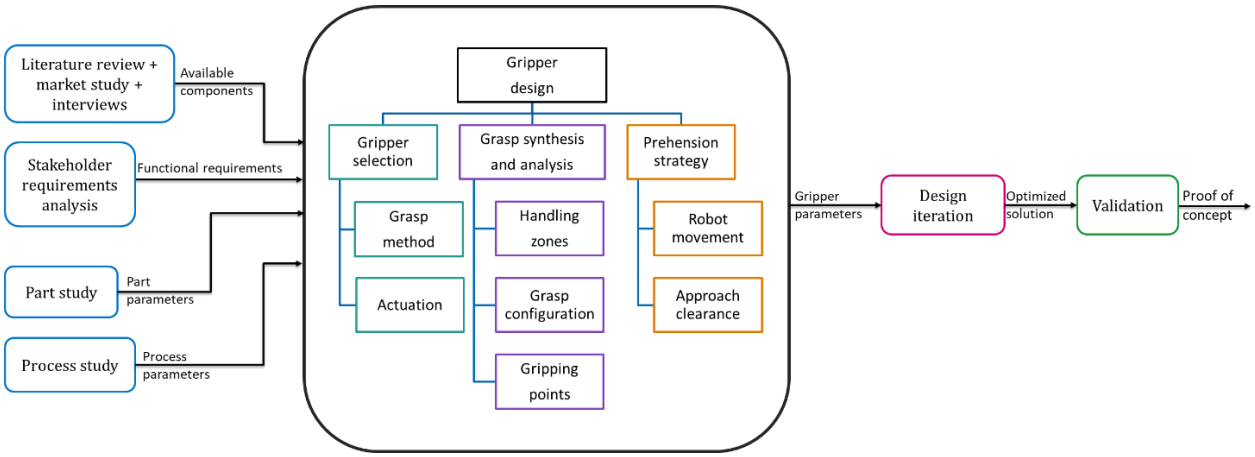

Figure 23. EOAT design strategy based on the components of finger-design flowchart by Honarpardaz et al. (2017) and the gripper selection framework by Fantoni et al. (2014), depicting the sequential chain of events leading to the proof of concept.

The design iteration followed the modeling and analysis of the gripper fingers, jaws, and interfacing components using NX12 CAD modeling software. The designs were then prototyped in Polyamide (PA) 12 (Appendix A), and Agilus30 (Appendix B) materials, using HP multi-jet fusion (MJF) (Appendix C) and Stratasys j750 (Appendix D) 3D printers, respectively. The experimental validation was performed by attaching the flexible EOAT to a Universal UR5 robot arm (Appendix E). The tools used were selected based on their ease of availability at DTN.

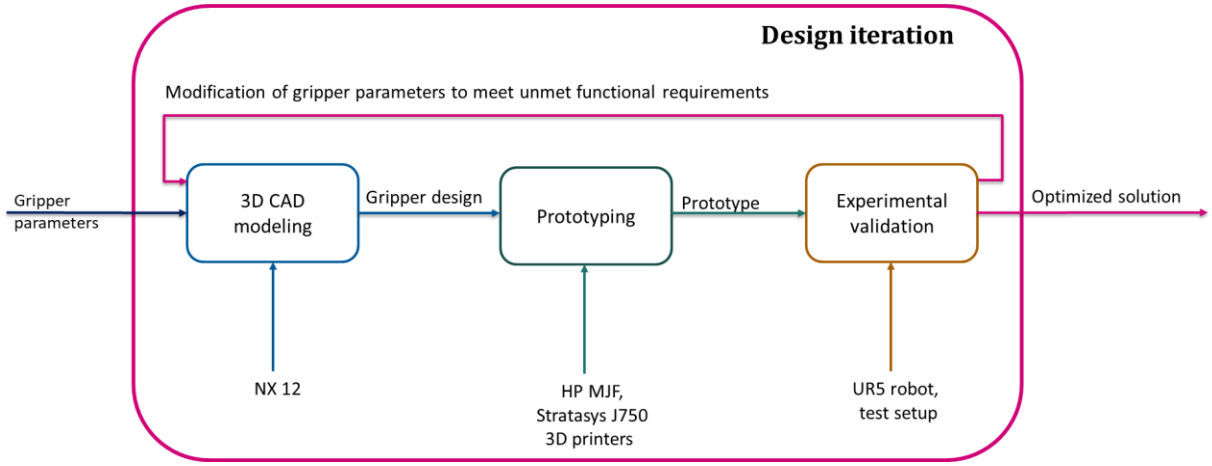

Figure 24. The design iteration for gripper components not available readily in the maket.

4.2. Part and process study

The parts that are currently lacquered in the lacquering line at DTN are listed and picturized in Figure 25. 2 sets of parts – 2 variants of Hera s3000 front panel; Poseidon and Atlas chests - have similar dimensions and shape and hence considered equivalent for grasping. The parts are referred to by their numbers throughout the report for ease of readability.

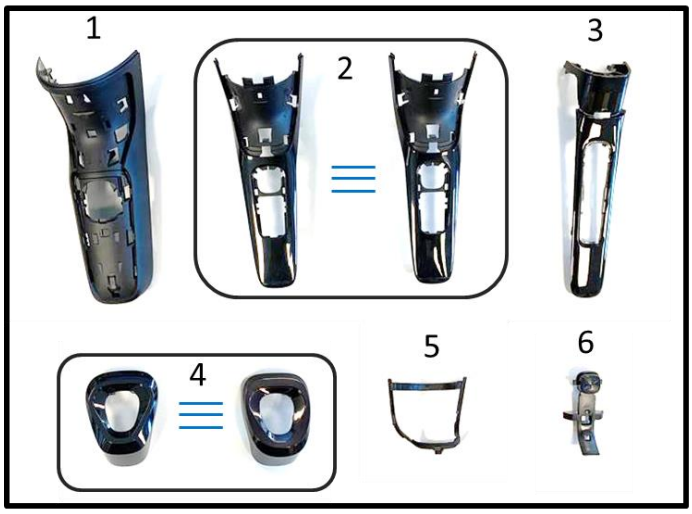

Part list (current variation):

1. Hera s1000 front panel
2. Hera s3000 front panel
3. Poseidon s7000 front panel
4. Poseidon s7000 chest ≡ Atlas s5000 chest
5. Hera s3000 deco panel
6. Hera s3000 button

Property	Unit	Value
Density	kg/dm³	1.14
Tensile strength	MPa	55
Tensile modulus	MPa	2700
Izod impact strength	kJ/m²	7
Charpy impact strength	kJ/m²	8

Figure 25. Pictorial representation of the list of all the parts that are currently lacquered in the lacquering line at DTN with the similarly shaped parts considered equivalent for grasping and their material properties

The generic material properties of the parts are listed in the table within Figure 25, with part-specific properties discussed in later sections, as and when they are used. The material data sheet for the part as well as the lacquer materials are given in Appendix F.

(Dis)mounting mechanism

The (dis)mounting of the parts on/from the jig is achieved through 2 jig-features:

1. Place: The pivoting feature on which the part is initially placed, and then pivoted about.
2. Click: The cantilever beams which deform to snap-fit the beams on the part.

The part is initially placed on the "place" feature of the jig before pivoting about it to then "click" it.

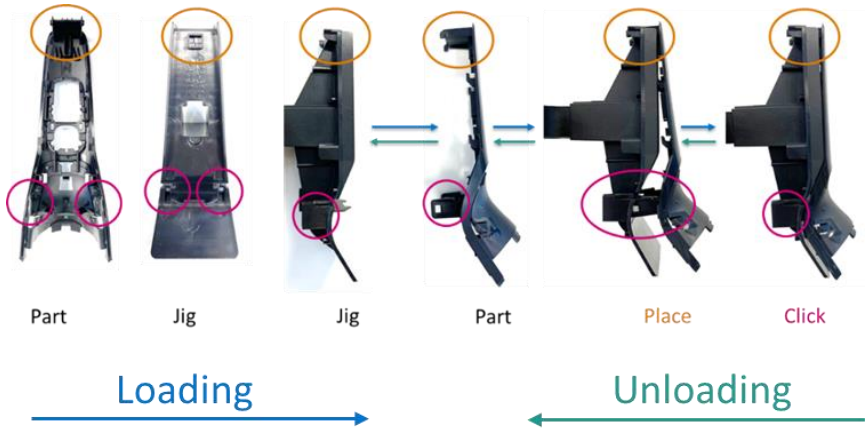

Figure 26. Pictorial representation of the (dis)mounting mechanism for Part 2 (example) showing the place (pivot) and click (snap-fit cantilever beam) features of the part and the jig.

4.3. Gripper selection

The suitability of each grasping method was checked for each of the part against the functional requirements and part and process constraints to find the method(s) suitable to most or all of the parts, as explained below and summarized in the selection matrix in Table 3:

1. Contigutive type of grasping is not feasible for any of the parts because of unsuitability of the part material for the reactive grasping method.
2. Non-intrusive hook and loop type of ingressive grasping would be difficult due to the varying hole dimensions of the part as well as the use of the hole edges in certain part-jig assemblies and the fragility of Part 5.
3. While magnet and electro-adhesion based astrictive grasping methods are not possible due to the nature (non-magnetic, non-conducting, and curvature) of the parts, vacuum suction is difficult due to the lack of a sufficiently large feasible suction area – non-porous flat surface - on the parts.
4. Impactive grasping is possible for all the parts without much difficulty, and hence most suitable for the problem context.

Table 3. Grasping method selection matrix based on the feasibility of grasping each part.

Part	Impactive	Ingressive	Astrictive	Contigutive
1 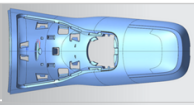	Yes	Difficult	Yes	No
2 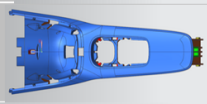	Yes	Difficult	Yes	No
3 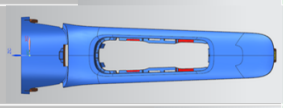	Yes	Difficult	Yes	No
4 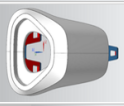	Yes	Difficult	Difficult	No
5 	Yes	No	No	No
6 	Yes	Difficult	Difficult	No

A similar selection matrix was drawn-up (Table 4) for the selection of the type of impactive gripper based on the following parameters:

1. Type of closure: Force closure is difficult due to the curved edges of the Chest, and the dimensional constraints and fragility of the deco-panel and button. Although form closure is possible for all the parts, combined force closure is selected since it allows for a more secure grasping of the object.
2. Jaw movement relative to gripper axis: Angular movement of the jaws is not preferred due to the larger footprint potentially colliding with the parts placed beside the one being grasped, as well as

those in the jig. Parallel movement of the gripper fingers offers a better approach clearance and hence parallel gripper with position control is selected.

3. Jaw movement relative to part features: Internal gripping is limited due to the varying hole dimensions of the parts and hence external gripper type is selected.

Table 4. Gripper type selection matrix based on the feasibility of grasping each part.

Part	Form closure	Force closure	Angular jaws	Parallel jaws	Internal gripping	External gripping
1 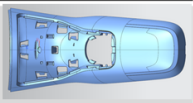	Possible	Yes	Not preferred due to part positioning in the tray	Yes	Limited	Yes
2 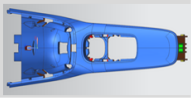	Possible	Yes		Yes	Possible	Yes
3 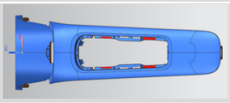	Possible	Yes		Yes	Limited	Yes
4 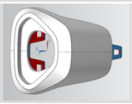	Possible	Difficult		Yes	Limited	Yes
5 	Preferred	Fragile		Yes	Possible	Yes
6 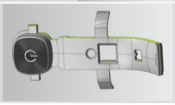	Possible	Difficult		Yes	No	Yes

The selected gripper is thus described as a mechanical gripper with the following parameters:

1. Suitable drive to allow parallel movement of the fingers.
2. Force control to allow combined form and force closure.
3. Position control to allow collision-less approach.
4. Jaw positioning of the fingers to facilitate external gripping.

4.4. Grasp synthesis and analysis

In this section, the handling zones – the allocation of each surface and edge of the part to a particular function – are defined for the 6 lacquering parts. The gripping points are then defined as the points lying on the axis of symmetry of the parts, along the feasible grasp configuration for part picking and (dis)mounting.

4.4.1. Handling zones

1. **Forbidden zone**: Surfaces of the parts which should not be used for grasping in order to prevent potential part damage.
2. **Reserve zone**: The surfaces of the parts reserved for mounting and dismounting i.e., the place and click feature surfaces on the parts.
3. **Support zone**: Inaccessible or difficult to access surfaces of the parts when they are placed on the tray or when mounted on the jig.
4. **Prehension zones** are the surfaces of the parts where they can be potentially grasped while meeting the object and operation constraint i.e., the zones which do not overlap with the other handling zones.

Part 1 (Figure 27)

For Part 1, the pick and place features, and the surfaces in contact with the tray (during feeding) or jig (during assembly/disassembly) form the red zones. Hence, the surfaces of the part at the top and bottom of the part (along its length) are selected as the prehension zones, with the gripping points along the axis of symmetry of the part.

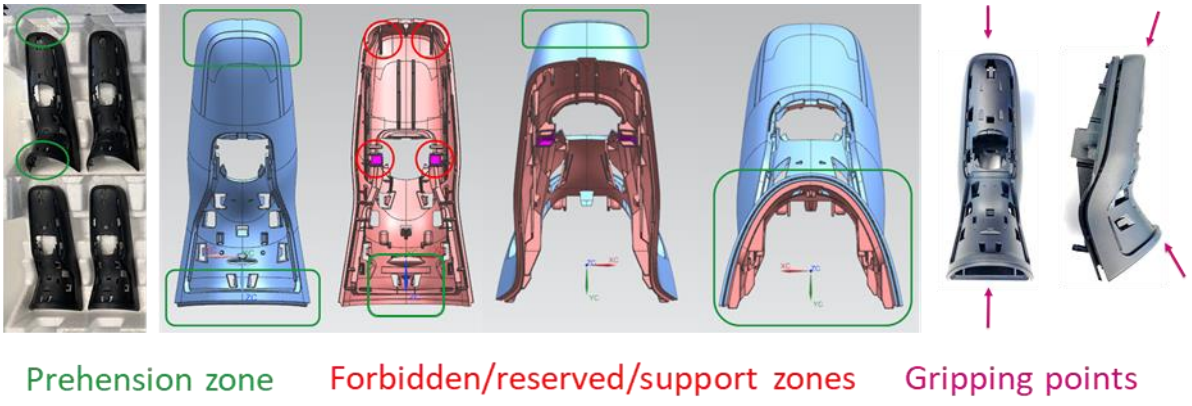

Figure 27. Pictorial representation of the handling zones depicting the prehension zones for Part 1 (Hera s1000 front panel) and the gripping points selected within the prehension zones.

Part 2 (Figure 28)

Part 2 has similar surface shapes as Part 1 and hence similar prehension zones and gripping points are chosen.

Figure 28. Pictorial representation of the handling zones depicting the prehension zones for Part 2 (Hera s3000 front panel) and the gripping points selected within the prehension zones.

Part 3 (Figure 29)

The positioning of part 3 in the tray makes it difficult to grasp the parts in the upper row of the tray with little to no clearance between the parts. This was solved by defining a pick sequence which ensures the parts in the lower row of the tray are picked first, thus ensuring collision prevention during the picking of parts in the upper row.

Figure 29. Pictorial representation of the handling zones depicting the prehension zones for Part 3 (Poseidon s7000 front panel) and the gripping points selected within the prehension zones. The part positioning in the tray causing potential collision during part picking is circled in red, and the part-picking sequence which solves the problem shown alongside.

Part 4 (Figure 30)

Due to the smooth curved bottom surfaces of Part 4, a part of the place feature with sharp edges is included within the prehension zone of the part. Since this part feature is inaccessible when placed in the tray (see red marking in the tray picture), 2 sets of gripping points, marked 1 and 2 in the picture, are defined for (dis)mounting and part picking, respectively.

Figure 30. Pictorial representation of the handling zones depicting the prehension zones for Part 4 (Atlas chest shown in picture) and the gripping points selected within the prehension zones. The tray hole used for part placement and the smooth curvature of the bottom surface of the part are circled in red.

Part 5 (Figure 31)

Part 5 is limited to a small prehension zone – at the groove within the jig - due to the dimensions of the part as well as the jig design.

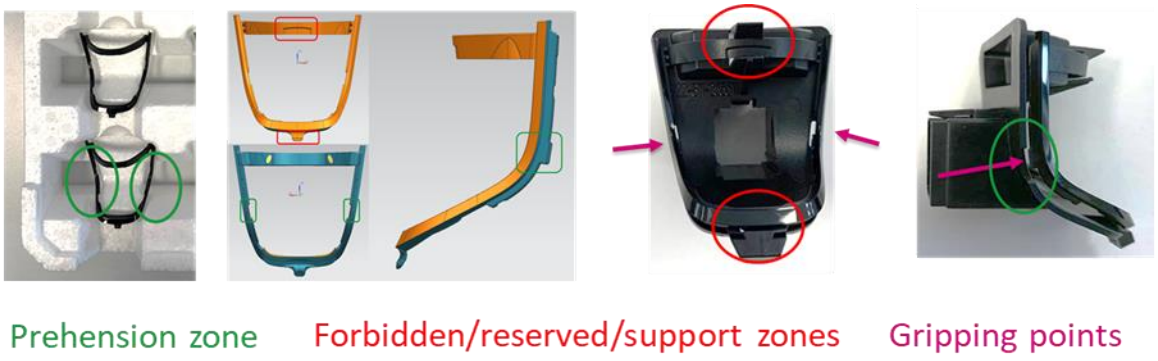

Figure 31. Pictorial representation of the handling zones depicting the prehension zones for the Hera s3000 deco panel and the gripping points selected within the prehension zones.

Part 6 (Figure 32)

The prehension zone for Part 6 is limited by the dimensions of the part, clearance at the tray, as well as the jig features.

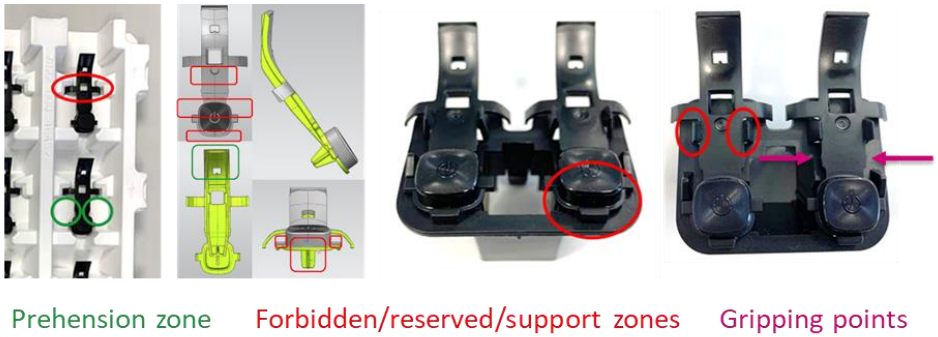

Figure 32. Pictorial representation of the handling zones depicting the prehension zones for the Hera s3000 on/off button and the gripping points selected within the prehension zones.

4.4.2. Grip configuration

The grip configuration is the axis of grasp i.e., the axis of movement of the parallel fingers. The three configurations for a grasp and their suitability for part picking and (dis)mounting are explained below:

1. **Vertical configuration** is selected for both part-picking and (dis)mounting of the parts: 1,2, and 3, due to the un-hindered availability of sharp corners and edges in the prehension zone along their vertical axis. The jig features facilitate vertical (dis)mounting of parts 1,2,3, and 4.
2. **Horizontal configuration**: Due to the tray placement of part 5 on a feature located on the vertical axis, as explained in the previous section, horizontal configuration is selected for part-picking of 5. Horizontal configuration is also the preferred choice for the part-picking an (dis)mounting of parts 5 and 6, due to the location of prehension zones along the horizontal axis.
3. **Distal configuration** is not feasible due to the reservation of those surfaces for part placement as well as (dis)mounting.

Table 5. Grasp configurations for each of the parts for part-picking from the tray and (dis)mounting.

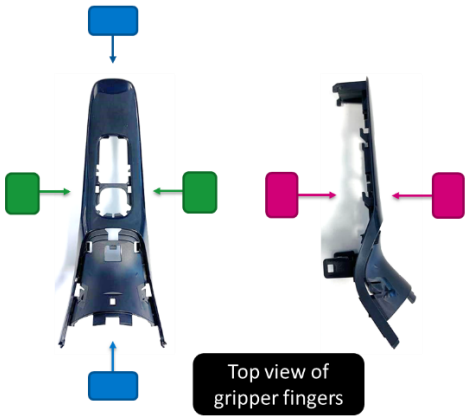

Part	Grasp configuration	
	Part-pick	(Dis)mount
1	Vertical	Vertical
2	Vertical	Vertical
3	Vertical	Vertical
4	Horizontal	Vertical
5	Horizontal	Horizontal
6	Horizontal	Horizontal

Vertical (along part length)
Horizontal (along part width)
Distal (along part height)

Figure 33. Pictorial representation of grasp configurations: vertical, horizontal, and distal, along the part length, width, and height, respectively, with the gripper fingers.

4.5. Prehension strategy

4.5.1. Grasp procedure

Based on the selected gripper selection and grasp synthesis, a procedure of steps depicting the sequence of steps to be followed to achieve the (un)loading processes - termed as the grasp procedure - is defined below:

1. Loading:
    a. Approach: The robot arm moves the gripper towards the part placed in the tray.
    b. Align: The part is aligned with the gripper fingers.
    c. Grasp: The gripper closes the fingers to grasp the part.
    d. Transport: The robot arm moves the grasped part to the location of the jig while re-orienting the part to align with the jig.
    e. Mount: The gripper performs snap-fit assembly to mount the part onto the jig.
        i. Place: The robot arm moves the part to the place feature of the jig; the gripper fingers open to release the part.
        ii. Click: The robot arm pushes the part using the fingers to perform snap-fit assembly.
    f. Release: The gripper fingers open to release the part mounted on the jig.
2. Unloading:
    a. Grasp: The gripper fingers close to grasp the part.
    b. Dismount: The gripper performs snap-fit disassembly dismount the part from the jig.
    c. Transport: The robot moves the grasped part to the tray location, while re-orienting the part to align with the tray.
    d. Release: The gripper fingers open to release the part in the tray.

4.5.2. Robot arm programming

The programming of a robot arm involves the definition of the following primary parameters to achieve the grasp procedure:

1. Waypoints: the positions and orientations of the EOAT relative to the robot.
    a. **Home:** A roughly equidistant position from the tray and the jig was chosen as the waypoint from/at which the robot arm begins and ends the program.
    b. **Tray:** The position at the center of the gripping points of the part when aligned and placed in the tray with the orientation of the gripper aligned with the grasp configuration.
    c. **Place:** the position and orientation of the gripper which aligns the part with the jig at some distance from the place feature such that when the part is released at this waypoint, the part maintains the alignment with the jig.
    d. **Click:** The gripper position at which the snap-fit assembly is achieved.
    e. **Tray safe**, f. **Pre-place** and g. **Pre-click** are the positions at a distance from the tray, place, and click positions respectively, such that there is no collision during joint movements of the robot from/to these positions, while the orientations match that of the tray and jig waypoints respectively.
2. Mode of movement between the waypoints. The 2 modes used for the purpose of (un)loading:
    a. Joint movement (**Mov J**): takes the fastest possible path between waypoints.

   b. Linear movement (**Mov L**): ensures linear movement of the tool between the waypoints and is hence used for collision prevention.
3. Output signal to the EOAT controller to open/close the fingers.
   a. **Grasp**: The fingers move towards each other until a pre-defined finger-distance is reached, to grasp the object. The finger-distance (distance between the parallel fingers) is determined by the distance between the gripping points
   b. **Release**: The fingers move away from each other to release the object.
   c. **Align**: The fingers move towards each other to re-orient the part and then away from each other.

The robot programs for each part are given in Appendix G. The generic robot-arm program parameters for the loading and unloading functions are summarized in Tables 6 and 7, respectively:

Table 6. Robot-arm program for the loading function with part-specific waypoints

Step	Movement	Mode	Waypoint
1	Robot arm	MovJ	Home
2	Robot arm	MovJ	Tray safe
3	Gripper	Open	Distance between gripping points + releasing allowance
4	Robot arm	MovL	Tray
5	Gripper	Align	Part dimension along the alignment axis
6	Gripper	Close	Distance between gripping points – grasping allowance
7	Robot arm	MovL	Tray safe
8	Robot arm	MovJ	Jig safe
9	Robot arm	MovL	Place
10	Gripper	Open	Distance between gripping points + releasing allowance
11	Robot arm	MovL	Pre-click
12	Griper	Close	Distance between gripping points – grasping allowance
13	Robot arm	MovL	Click
14	Robot arm	MovJ	Home

Table 7. Robot-arm program for the unloading function with part-specific waypoints

Step	Movement	Mode	Waypoint
1	Robot arm	MovJ	Pre-click
2	Robot arm	MovL	Click
3	Gripper	Close	Distance between gripping points – grasping allowance
4	Robot arm	MovL	Pre-click
5	Robot arm	MovL	Place
6	Robot arm	MovL	Pre-place
7	Robot arm	MovJ	Tray safe
8	Robot arm	MovL	Tray

9	Gripper	Open	Distance between gripping points + releasing allowance

4.5.3. Approach clearance

The 3-dimensional space around the parts located in the tray available for the gripper to approach the part located in the tray (Tray safe -> Tray) without colliding with any of the parts or the tray, is called the approach clearance, and is defined using the dimensions of the part and those of the tray, seen in Table 8.

Table 8. Approach clearance in terms of the part and tray dimensions (in mm)

Part	**Length**	**Width**	**Height**	**Least distance from the**			
				Neighboring part along		Tray boundary along	
				length	width	length	width
	x	y	z	x_p	y_p	x_t	y_t
1	35-55	140	25	15	22	19	50
2	20-48	127	20	22	25	18	50
3	20-35	142	35	11	0	21	22
4	30-45	60	30	15	10	22	20
5	30-45	55	5	25	20	20	20
6	10	50	3	15	15	8	20

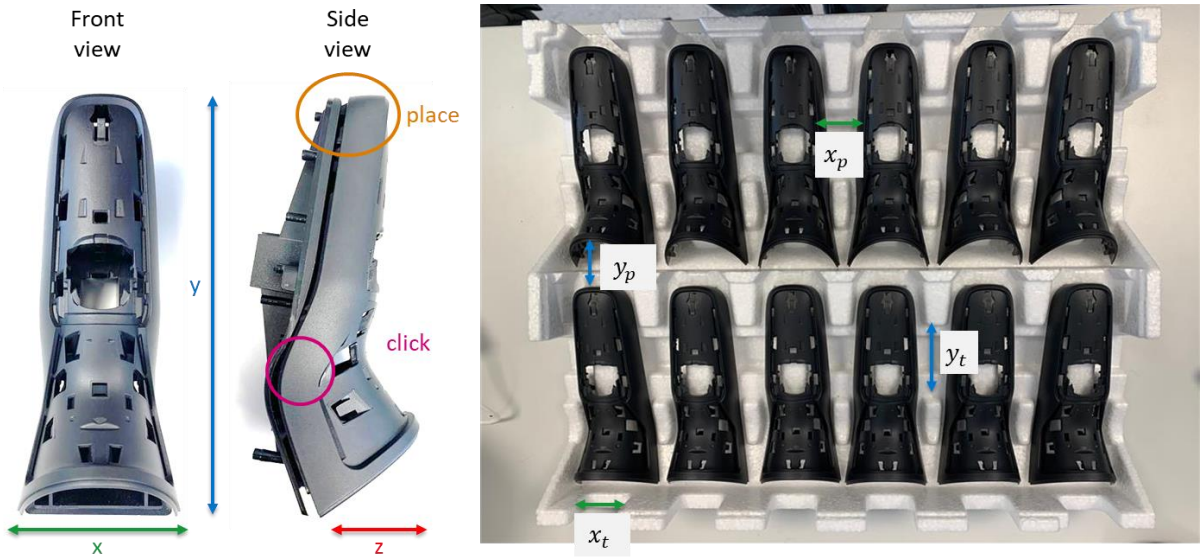

Figure 34. Dimensional legend for Table 8 depicting the length (y), width (x), height (z), distance between the neighboring objects (x_p and y_p), and the distance between the tray boundaries (x_t and y_t) of Part 1 (example)

The dimensional constraints posed by the approach clearance for the 2 grasp configurations is summarized below:

Table 9. Constraints posed by the approach clearance on the dimensions of the fingers and jaws for (a). Vertical grasp and (b). Horizontal grasp

Dimension	Vertical grasp (V)		Horizontal grasp (H)	
	Maximum	Minimum	Maximum	Minimum
Longitudinal (finger)	-	$z = 35$	-	$z = 35$
Lateral (jaw)	$x_t = 8$	-	$y_t = 20$	-
Orthogonal (finger and jaw)	$y + y_p = 152$	$y = 50$	$x + x_p = 66$	$x = 10$

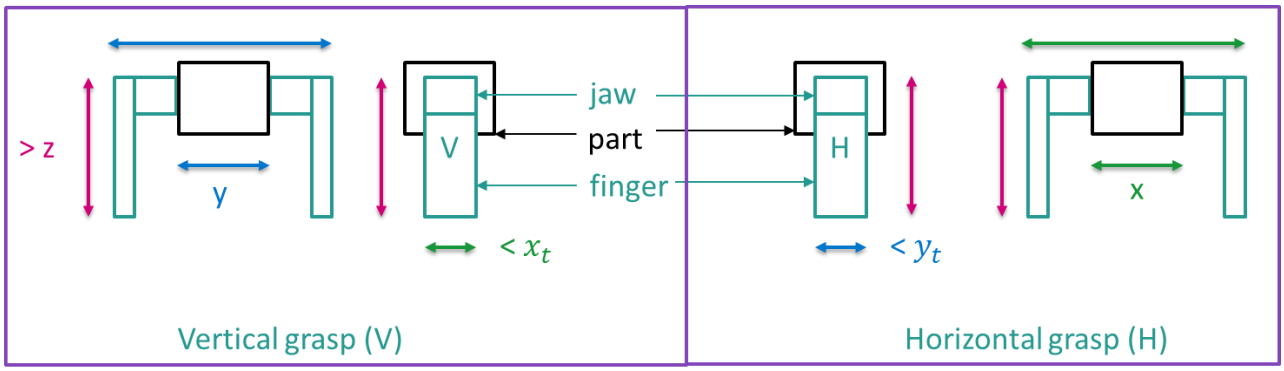

Figure 35. Constraints posed by the approach clearance on the dimensions of the fingers and jaws for (a). Vertical grasp and (b). Horizontal grasp

4.6. Flexible EOAT design

In this section, the design of the flexible EOAT is explained in terms of the following primary components of a mechanical gripper drive which achieve the required finger movement:

1. **Prime mover** converts a form of energy (source) to mechanical energy.
2. **Force convertor** to convert the mechanical energy to the required finger translation.
3. **Fingers** move to bring the jaws in contact with the object.
4. **Jaws** achieve grasping by exerting force on the object through direct contact.
5. **Collision prevention system** to avoid collision of one set of fingers when the other is in use.

The conflicting dimensional constraints on the gripper fingers and jaws for the vertical and horizontal grasp facilitate the need for 2 parallel sets of fingers and jaws for the 2 grasp configurations. Since such an EOAT - with 2 parallel sets of fingers with independent movement control for each set - was not readily available in the market (not part of the portfolio of 3 of the largest gripper manufacturers in the world: Schunk, Festo, and Gimatic) as of 16/12/2021, the 2 sets of fingers and jaws were custom designed to meet the requirements. The drive components designed/selected for each set of fingers is summarized in Table 10 and elaborated in the following sections.

Table 10. Components of the flexible EOAT for vertical and horizontal grasp configurations.

Drive components	Vertical grasp	Horizontal grasp
Prime mover	Electromechanical (Motor)	Pneumatic
Force convertor	Rack and pinion	Cylinders
Fingers	Designed in NX 12, 3D printed in PA-12 material	Designed in NX 12, 3D printed in PA-12 material; single component
Jaws	Designed in NX 12, 3D printed in Agilus30 material	
Collision prevention system	Fixed (primary fingers)	Pneumatic cylinders

4.6.1. Vertical grasp

The vertical grasp is considered as the primary configuration since it is feasible for more parts than the horizontal one and hence does not require a collision-prevention system. A force and position control electric gripper - hand-e manufactured by Robotiq (Appendix H) - was chosen as the drive system for the vertical fingers. The hand-e gripper has an electric motor driven rack and pinion mechanism for opening and closing the fingers, as seen in Figure 36. The vertical fingers were designed such that the dimensional constraints for the vertical grasp were met while being able to mount onto the racks of the hand-e gripper. The vertical fingers have the following features:

1. Base with 4 screw clearance holes to mount the fingers onto the racks of the hand-e gripper.
2. Column with an offset to align the jaws of the 2 parallel fingers.
3. Spring element to provide flexibility.
4. Jaw mounting pin for a press-fit with the slightly smaller jaw hole.

The jaw was separated from the finger to allow different materials for the finger and the jaw, so as to achieve soft-finger contact with a flexible material jaw.

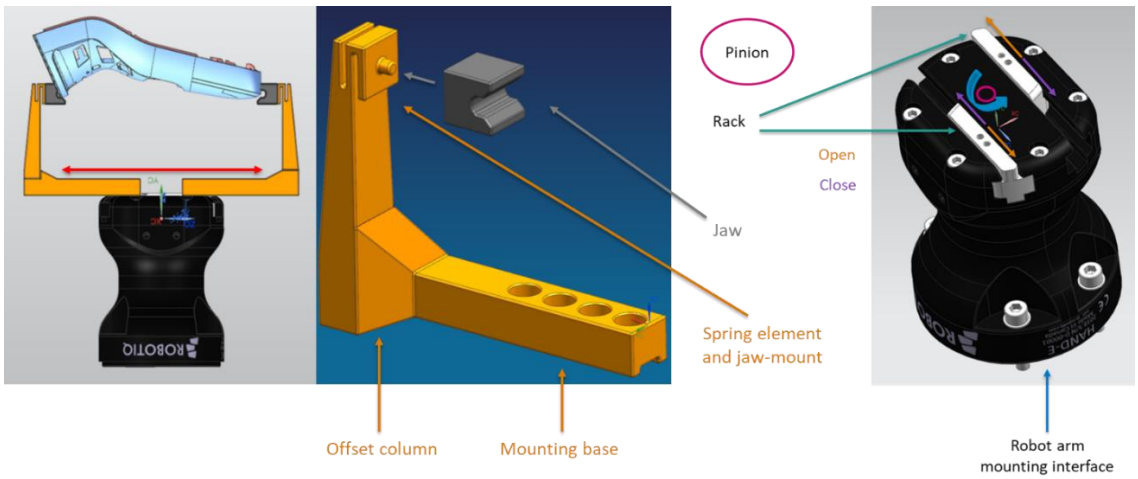

Figure 36. Schematic representation of (a) Vertical finger and jaw assembly mounted onto a Robotiq gripper (b) vertical finger features including mounting base with 4 screw-clearance holes, offset column for alignment of parallel fingers, and a spring-element at the jaw-mount (c) Rack and pinion mechanism of the Robotiq hand-e gripper with mounting holes on the racks.

4.6.2. Horizontal grasp

The horizontal grasp was the secondary configuration and hence required a collision prevention system (CPS) to avoid the collision of 1 set of fingers when the other is in use. A pneumatic mechanism was chosen for actuating both the fingers as well as the CPS. 2 sets of Festo mini slide pneumatic cylinders (Appendix I) each were used for the fingers and the CPS, providing vertical and horizontal translation, respectively, as seen in Figure 37. The CPS was mounted to the Hand-e using a mounting block, while the cylinders driving the fingers were mounted to a platform which rested on the groove of the mounting block. The cylinders were controlled using a Festo solenoid valve (Appendix J) with digital inputs from the Robot. A digital input of "high" for the CPS extends the cylinders while "low" retracts them back. A digital input of "high" for the fingers closes the fingers i.e., moves them towards each other, while "low" digital output retracts them to open the fingers i.e., moves them away from each other.

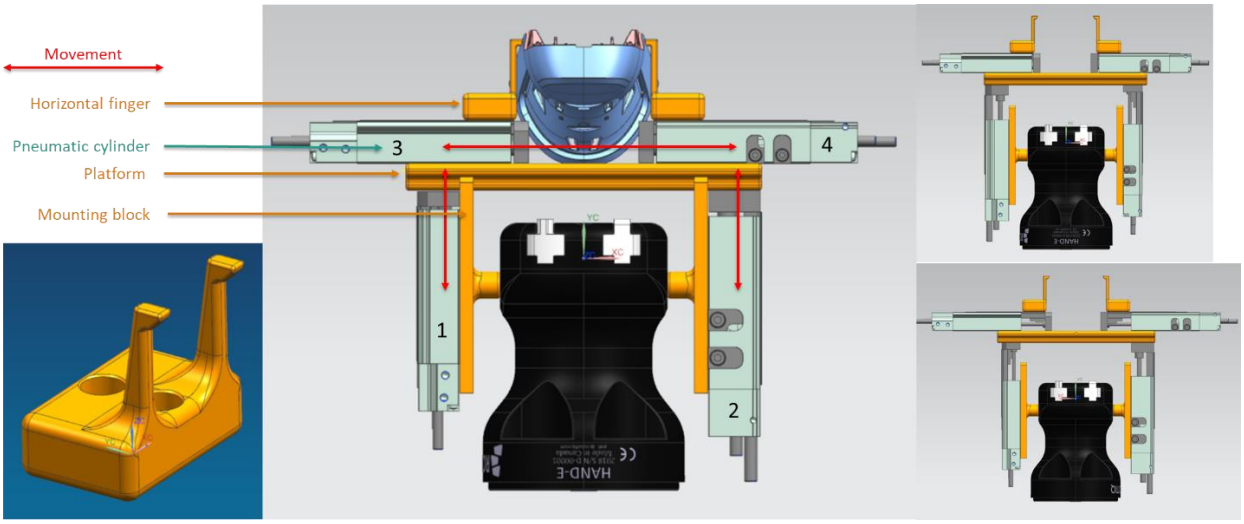

Figure 37. Schematic representation of the (a) horizontal finger (b) pneumatic mechanism for collision protection and actuation of horizontal fingers (c) extended cylinders for CPS in the top image and for the fingers in the bottom image.

The horizontal fingers were designed to meet the dimensional requirements of the horizontal grasp, with the 2 fingers each having 2 parallel jaws built-in to achieve horizontal part-alignment.

4.6.3. Integration

The vertical and horizontal fingers were integrated together to arrive at the flexible EOAT assembly, as seen in Figure 38.

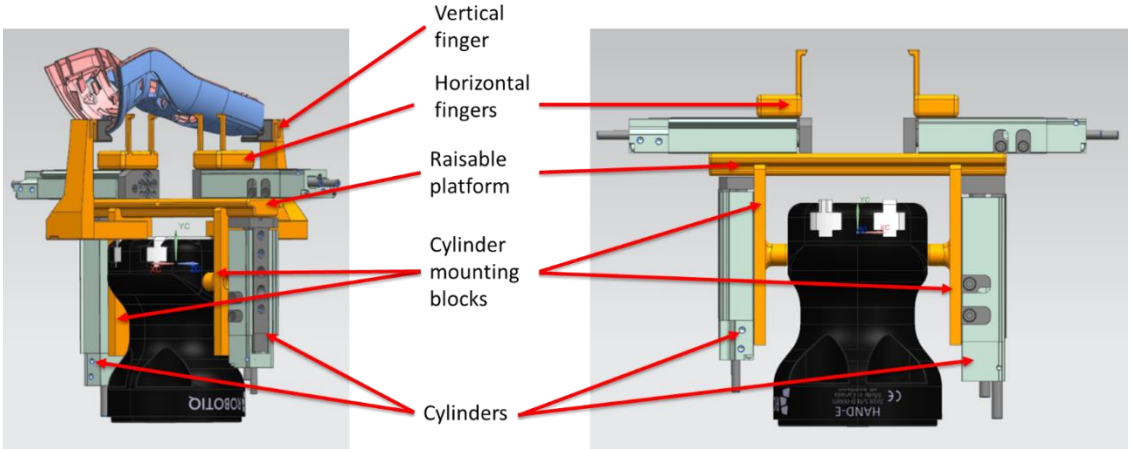

Figure 38. Flexible EOAT assembly design depicting the vertical and horizontal fingers, and their drive and mounting components.

4.6.4. Jaw profile

Based on the object parameters, approach clearance constraints, and the flexibility requirements of the gripper, a C-shaped fingertip profile was selected to facilitate the stable grasping of the parts. The jaws for the vertical fingers (vertical jaws) have chamfers corresponding to the angles of the grasping surfaces are made of a flexible material (to achieve soft finger contact) and then mounted onto the fingers.

4.6.5. Flexibility

The parameters of the gripping points affecting the flexibility of the gripper to achieve a stable grasp for all the parts are explained below:

1. Distance between the gripping points: The gripper fingers need to be opened for a minimum value of the part dimension along which the gripping points are defined, plus an allowance based on the approach clearance of the gripper. The appropriate gripper stroke (distance between open and closed gripper fingers) is determined by the difference between the maximum and minimum distances between the gripping points for all the parts. The minimum gripping stroke is calculated based on the distances seen in Table 11, as 118.8568 – 10.7986 = 108.0582 mm without allowance.
2. Angle between the gripping surfaces: The angle between the gripping surfaces needs to be matched by the angle of the gripper jaw. The maximum angle between the gripping surfaces of all the parts is 34.5^0, as seen in Table 11. The angle match is achieved by a cantilever flat spring feature in the vertical finger providing an angular compliance of about 23^0 along the axis normal to finger column.
3. Contour of the gripping surface: The contour of the surface needs to be matched with the jaw profile to maximize the contact area. This is achieved by using a flexible material with the selected fingertip profile for a stable grasp.

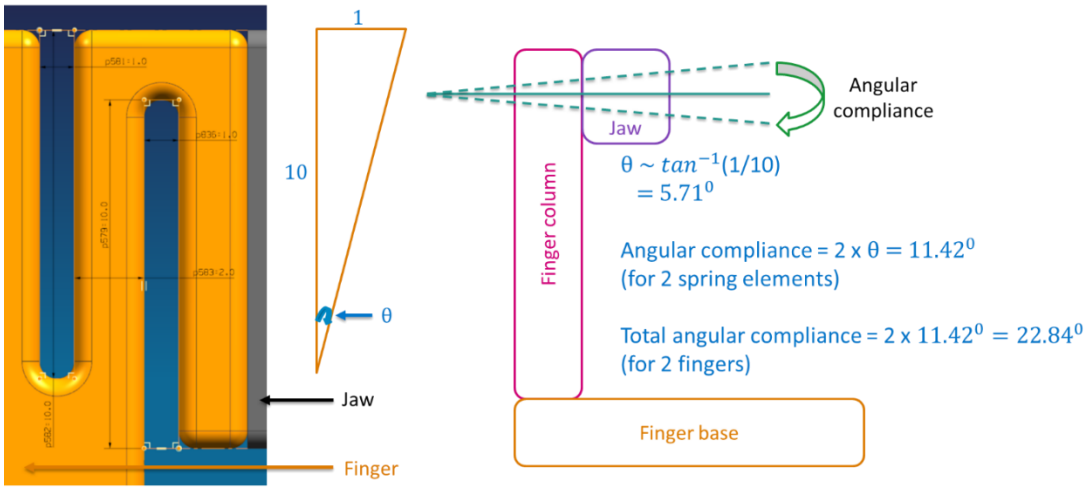

Figure 39. Pictorial representation of the angular compliance introduced by the spring element in the vertical jaw.

Table 11. Distance and angle between the gripping points defined for the 6 representative parts.

Part	Distance between gripping points (in mm)	Angle between the gripping surfaces (in degrees)
1	119	8
2	116	34
3	127	28
4	58	7
5	53	21
6	11	2

4.6.5. Prototype

The flexible EOAT was prototyped by 3D printing the vertical and horizontal fingers in the 3D printers at the Philips Drachten site, the particulars of which are seen in Table 12, and then assembling them with the Robotiq hand-e gripper.

Table 12. Specifications of the 3D printed components

Component	Material	3D Printer
Vertical finger	PA-12	HP MJF
Vertical jaw	Agilus30	Stratasys j750
Horizontal finger & jaw	PA-12	HP MJF

4.7. Validation

The artifact of the project – proof of concept of the flexible EOAT – is validated using experimental and simulative analysis of the prototype by checking for the following parameters:

Table 13. Parameters and tests for each validation function

Function	Parameter	Test
Grasp stability	Part position relative to finger	Repeatability
Grasp safety	Part damage (scratches/stains/pollution)	Cross-cut test, visual quality check
(Dis)mounting success	Place and click features	Drop during spindle rotation, conveyor movement
Part alignment	Part position relative to tray	Repeatability
Finger/jaw life	Stress, displacement, and fatigue study	Simulation
Cost and time	Check if budget > cost of [the no. of robots + EOATs required to meet Cycle time requirement (<2 seconds/part) + out of scope components]	

4.7.1. Experimental setup

The experimental setup (Figure 40) for the validation included a Universal Robots UR5 robot arm mounted on a T-slot table-top and a fixturing assembly (Appendix K) - representing the spindles in the lacquering line – to hold the jig, at the robotics lab of the innovation cluster Drachten (ICD) facility at Philips, Drachten.

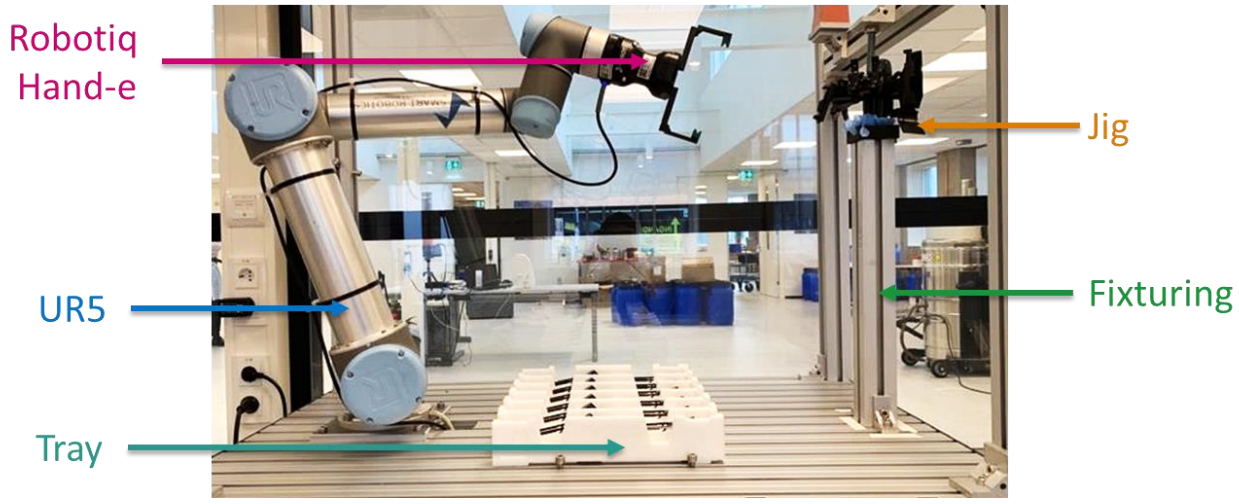

Figure 40. Experimental setup at the ICD robotics lab at Philips, Drachten.

4.7.2. Grasp stability

The stability of the grasp is the ability of the gripper to firmly hold the object to prevent changes in the object's position or orientation during the robot movements after grasping and before releasing the object. This was tested by programming a full-speed robot movement with linear and circular movements of the gripper to check the position of certain part features relative to those of the finger for each representative part before (once) and after (each) 5 repetitions of the following robot movements:

1. Translation of the EOAT: the tool was moved between 3 waypoints with the first 2 in the vertical plane and the next 2 in the horizontal plane, as seen in Figure 43 (a).
2. Rotation of the EOAT: The tool was rotated in the same waypoint through 180° rotation of the 3 wrist joints seen in Figure 43 (b).

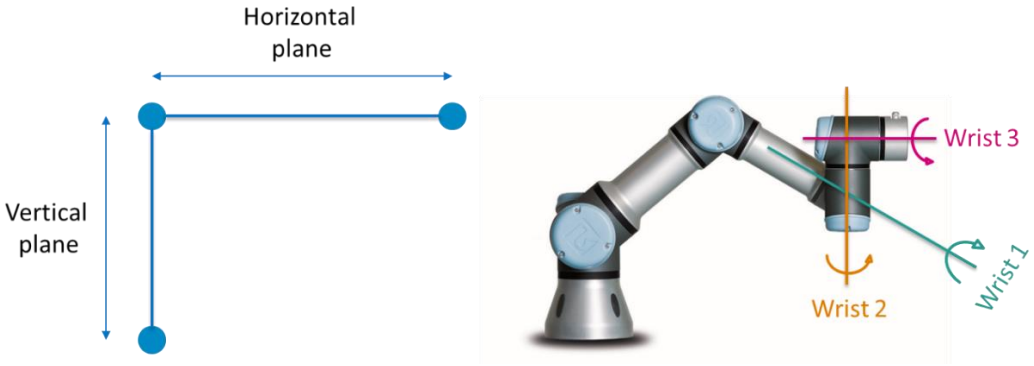

Figure 41. (a) Tool movement between 3 waypoints (b) Tool re-orientation through rotation of the 3 wrist joints

The positional changes measured by the distances between part and jig features were then compared with the positional inaccuracies allowed by the jig design (chamfers), measured by the distance between the part and jig features at extreme positions of the part (Figure 44) which still allow successful mounting of the part onto the jig. The grasp stability was considered successful if the largest value of the positional changes were less than the smallest value of the allowable positional inaccuracy.

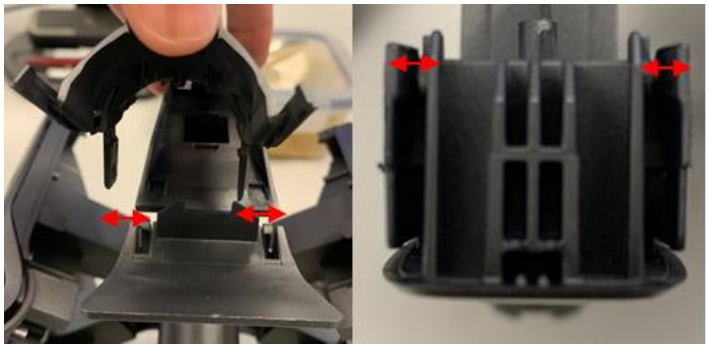

Figure 42. Pictorial representation of the allowable positional inaccuracy (API) measurement for Part 2 (example) depicting the distances measured between the part and jig features at jig chamfers.

4.7.3. Grasp safety

The safety of the grasp tests the effect of the EOAT on the quality of the lacquering process measured as:

1. Damages to the parts visible as scratches, stains, or dents caused by the force exerted by the gripper validated by a visual check by quality personnel.
2. The effect of the gripper material on the quality of lacquer adhesion validated by a cross-cut test.

Cross-cut test

The lacquering quality parameters include the consistency of the lacquer which is largely dependent on the adhesion of the lacquer to the substrate (part). In the manual (un)loading process, the operators use gloves with a moisture repellent aqua-polymer foam coating to prevent contamination (and hence improve adhesion) of the Poseidon parts (3 and 4) which are lacquered with the Ultra-deep-shine lacquer (UDSL), which is most vulnerable to contamination.

To check for the UDSL adhesion for gripper loaded parts, Philips ISO 2409 standard cross-cut test was used. The test assesses the resistance of the coating (lacquer) to substrate (part) separation by cutting a lattice structure (2 perpendicular cuts repeated 6 times) through the coating using a blade, and then using (applying and removing) a pressure-sensitive adhesive tape over the lattice structure to remove any loose paint. Additionally, the UDS lacquered part is first placed in a hot (40°) water bath for 24 hours to build up tension in the lacquered surface, to get accurate results.

4.7.4. (Dis)mounting success

The jigs with the gripper loaded parts were driven through the conveyor line to check for the mounting success. The mounting success was measured as the number of parts falling out during the rotation of the spindle or the movement of the conveyor line, with 0 being a success and a higher number indicating failure. Dismounting success was checked visually.

4.7.5. Part alignment

The horizontal jaws were used to align the parts while picking the parts from the corresponding trays to ensure grasp repeatability and hence mount repeatability. The part alignment using horizontal jaws was checked by measuring the consistency of the distance between the part features and tray features after grasping. The boundary of the aligned part was marked with a ball-point pen with the visibility of the markers indicating the success of the part-alignment. The parts were placed in extreme positions (picturized in Appendix L) - such that the part would cover some of the markers - to simulate potential inaccuracies in part positioning, and then grasped with the horizontal jaws and released.

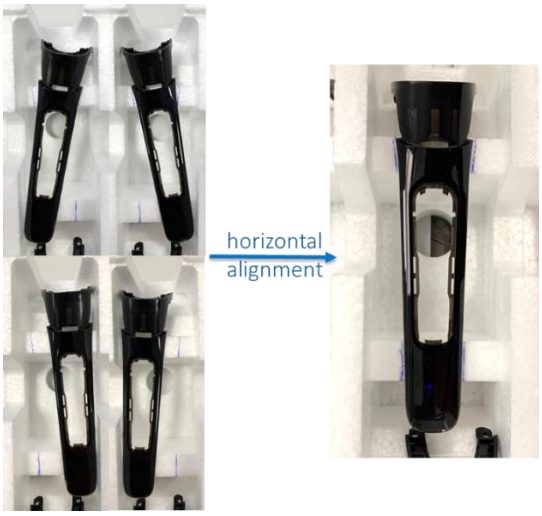

Figure 43. Pictorial representation of the part-alignment test for Part 3 depicting (a) the potential extreme positions of the part where the 4 markers are not visible and (b) the aligned part with the 4 markers visible.

4.7.6. Simulation

The vertical finger and jaw designs were simulated in SolidWorks 2019 software for stress, displacement, and fatigue failure analysis. A linear static study was performed for the stress and displacement analysis with the following parameters:

1. Material: Agilus30 and PA-12 material were assigned to the jaw and the finger, respectively.
2. Contact set for the assembly: A shrink-fit was defined for the jaw-finger attachment to simulate the press-fit.
3. Fixtures: While fixed geometry was applied to 2 of the mounting holes and the surface of the finger which rests on the rack, the other bottom surfaces which slides on the surface of the Robotiq Hand-e gripper, were defined as sliding fixtures.
4. External loads: a normal force of 55N (determined from compression spring force calibration) was applied to the surfaces of the jaw.

Figure 44. SOLIDWORKS simulation parameters for the linear static study of the vertical finger and jaw depicting the material, contact sets, fixtures, and external loads assigned to the study.

The parameters for the fatigue analysis include – apart from the ones carried over from the static study - a stress-life cycle (S-N) curve for the materials. The S-N curves of SLS-PA 12 components (Van Hooreweder et. al., 2013) and S-N curves for rubber materials (Luo, R.K. et. al., 2003) were used as an approximation for the finger and jaw materials, respectively.

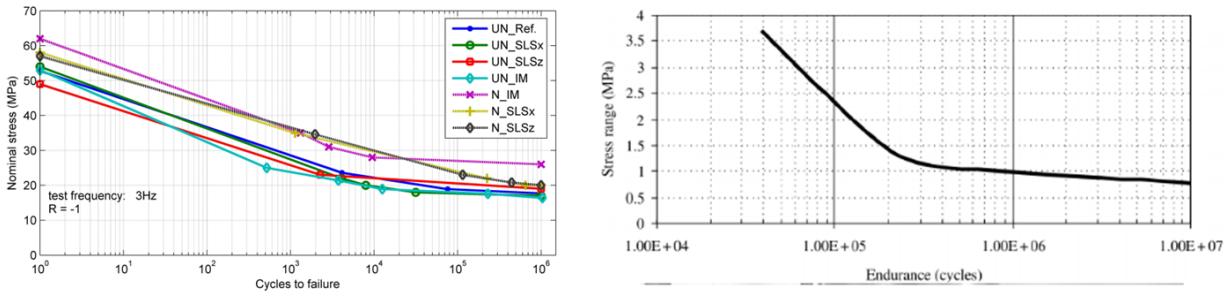

Figure 45. S-N curves for (a) PA-12 (Van Hooreweder et. al., 2013) and (b) rubber material (Luo, R.K. et. al., 2003)

4.7.7. Force calibration

The Robotiq hand-e allows force control of the fingers from 20 N to 185 N, with the force being exerted displayed in percentage values in the UR5 display. Since the force exerted on the finger jaws is lesser than the force generated, the force readings were calibrated to get the force values in N for force increments in steps of 5%. The gripper fingers (and hence the jaws) were closed with a calibrated compression spring in between the fingers, as seen in Figure 48. The displacement of the spring for every 5% force increase was measured using digital calipers. The tests were repeated for 2 Tevema D12680 compression springs (Appendix M) with 5 readings each to minimize reading errors. The average of the 5 readings for the 2 springs for 100% force exertion was then considered as the maximum force at the jaws and was used for the simulation study. The force calibration was also used to define the force applied for grasping each part, in its robot program.

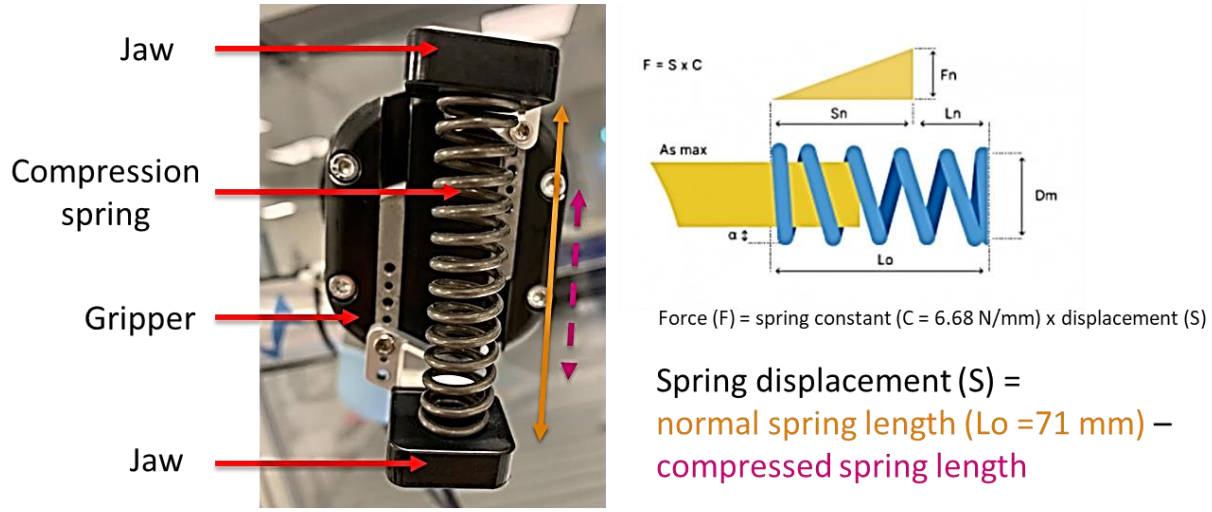

Figure 46. Pictorial representation of the Robotiq hand-e gripper force calibration using Tevema D12680 compression spring with a spring rate of 6.68N/mm.

4.7.9. Cost and time

Due to the interdependency of the financial and temporal constraints, the number of robots (with a flexible EOAT each) required to meet the cycle time (CT) requirements were first calculated. The expenses for these components were then compared to the project budget as well as the cost of a part-specific gripper and robot setup to meet the CT requirements. The costs were estimated using the CAPEX estimate tool available at Philips (generated by experts). The net present value (NPV) for the flexible EOAT was then compared against the part-specific EOAT and the manual loading costs to estimate the returns on the investment (ROI). The CAPEX estimate break-down is given in Appendix N.

5. Results

5.1. Grasp stability

The grasp stability was measured as the difference between the allowable positional inaccuracy and the total positional variance. The grasp stability was considered successful i.e., the grasp was stable enough to get repeatable (dis)mounting of the parts since the grasp stability values were significantly greater than the repeatability of the robot arm (0.06 mm for the UR5).

Table 14. Grasp stability (API – TPV) for each part

Part	Allowable positional inaccuracy (API)	Total positional variance (TPV)	Grasp stability (API – TPV)
1	2,80	0,26	2,54
2	2,56	0,30	2,26
3	1,26	0,21	1,05
4	1,25	0,13	1,12
5	0,97	0,19	0,78
6	0,65	0,29	0,36

Allowable positional inaccuracy (API)

The chamfer dimensions of the jig click and place features compensating for the positional inaccuracies of the part were measured (Appendix O) for each representative part, as listed in Table 14.

Table 15. Allowable positional inaccuracy (API) for the 6 parts

Part	Allowable inaccuracy on each side left/right (+/-)		API =
	Position (in mm)	Orientation (in mm)	**min (position, orientation)**
1	2.80	6.07	2.80
2	2.56	7.36	2.56
3	1.26	1.27	1.26
4	1.25	1.60	1.25
5	0.97	3.95	0.97
6	0.65	0.65	0.65

Positional variation (PV)

The positional variation was calculated as the difference of the **maximum** and the **minimum** values of the average (of the 5 readings) variation measured. The PV readings for each part is given in Appendix P.

5.2. Visual check

The results of the visual check performed for the part-damage (scratches/stains/dents) tests for both loading (pre-lacquer) and unloading (post-lacquer) and the (dis)mounting success are summarized in Table 16:

Table 16. Visual check results showing the number of samples checked for each part and the number of parts that successfully prevented part damage (pre-and post- lacquer), mounted on the jig, and dismounted from the jig.

Part	Sample size	Part-damage prevention		Mounting success	Dismounting success
		Pre-lacquer	Post-lacquer		
1	6	6	6	6	6
2	6	6	6	6	6
3	6	6	6	6	6
4	6	6	6	6	6
5	6	6	6	6	6
6	12	12	12	12	12

1 spindle size (6 each for parts 1 to 5; 12 for part 6) of parts were loaded using the flexible EOAT and then checked for scratches/stains/dents. All the samples were accepted by quality personnel and hence, pre-lacquer part damage prevention was considered successful. They were then processed in the lacquering line, following which the number of parts remaining on the jig were counted and since all the samples were found on the jigs, mounting was considered successful. The parts were then unloaded from the jigs and placed on the tray. Since all the parts were placed on the tray, dismounting was also considered successful. The parts were then checked by the quality personnel and all the parts were accepted and hence, post-lacquer part damage was considered successful.

5.3. Cross-cut test

12 samples each of Parts 3 and 4 were loaded with the flexible EOAT before lacquering with UDS lacquer for the cross-cut test. Since no loose paint was observed on the tape used on the cuts, the adhesion resistance was considered to be not affected by the jaw material.

5.4. Part alignment

The part alignment test was conducted for parts 1 to 5 since the tray design already aligns part 6 sufficiently. Both the variants of Part 4 – Poseidon and Atlas – were tested since the tray designs differ for the 2 variants. The number of markers before and after alignment is seen in Table 17, with multiple readings indicating multiple extreme positions, and the alignment considered successful if the number of markers visible after alignment matches the total number of markers. It was found that part alignment for Part 4 Poseidon was not feasible due to the tray design with the horizontal jaws not being able to reach the part when placed in the extreme positions. All the other parts were successfully aligned.

Table 17. Part-alignment results measured as a success if all the markers are visible after alignment.

Part	Total markers	**No. of markers visible**		**Alignment success**
		Before alignment	After alignment	
1	4	2	4	Yes
	4	2	4	Yes
	4	2	4	Yes
	4	2	4	Yes
2	4	2	4	Yes
	4	2	4	Yes
	4	2	4	Yes
	4	2	4	Yes
3	4	2	4	Yes
	4	2	4	Yes
	4	1	4	Yes
	4	1	4	Yes
4 (Poseidon)	2	1	1	Error
	2	1	1	
4 (Atlas)	2	1	2	Yes
	2	1	2	Yes
5	2	1	2	Yes
	2	1	2	Yes

5.5. Simulation study

5.5.1. Force calibration

The results of the compression spring displacement test to calibrate the force exerted by the Robotiq hand-e at the finger jaws are displayed in Table 18, showing the force values (in N) at 5% (UR5 display) increments. The maximum value of force of 110N was input as the load at the vertical finger jaw for the simulation study.

Table 18. Force calibration results: Force (in N) for every 5% increase in Force% displayed in the UR5

force (%) displayed in UR	F_avg
0	0
5	29
10	37
15	45
20	52
25	58
30	64
35	66
40	72
45	79
50	81
55	84
60	87
65	93
70	95
75	97
80	101
85	105
90	108
95	109
100	110

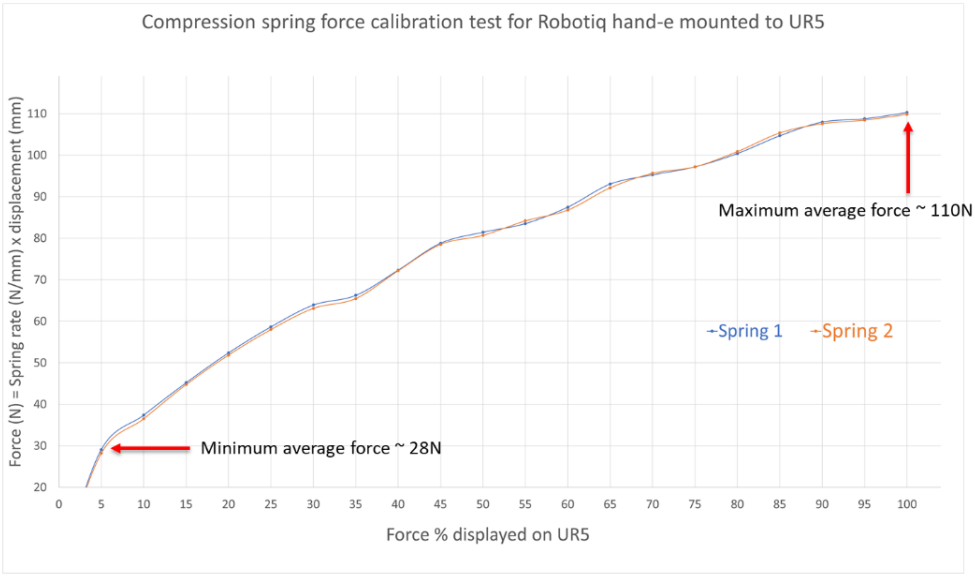

Figure 47. Force calibration test graph depicting the relationship between the force % displayed on the UR5 and the actual force exerted by the fingers.

5.5.2. Stress and displacement analysis

The von Mises stress results indicate maximum stress induced in the fingers at the spring elements with a value of 38 MPa, which is lower than the yield strength (53 MPa) of the finger material (PA-12). The other vulnerable points of the design include the points at which the finger column is attached to the base and parts of the column due to the nature of the load applied, fixtures, and the design of the fingers.

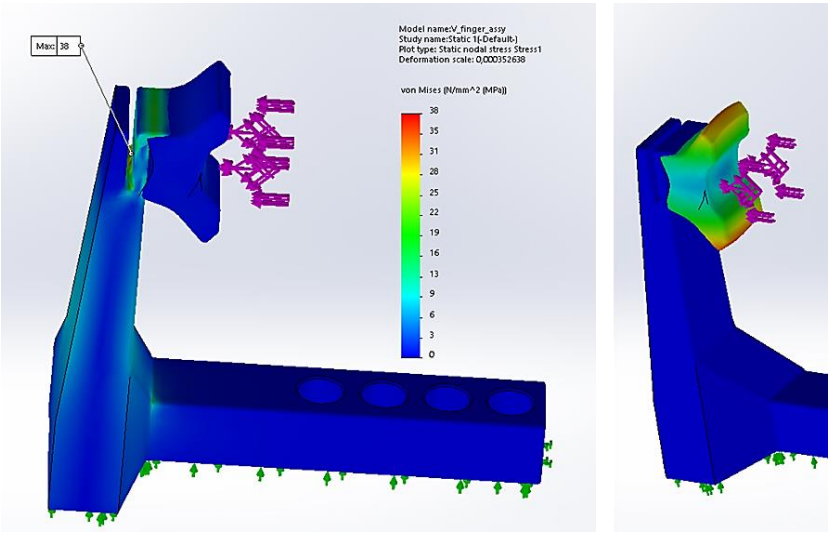

Figure 48. SolidWorks simulation results depicting (a) von Mises stress and (b) static displacement

The displacement plot shows the nature of displacement of the jaws at maximum force, which meets the requirement of contact area maximization during grasping for stable grasp.

5.5.3. Fatigue failure analysis

The fatigue-life plot shows the least life of the assembly at a jaw location at 100k cycles. Although the value is an approximation due to the material properties assigned being of a similar material, it serves as a good reference point for the number of cycles for the repeatability test. The fatigue-damage plots show maximum damage occurring at the valley of the C-shape jaw profile due to the repetitive stressing and displacement of the jaw during contact.

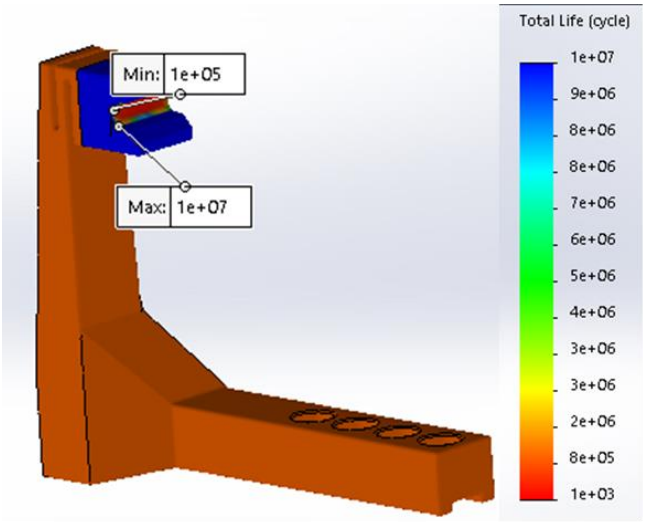

Figure 49. Fatigue plots showing the fatigue (a)life and (b)damage of the finger-jaw assembly locations.

The least life of 1e5 (100k) cycles is seen at the jaw, indicating that the jaw needs to be replaced after grasping every 100k parts, if the maximum force is used. Since the force used for the parts averages at about 50% (81 N), the fatigue life can be estimated to be about twice the simulated result i.e., 200k parts. Similarly, the finger has a life of about 3e6 (3M) cycles which can be estimated to be about 6M parts before it needs replacement. The material and printing costs for the replacements needed per year are also considered in the NPV calculations.

5.6. Cost and time

The average cycle time for loading and unloading using the flexible EOAT with the UR5 parameters listed in Table 19, was determined to be 8.35 seconds per part. To meet the cycle-time requirements of 2 seconds per part a minimum of 5 robot arms with flexible EOATs are required. The estimated capital expenditure (CAPEX) for the flexible EOAT compared with that of a complex (capable of pick and place + (dis)assembly), part-specific gripper is given in Table 20. To account for the change-over time for a part-specific EOAT, 2 additional robot arms (7 in total) are considered with 8 EOATs per robot (for the 8 parts).

Table 19. Robot arm parameters of speed and acceleration of the joint for MovJ and tool for MovL

Movement mode	Speed	Acceleration
MovJ (joint parameters)	180 °/s	2292 °/s²
MovL (tool parameters)	3000 mm/s	150000 mm/s²

Table 20. CAPEX estimate of the automation components for a flexible EOAT compared to that of part-specific EOAT

Parameter	For part-specific EOAT	For flexible EOAT
Individual EOAT cost (in k€)	17	7
Number of robots required to meet cycle time requirement (max. 2 seconds per part)	7	5
Number of EOATS required to meet CT requirement	56 = 8x7 (1/part x 1/robot)	5 =1x5 (1/robot)
No. of tool change systems	7 (1/robot)	0
CAPEX estimate of total automated setup (in k€) (Robots + EOATs + tool and jig handling + engg.)	1500	900

Net Present value (NPV)

The NPV was calculated (graphed in Figure 58) using the Philips tool and was assessed by the Problem Owner, Eric Sloot, and the cost engineer, Oeds van der Wijk. The CAPEX estimate (€900k) as well as the payback period (1.75 years) meet the financial requirements (budget = €1200k, payback period < 2 years).

Table 21. Net Present Value particulars for the 3 alternatives.

Alternatives	Payback period (in years)	ROI	Cumulative NPV (in k€)	CAPEX (in k€)
Manual (un)loading	Ref.			
Part-specific EOAT	3	1.58	865	1500
Flexible EOAT	1.75	2.62	1461	900

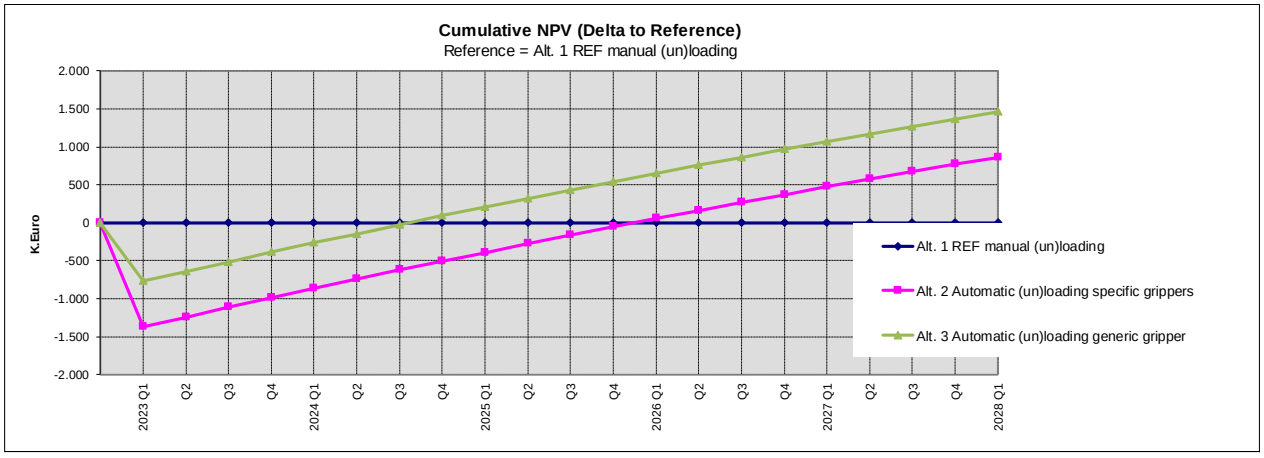

Figure 50. Cumulative NPV for the period 2023 Q1 until 2028 Q1 with the manual (un)loading as reference.

6. Conclusion

A flexible – capable of handling 8 part-families - EOAT was designed for the loading and unloading processes of the lacquering line at Philips, Drachten. The design was achieved through a framework of gripper selection, grasp synthesis and analysis, and prehension strategy, formulated through literature review. The design was prototyped using 3D printers at Philips, Drachten, and was validated against the functional requirements (defined through part and process study, and stakeholder analysis). The validation is summarized in Table 22. The part-alignment and EOAT life requirements were not completely validated due to the tray-design of Part 5 (Poseidon) and assumptions made for the vertical jaw material, respectively. The potential solutions to these issues are discussed in the following section.

Table 22. Validation of the flexible EOAT design against the functional requirements, along with the tests used for validation and their results.

Requirement			Test	Result	Validation
Quality	Process repeatability	Grasp stability	Grasped part position before and after robot movement at max speed	TPV<<API	Success
		Part alignment	Visibility of marker on the tray before (extreme inaccurate part positions) and after alignment	Fingers unable to reach Part 5 (Poseidon variant)	Success (all except Part 5)
		Mounting success	Number of parts on the jig before and after spindle rotation during lacquering	Successful (dis)mounting	Success
		Dismounting success	Number of parts on the tray relative to the number of parts on the jig		Success
		EOAT life	FEM analysis to check for stress, displacement and fatigue life of vertical finger and jaw for maximum load (55N)	Max. stress < Material strength; 50k load cycles	Success (with assumptions)
	Part Safety	Scratch/stain /dent prevention	Visual check by quality personnel for loaded and unloaded parts	All samples accepted	Success
		Lacquer adhesion	Cross-cut test (Philips ISO 2409) adhesive resistance to blade cut	No loose paint -> good adhesive resistance	Success
Time	Cycle time = 2 seconds / part		Avg. loading and unloading cycle time	8.35 seconds / part	Success (CAPEX< budget, payback period < required)
Cost	Budget = €1.2M (< 2 years payback time)		Estimated CAPEX	€900k	
			Payback period	1.75 years	
			Estimated ROI	2.62	
			Estimated cumulative NPV (scope: 5 years)	€1461k	

Limitations and future work

The limitations of the flexible EOAT design and potential solutions to reduce (or eliminate) them are:

1. Flexibility: the range of parts the EOAT can handle is limited by
    a. Part design: the dimensions of the lacquering parts need to satisfy the distance and angle limitations of the gripping point to achieve a stale grasp with the same EOAT design.
    b. Jig design: the chamfers provided on the jig should ensure a larger allowable positional inaccuracy (API) than the total positional variation (TPV) of the part when grasped by the EOAT. The ease of automated (dis)mounting of parts on/from the jig should be included as a parameter for future jig designs.
    c. Tray design: The tray dimensions should allow the same (if not larger) approach clearance for collision-free flexible EOAT (un)loading. The current design of Poseidon chest does not allow part-alignment for certain part positions in the tray, which can be solved by redesigning the Poseidon chest tray, or by using the Atlas chest tray for the Poseidon chest. Future tray designs should consider the reachability of the EOAT as well as the positional accuracy of the part within the tray.
    d. EOAT stroke: The range of movement of the fingers is currently limited to 50mm due to the choice of the gripper, which requires the finger mounting positions to be changed when switching between a shorter part family (4, 5, 6) and a longer part family (1, 2, 3). This can be solved by increasing the rack length to get a larger stroke.
2. Finger and jaw material: The life of the EOAT is limited by the material properties of the fingers and jaws. The fatigue simulation was performed with assumptions made on the jaw material due to the non-availability of S-N curves for the Agilus30 material. While the assumed material is similar to Agilus30 and the fatigue analysis serves as a good estimate, extensive tests are required to get accurate results. The materials themselves were chosen based on availability, which facilitates the need for further material tests.
3. Lack of position and force control of horizontal grasp: One of the ways to get around the constraints posed by the part, tray, and jig designs, is to control the position and force of the horizontal finger movement, which is not possible with the current solenoid valve used to control the pneumatic cylinders. The addition of a control system for the actuation of horizontal fingers needs consideration.
4. Jig and tray positioning accuracy: The repeatability of the automated (un)loading process is dependent on the repeatability of the tray and jig positioning (outside the scope of this project). Tray and jig handling which allow the positioning of the tray and jig, within the required positional accuracy for successful (dis)mounting needs to be researched.

7. Bibliography

Amend, J.R., Brown, E., Rodenberg, N., Jaeger, H.M. and Lipson, H., 2012. A positive pressure universal gripper based on the jamming of granular material. *IEEE transactions on robotics*, *28*(2), pp.341-350.

Annamalai, N., Kamaruddin, S., Abdul Azid, I. and Yeoh, T.S., 2013. Importance of problem statement in solving industry problems. In *Applied Mechanics and Materials* (Vol. 421, pp. 857-863). Trans Tech Publications Ltd.

Arai, F., Chaillet, N. and Martel, S., 2021. *Technical Committee on Micro/Nano Robotics and Automation*. [online] Rastc-mnra.in2p3.fr. Available at: <http://rastc-mnra.in2p3.fr/imagesTC/capillarygripper.png> [Accessed 17 November 2021].

Babin, V. and Gosselin, C., 2021. Mechanisms for Robotic Grasping and Manipulation. *Annual Review of Control, Robotics, and Autonomous Systems*, *4*, pp.573-593.

Bajd, T., Mihelj, M., Lenarčič, J., Stanovnik, A. and Munih, M., 2010. *Robotics* (Vol. 43). Springer Science & Business Media.

Birglen, L. and Schlicht, T., 2018. A statistical review of industrial robotic grippers. *Robotics and Computer-Integrated Manufacturing*, *49*, pp.88-97.

Blunck, E. and Werthmann, H., 2017, October. Industry 4.0–an opportunity to realize sustainable manufacturing and its potential for a circular economy. In *DIEM: Dubrovnik International Economic Meeting* (Vol. 3, No. 1, pp. 644-666). Sveučilište u Dubrovniku.

Boubekri, N. and Chakraborty, P., 2002. Robotic grasping: gripper designs, control methods and grasp configurations–a review of research. *Integrated Manufacturing Systems*.

Bouchard, S., 2018. Lean Robotics: A guide to making robots work in your Factory. Samuel Bouchard.

Bukoschek, R.L., US Philips Corp, 1993. *Electric shaver*. U.S. Patent 5,207,731.

Causey, G.C. and Quinn, R.D., 1998, May. Gripper design guidelines for modular manufacturing. In *Proceedings. 1998 IEEE International Conference on Robotics and Automation (Cat. No. 98CH36146)* (Vol. 2, pp. 1453-1458). IEEE.

Chandrasekaran, B., 1990. Design problem solving: A task analysis. *AI magazine*, *11*(4), pp.59-59.

Chaudhari, N. and Shinde, V.B., 2014. Recent trends in robotic end of arm tooling (gripper). *International Journal of Mechanical Engineering and Robotics Research*, *3*(2), p.171.

Custodio, L. and Machado, R., 2020. Flexible automated warehouse: a literature review and an innovative framework. *The International Journal of Advanced Manufacturing Technology*, *106*(1), pp.533-558.

Dalenogare, L.S., Benitez, G.B., Ayala, N.F. and Frank, A.G., 2018. The expected contribution of Industry 4.0 technologies for industrial performance. *International Journal of Production Economics*, *204*, pp.383-394.

Datta, R. and Deb, K., 2011, July. Multi-objective design and analysis of robot gripper configurations using an evolutionary-classical approach. In *Proceedings of the 13th annual conference on Genetic and evolutionary computation* (pp. 1843-1850).

Doltsinis, S., Krestenitis, M. and Doulgeri, Z., 2019. A machine learning framework for real-time identification of successful snap-fit assemblies. *IEEE Transactions on Automation Science and Engineering*, *17*(1), pp.513-523.

Dym, C.L., 2004. Design, systems, and engineering education. *International Journal of Engineering Education*, *20*(3), pp.305-312.

Fantoni, G., Capiferri, S. and Tilli, J., 2014. Method for supporting the selection of robot grippers. Procedia CIRP, 21, pp.330-335.

Fantoni, G., Santochi, M., Dini, G., Tracht, K., Scholz-Reiter, B., Fleischer, J., Lien, T.K., Seliger, G., Reinhart, G., Franke, J. and Hansen, H.N., 2014. Grasping devices and methods in automated production processes. *CIRP Annals*, *63*(2), pp.679-701.

Farahhanis, 2017. *The fourth industrial revolution*. [online] farahhanis. Available at: <https://farahhhanis702.wordpress.com/> [Accessed 18 October 2021].

Feldmann, K., Trautner, S. and Meedt, O., 1998. Innovative disassembly strategies based on flexible partial destructive tools. *IFAC Proceedings Volumes*, *31*(7), pp.1-6.

Frank, A.G., Dalenogare, L.S. and Ayala, N.F., 2019. Industry 4.0 technologies: Implementation patterns in manufacturing companies. *International Journal of Production Economics*, *210*, pp.15-26.

Honarpardaz, M., Tarkian, M., Ölvander, J. and Feng, X., 2017. Finger design automation for industrial robot grippers: A review. *Robotics and Autonomous Systems*, *87*, pp.104-119.

Jonassen, D.H., 2010. Learning to solve problems: A handbook for designing problem-solving learning environments. Routledge.

Lancioni, R.A., 2005. A strategic approach to industrial product pricing: The pricing plan. *Industrial marketing management*, *34*(2), pp.177-183.

Landuré, J., Gosselin, C., Laliberté, T. and Abdallah, M., 2021. Analysis and synthesis of assistive tools for insertion tasks. *Proceedings of the Institution of Mechanical Engineers, Part B: Journal of Engineering Manufacture*, p.09544054211019655.

LaSalata, J., 2021. *Philips Announces New Range Of 'Star Wars' Shavers*. [image] Available at: <https://www.jedinews.com/misc/articles/philips-announces-new-range-star-wars-shavers/> [Accessed 9 August 2021].

Lenders, C., Valsamis, J.B., Desaedeleer, M., Delchambre, A. and Lambert, P., 2008, February. Assembly of a micro ball-bearing using a capillary gripper and a microcomponent feeder. In *International Precision Assembly Seminar* (pp. 265-274). Springer, Boston, MA.

Löfving, M., Almström, P., Jarebrant, C., Wadman, B. and Widfeldt, M., 2018. Evaluation of flexible automation for small batch production. *Procedia Manufacturing*, *25*, pp.177-184.

Luo, R.K., Cook, P.W., Wu, W.X. and Mortel, W.J., 2003. Fatigue design of rubber springs used in rail vehicle suspensions. *Proceedings of the Institution of Mechanical Engineers, Part F: Journal of Rail and Rapid Transit*, *217*(3), pp.237-240.

Malvezzi, M., Gioioso, G., Salvietti, G. and Prattichizzo, D., 2015. Syngrasp: A matlab toolbox for underactuated and compliant hands. *IEEE Robotics & Automation Magazine*, *22*(4), pp.52-68.

Melnyk, L.H., Kubatko, O.V., Dehtyarova, I.B., Dehtiarova, I.B., Matsenko, O.M. and Rozhko, O.D., 2019. The effect of industrial revolutions on the transformation of social and economic systems.

Michalakoudis, I., Childs, P.R., Aurisicchio, M., Pollpeter, N. and Sambell, N., 2014, November. Using functional analysis diagrams as a design tool. In *ASME International Mechanical Engineering Congress and Exposition* (Vol. 46606, p. V011T14A011). American Society of Mechanical Engineers.

Monkman, G.J., Hesse, S., Steinmann, R. and Schunk, H., 2007. Introduction to prehension technology. *Robot grippers*, pp.1-18.

Mostow, J., 1985. Toward better models of the design process. *AI magazine*, *6*(1), pp.44-44.

NC state, 2019. *Thermal actuated Kirigami gripper*. [online] Youtube.com. Available at: <https://www.youtube.com/watch?v=4U2ARa83188> [Accessed 17 November 2021].

Nguyen, V.D., 1987, March. Constructing force-closure grasps in 3D. In *Proceedings. 1987 IEEE International Conference on Robotics and Automation* (Vol. 4, pp. 240-245). IEEE.

OECD (2021), Unit labour costs (indicator). doi: 10.1787/37d9d925-en (Accessed on 10 September 2021)

Omega, 2021. *Pneumatic gripper*. [online] Omega.nl. Available at: <https://www.omega.nl/prodinfo/grippers.html> [Accessed 17 November 2021].

OnRobot. 2021. *Magnetic Gripper for Collaborative Applications*. [online] Available at: <https://onrobot.com/en/products/mg10> [Accessed 17 November 2021].

Oztemel, E. and Tekez, E.K., 2009. A general framework of a reference model for intelligent integrated manufacturing systems (REMIMS). *Engineering Applications of Artificial Intelligence*, *22*(6), pp.855-864.

Parthasarthy, R. and Sethi, S.P., 1992. The impact of flexible automation on business strategy and organizational structure. *Academy of Management review*, *17*(1), pp.86-111.

Pedrazzoli, P., Rinaldi, R. and Boer, C.R., 2001, May. A rule based approach to the gripper selection issue for the assembly process. In *Proceedings of the 2001 IEEE International Symposium on Assembly and Task Planning (ISATP2001). Assembly and Disassembly in the Twenty-first Century.(Cat. No. 01TH8560)* (pp. 202-207). IEEE.

Pham, D.T. and Yeo, S.H., 1988. A knowledge-based system for robot gripper selection: criteria for choosing grippers and surfaces for gripping. *International Journal of Machine Tools and Manufacture*, *28*(4), pp.301-313.

Pham, D.T. and Yeo, S.H., 1991. Strategies for gripper design and selection in robotic assembly. *The International Journal of Production Research*, *29*(2), pp.303-316.

Philips, 2021. *Manufacturing Systems & Industry 4.0 | Philips Engineering Solutions*. [online] Philips Engineering Solutions. Available at: <https://www.engineeringsolutions.philips.com/looking-expertise/manufacturing-systems-industry-40/> [Accessed 10 September 2021].

Popkova, E.G., Ragulina, Y.V. and Bogoviz, A.V. eds., 2019. *Industry 4.0: Industrial revolution of the 21st century* (p. 253). Springer.

Pugh, S., 1990. Engineering design—unscrambling the research issues. *Journal of Engineering Design*, *1*(1), pp.65-72.

Reddy, P.V.P. and Suresh, V.V.N.S., 2013. A review on importance of universal gripper in industrial robot applications. *Int. J. Mech. Eng. Robot. Res*, *2*(2), pp.255-264.

Robotiq. 2021. *Vacuum Grippers - Robotiq*. [online] Available at: <https://robotiq.com/products/vacuum-grippers> [Accessed 17 November 2021].

Schmalz.com. 2021. *Needle Grippers SNG-DL > Special Grippers | Schmalz*. [online] Available at: <https://www.schmalz.com/en/vacuum-technology-for-automation/vacuum-components/special-grippers/needle-grippers/needle-grippers-sng-dl-306154/> [Accessed 17 November 2021].

Schumacher, P. and Jouaneh, M., 2013. A system for automated disassembly of snap-fit covers. *The International Journal of Advanced Manufacturing Technology*, *69*(9-12), pp.2055-2069.

Shimoga, K.B., 1996. Robot grasp synthesis algorithms: A survey. *The International Journal of Robotics Research*, *15*(3), pp.230-266.

Solidworks.com. 2021. *Fatigue Plots - 2021 - SOLIDWORKS Help*. [online] Available at: <https://help.solidworks.com/2021/english/SolidWorks/cworks/c_Fatigue_Plots.htm?id=ac0a5efef9114145be36d79f4ef7499a#Pg0> [Accessed 7 December 2021].

Tameson.com. 2021. *Parallel Double Acting Pneumatic Gripper Standard Jaws*. [online] Available at: <https://tameson.com/317620-medium_default/mchc-20-20-mm-2-jaw-parallel-double-acting-gripper-standard-jaws.jpg> [Accessed 17 November 2021].

Tech & Lifestyle, 2021. *Philips Aquatouch AT620 /AT610 Shaver - Disassembly*. [online] Youtube.com. Available at: <https://www.youtube.com/watch?v=CT-65YDfshk> [Accessed 6 August 2021].

Trading economics, 2021. *Labour Costs Index | 2011-2021 Data*. [online] Tradingeconomics.com. Available at: <https://tradingeconomics.com/china/labour-costs> [Accessed 10 September 2021].

Universal robots UR5e. [image] Available at: <https://www.universal-robots.com/img/animations/ur5e.mp4> [Accessed 9 August 2021].

Van Boeijen, A., Daalhuizen, J. and Zijlstra, J., 2020. *Delft Design Guide: Perspectives, Models, Approaches, Methods*. BIS Publishers.

Van Hooreweder, B., Moens, D., Boonen, R., Kruth, J.P. and Sas, P., 2013. On the difference in material structure and fatigue properties of nylon specimens produced by injection molding and selective laser sintering. *Polymer Testing*, *32*(5), pp.972-981.

Velasco, V.B. and Newman, W.S., 1998, May. Computer-assisted gripper and fixture customization using rapid-prototyping technology. In *Proceedings. 1998 IEEE International Conference on Robotics and Automation (Cat. No. 98CH36146)* (Vol. 4, pp. 3658-3664). IEEE.

Wieringa, R.J., 2014. Design science methodology for information systems and software engineering. Springer.

Zol Bahri, R., Mohammad Haniff, O. and Mohd Hisam, D., 2016. Optimum Design of Multi-Function Robot Arm Gripper for Varying Shape Green Product. MATEC Web Conf. 78 01006

8. Appendices

Appendix A: PA-12 material datasheet

Table 23. PA-12 MJF printing properties and material datasheet (GetDocument.aspx (hp.com))

Standard lead time	5 working days (online & offline orders)
Standard accuracy	±0.3% (with lower limit on ±0.3 mm)
Layer thickness	0.08 mm
Minimum wall thickness	1 mm, but living hinges are possible at 0.5 mm
Minimum detail	0.25 mm
Minimum clearance	0.4 mm between parts that need to be assembled 0.5 mm between shells of an interlocking part
Maximum part dimensions	256 x 340 x 360 mm
Interlocking or enclosed parts?	Yes
Surface structure	Unfinished parts typically have a smooth surface, without visible layers, and a stone-grey color. Multi Jet Fusion parts can be sandblasted and colored/impregnated.

Datasheet

MEASUREMENT	VALUE	STANDARD
Density of parts	1.01 g/cm^3	ASTM D792
Tensile Strength, Max Load - XY	48 MPa/6960 psi	ASTM D638
Tensile Strength, Max Load - Z	48 MPa/6960 psi	ASTM D638
Tensile Modulus[4] - XY	1700 MPa/245 ksi	ASTM D638
Tensile Modulus[4] - Z	1800 MPa/260 ksi	ASTM D638
Elongation at Break[4] - XY	20%	ASTM D638
Elongation at Break[4] - Z	15%	ASTM D638
Heat Deflection Temperature - Z	 175°C 95°C	ASTM D648 @ 0.45 MPa @ 1.82 MPa

Appendix B: Agilus 30 material datasheet

Table 24. Agilus30 material datasheet (Agilus 30: A Flexible Photopolymer 3D Printing Material | Stratasys)

stratasys

Agilus30

Polyjet Rubber-Like Material

Agilus30™ is a superior Rubber-like PolyJet™ photopolymer family ideal for advanced design verification and rapid prototyping. Get more durable, tear-resistant prototypes that can stand up to repeated flexing and bending. With a Shore A value of 30 in clear, black and white, Agilus30 accurately simulates the look, feel and function of Rubber-like products. 3D print rubber surrounds, overmolds, soft-touch coatings, living hinges, jigs and fixtures, wearables, grips and seals with improved surface texture.

Mechanical Properties	Test Method	Value	
		Black / Translucent	White
Tensile Strength	ASTM D-412	2.4 – 3.1 MPa (348 – 450 psi)	2.1-2.6 MPa (305 – 377 psi)
Elongation at Break	ASTM D-412	220 – 270%	185 – 230%
Compressive Set	ASTM D-395	6 – 7%	6 – 7%
Tensile Tear Resistance	ASTM D-624	4 – 7 Kg/cm (22 – 39 lb/in)	4 – 7 Kg/cm (22 – 39 lb/in)

Other	Test Method	Value	
		Black / Translucent	White
Shore Hardness	ASTM D-2240	30 – 35 Scale A	30 – 40 Scale A
Polymerized Density	ASTM D-792	1.14 – 1.15 g/cm^3	1.14 – 1.15 g/cm^3

System Availability	Layer Thickness Capability	Support Structure	Available Color
Objet260/350/500 Connex1/2/3™	High Speed mode: 30 microns (0.0012 in.)	SUP705 (WaterJet removable) SUP706B (soluble + WaterJet removable)	☐ Translucent
Stratasys J735™/ Stratasys J750™	High speed mode: 27 microns (0.0011 in.)	SUP705 (WaterJet removable) SUP706B (soluble + WaterJet removable)	■ Black ☐ Translucent ☐ White
J4100™	High Speed mode: 27 microns (0.001 in.)	SUP705 (Water Jet removable)	■ Black ☐ Translucent

Appendix C: HP MultiJet fusion 3D printer specifications

Table 25. HP MJF 3D printer specifications (GetDocument.aspx (hp.com))

Printer performance	Technology	HP Multi Jet Fusion technology
	Effective building volume	380 x 284 x 380 mm (15 x 11.2 x 15 in)
	Building speed[23]	Up to 4115 cm³/hr (251 in³/hr)
	Layer thickness	0.08 mm (0.003 in)
	Job processing resolution (x, y)	600 dpi
	Print resolution (x, y)	1200 dpi
Dimensions (w x d x h)	Printer	2210 x 1200 x 1448 mm (87 x 47 x 57 in)
	Shipping	2300 x 1325 x 2068 mm (91 x 52 x 81 in)
	Operating area	3700 x 3700 x 2500 mm (146 x 146 x 99 in)
Weight	Printer	750 kg (1653 lb)
	Shipping	945 kg (2083 lb)
Network[24]	Gigabit Ethernet (10/100/1000Base-T), supporting the following standards: TCP/IP, DHCP (IPv4 only), TLS/SSL	
Processor and memory	Processor	Intel® Core™ i7 4770TE (2.3 GHz, up to 3.3 GHz)
	Memory	16 GB DDR3
Hard disk	2TB (AES-256 encrypted, FIPS 140, disk wipe DoD 5220M)	
Software	HP SmartStream 3D Build Manager, HP SmartStream 3D Command Center	
	Compatible software	HP 3D API,[7] Center,[8] HP Universal Build Manager powered by Dyndrite[9]
	Supported file formats	3MF, STL, OBJ, and VRML (v2.0)
	Certified third-party software	Autodesk® Netfabb® with HP Work-space, Materialise Build Processor for HP Multi Jet Fusion technology, Siemens NX AM for HP Multi Jet Fusion technology
Power	Consumption	9 to 11 kW (typical)
	Requirements	Input voltage three phase 380-415 V (line-to-line), 30 A max, 50/60 Hz 200-240 V (line-to-line), 48 A max, 50/60 Hz

Appendix D: Stratasys J750 digital anatomy 3D printer specifications

Table 26. Stratasys j750 3D printer specifications (J750 Digital Anatomy 3D Printer for Lifelike Medical Models | Stratasys)

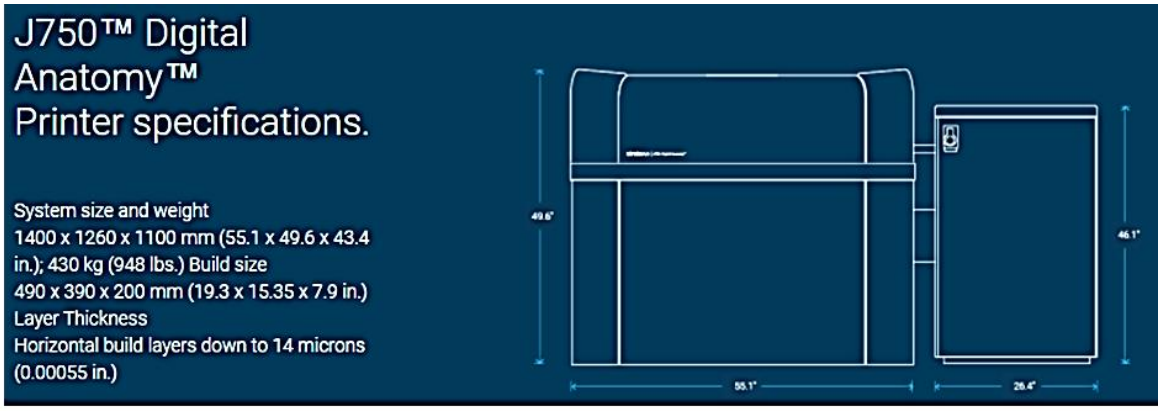

Product Specifications	
Model Materials	Vero™ family of opaque materials including neutral shades and vibrant VeroVivid™ colors Agilus30™, TangoPlus™ and TangoBlackPlus™ flexible materials VeroClear™, VeroUltraClear™ transparent materials TissueMatrix, BoneMatrix Biocompatible Clear
Digital Materials	**Unlimited number of composite materials including:** Over 500,000 colors Digital ABS Plus and Digital ABS2 Plus™ in ivory and green Rubber-like materials in a variety of Shore A values Ultra-soft rubber-like material with a Shore 00 value Translucent color tints User-developed digital materials with GrabCAD Voxel Print™
Support Materials	SUP705™ (waterjet removable) SUP706B™ (soluble) GelMatrix (waterjet removable)
Build size	490 x 390 x 200 mm (19.3 x 15.35 x 7.9 in.)
Layer Thickness	Horizontal build layers down to 14 microns (0.00055 in.)
Workstation Compatibility	Windows 7 and 8.1
Network Connectivity	LAN - TCP/IP
System Size and Weight	1400 x 1260 x 1100 mm (55.1 x 49.6 x 43.4 in.); 430 kg (948 lbs)
Material Cabinet	670 x 1,170 x 640 mm (26.4 x 46.1 x 25.2 in.); 152 kg (335 lbs)
Operating Conditions	Temperature 18 – 25 °C (64 – 77 °F); relative humidity 30-70% (non-condensing)
Power Requirements	100–120 VAC, 50–60 Hz, 13.5 A, 1 phase 220–240 VAC, 50–60 Hz, 7 A, 1 phase
Regulatory Compliance	CE, FCC, EAC
Software	GrabCAD Print Digital Anatomy, including the optional add-on GrabCAD Voxel Print
Build Modes	High Speed: up to 3 base resins, 27-micron (0.001 in.) resolution High Quality: up to 6 base resins, 14-micron (0.00055 in.) resolution High Mix: up to 6 base resins, 27-micron (0.001 in.) resolution
Accuracy	Typical deviation from STL dimensions, for models printed with rigid materials, based on size: under 100 mm: ±100µ; above100 mm: ±200µ or ± 0.06% of part length, whichever is greater. Please refer to material-specific spec sheets for accuracy estimates.

Appendix E: Universal robots UR5 specifications

Table 27. UR5 robot arm specifications (ur5_en.pdf (universal-robots.com))

6-axis robot arm with a working radius of 850 mm / 33.5 in

Weight:	18.4 kg / 40.6 lbs
Payload:	5 kg / 11 lbs
Reach:	850 mm / 33.5 in
Joint ranges:	+/- 360°
Speed:	All joints: 180°/s. Tool: Typical 1 m/s. / 39.4 in/s.
Repeatability:	+/- 0.1 mm / +/- 0.0039 in (4 mils)
Footprint:	Ø149 mm / 5.9 in
Degrees of freedom:	6 rotating joints
Control box size (WxHxD):	475 mm x 423 mm x 268 mm / 18.7 x 16.7 x 10.6 in
I/O ports:	Controlbox / Tool conn. Digital in 16 / 2 Digital out 16 / 2 Analog in 2 / 2 Analog out 2 / -
I/O power supply:	24 V 2A in control box and 12 V/24 V 600 mA in tool
Communication:	TCP/IP 100 Mbit: IEEE 802.3u, 100BASE-TX Ethernet socket & Modbus TCP
Programming:	Polyscope graphical user interface on 12 inch touchscreen with mounting
Noise:	Comparatively noiseless
IP classification:	IP54
ISO Class Cleanroom robot arm:	5
ISO Class Cleanroom control box:	6
Power consumption:	Approx. 200 watts using a typical program
Collaboration operation:	15 Advanced Safety Functions Tested in accordance with: EN ISO 13849:2008 PL d EN ISO 10218-1:2011, Clause 5.4.3
Materials:	Aluminum, PP plastic
Temperature:	The robot can work in a temperature range of 0-50°C
Power supply:	100-240 VAC, 50-60 Hz
Cabling:	Cable between robot and control box (6 m / 236 in) Cable between touchscreen and control box (4.5 m / 177 in)

Appendix F: Mechanical properties of the lacquering parts

Table 28. Mechanical properties of the lacquering parts (Philips)

Mechanical Properties			*2) ⇓
Tensile strength	ISO 527	MPa	55
Elongation at break	ISO 527	%	35
Tensile modulus	ISO 527	MPa	2700
Izod notched impact strength 23°C	ISO 180/A	kJ/m²	7
Charpy unnotched impact strength 23°C	ISO 179/U	kJ/m²	150
Charpy notched impact strength 23°C	ISO 179/A	kJ/m²	8

Appendix G: (un)loading robot (UR5) programs

UR5 programs attached in supplementary document.

Appendix H: Robotiq Hand-e gripper specifications

Table 29. Robotiq hand-e gripper specifications (Specifications (robotiq.com))

Specification	Metric Units	Imperial Units
Gripper opening	0 - 50 mm	0 - 1.97 in.
Maximum recommended payload, Form-fit grasp	5 kg	11 lbs
Maximum recommended payload, Friction grasp	3 kg	6.6 lbs
Gripper height (without fingertips)	100.5 mm	3.94 in
Gripper diameter	75 mm	2.95 in
Gripper weight (including coupling)	1070 g	2.3 lbs
Grip force	20 - 130 N	4.5 - 27 lbf
Finger speed	20 to 150 mm/s	0.8 to 5.9 in/s

Appendix I: Festo DGSL-4-20-PA mini slide pneumatic cylinder specifications

Table 30. Festo pneumatic cylinder specifications (Mini slide DGSL-4-20-PA (festo.com))

Feature	Value
Stroke	20 mm
Adjustable end-position range/front length	24.5 mm
Adjustable end-position range/rear length	13.5 mm
Piston diameter	6 mm
Drive unit operating mode	Yoke
Cushioning	Elastic cushioning rings/pads at both ends with fixed stop
Mounting position	Any
Guide	Ball bearing cage guide
Structural design	Yoke Piston Piston rod Slide
Position sensing	For proximity sensor
Symbol	00991263
Operating pressure	0.25 MPa ... 0.8 MPa
Operating pressure	2.5 bar ... 8 bar
Max. speed	0.5 m/s
Repetition accuracy	±0.01 mm
Mode of operation	Double-acting
Operating medium	Compressed air as per ISO 8573-1:2010 [7:4:4]
Information on operating and pilot media	Operation with oil lubrication possible (required for further use)
Corrosion resistance class (CRC)	0 - No corrosion stress
Ambient temperature	0 °C ... 60 °C
Impact energy in the end positions	0.005 J
Cushioning length	1.7 mm
Max. force Fy	368 N
Max. force Fz	368 N
Max. torque Mx	2 Nm
Max. torque My	2 Nm
Max. torque Mz	2 Nm
Theoretical force at 6 bar, retracting	13 N
Theoretical force at 6 bar, advancing	17 N
Moving mass	34 g
Product weight	96 g
Alternative connections	See product drawing
Type of mounting	With through-hole
Pneumatic connection	M3
Note on materials	Free of copper and PTFE RoHS-compliant
Cover material	Wrought aluminum alloy
Seals material	HNBR
Housing material	Wrought aluminum alloy
Piston rod material	High-alloy stainless steel

Appendix J: Festo MEH-5/2-1/8-P-B solenoid valve

Table 31. Festo solenoid valve specifications (Solenoid valve MEH-5/2-1/8-P-B (festo.com))

Feature	Value
Valve function	5/2, monostable
Actuation type	Electrical
Width	17.8 mm
Standard nominal flow rate	600 l/min
Pneumatic working port	G1/8
Operating voltage	24V DC
Operating pressure	2.5 bar ... 8 bar
Structural design	Piston gate valve
Reset method	Mechanical spring
Certification	c UL us - Recognized (OL)
Degree of protection	IP65
Nominal width	5 mm
Width dimension	18 mm
Exhaust air function	With flow control option
Sealing principle	Soft
Mounting position	Any
Manual override	Detenting via accessory
Type of control	Pilot-controlled
Pilot air supply port	Internal
Flow direction	Non-reversible
Symbol	00991035
Lap	Overlap
Pilot pressure	2.5 bar ... 8 bar
b-value	0.36
C value	2.55 l/sbar
Switching time off	28 ms
On switching time	10 ms
Duty cycle	100%
Coil characteristics	24 V DC: 1.5 W
Operating medium	Compressed air as per ISO 8573-1:2010 [7:4:4]
Information on operating and pilot media	Operation with oil lubrication possible (required for further use)
Vibration resistance	Transport application test with severity level 1 as per FN 942017-4 and EN 60068-2-6
Shock resistance	Shock test with severity level 2 as per FN 942017-5 and EN 60068-2-27
Corrosion resistance class (CRC)	2 - Moderate corrosion stress
Storage temperature	-20 °C ... 40 °C
Temperature of medium	-5 °C ... 50 °C
Noise level	75 dB(A)
Pilot medium	Compressed air as per ISO 8573-1:2010 [7:4:4]
Ambient temperature	-5 °C ... 50 °C
Product weight	105 g
Electrical connection	Connection diagram form C as per industrial standard, 9.4 mm Plug Rectangular design
Type of mounting	On terminal strip
Pilot exhaust air port 82/84	Sub-base
Pneumatic connection 1	Sub-base
Pneumatic connection 2	G1/8
Pneumatic connection 3	Sub-base
Pneumatic connection 4	G1/8
Pneumatic connection 5	Sub-base
Note on materials	RoHS-compliant
Seals material	HNBR NBR
Housing material	Die-cast aluminum

Appendix K: Fixturing assembly

The fixturing was made of an aluminum T-slot bar and a 3D printed adapter block interfacing the bar and the jig, as seen in Figure. The adapter is an assembly of a base with screw holes for mounting onto the bar, and a shaft with features matching those of the cylinder of the 6-folded cross (of the jig). The adapter base has a hexagonal pin to align the 6 attachments on the jig by locking the rotation of the shaft.

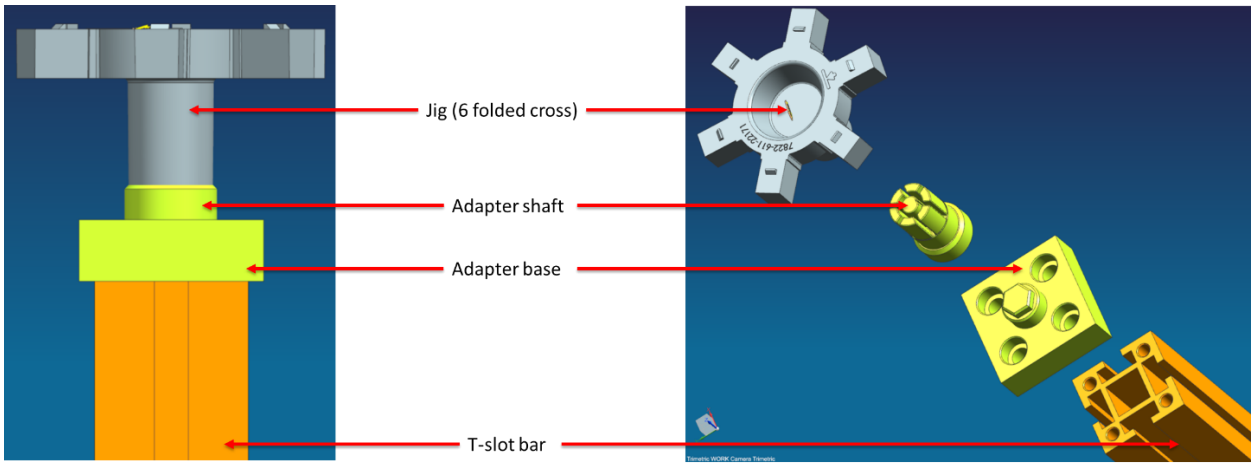

Figure 51. The fixturing assembly depicting how the 6-folded cross is held in place for the experimental validation.

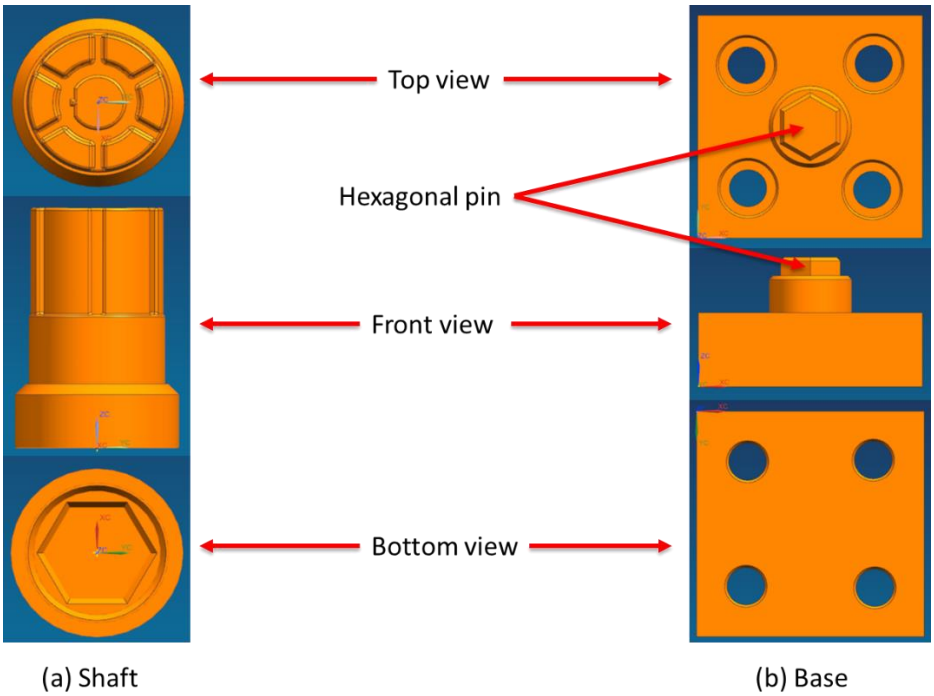

Figure 52. Top, front, and bottom views of the adapter (a) shaft and (b) base.

Appendix L: Part-alignment distance measurement images

Part 1 (Hera s1000 front panel)

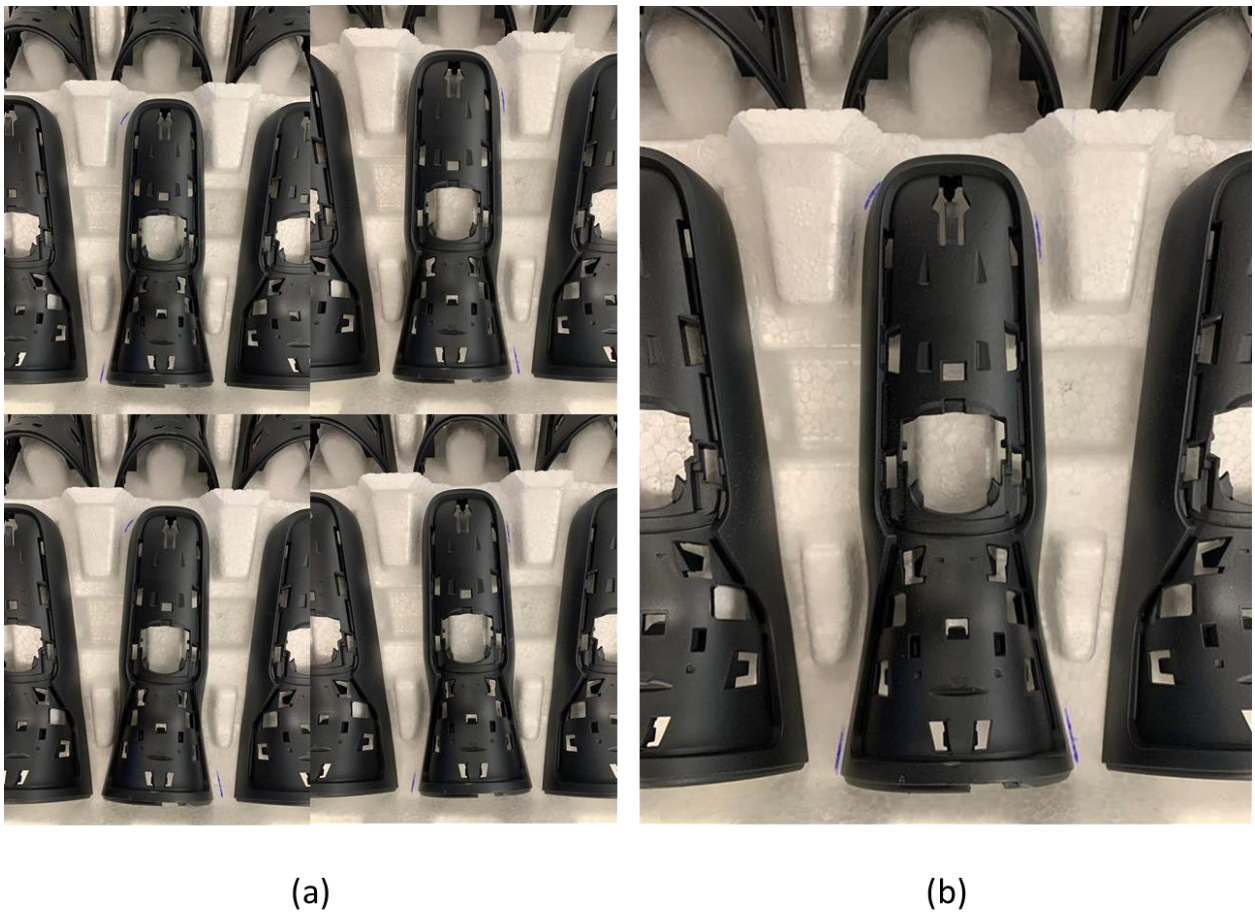

Figure 53. Images showing the visibility of markers (a) before and (b) after the horizontal alignment of Part 1

Part 2 (Hera s3000 front panel)

Figure 54. Images showing the visibility of markers (a) before and (b) after the horizontal alignment of Part 2

Part 4 (Poseidon chest)

(a) (b)

Figure 55. Images showing the visibility of markers (a) before and (b) after the horizontal alignment of the Poseidon chest.

Part 4 (Atlas chest)

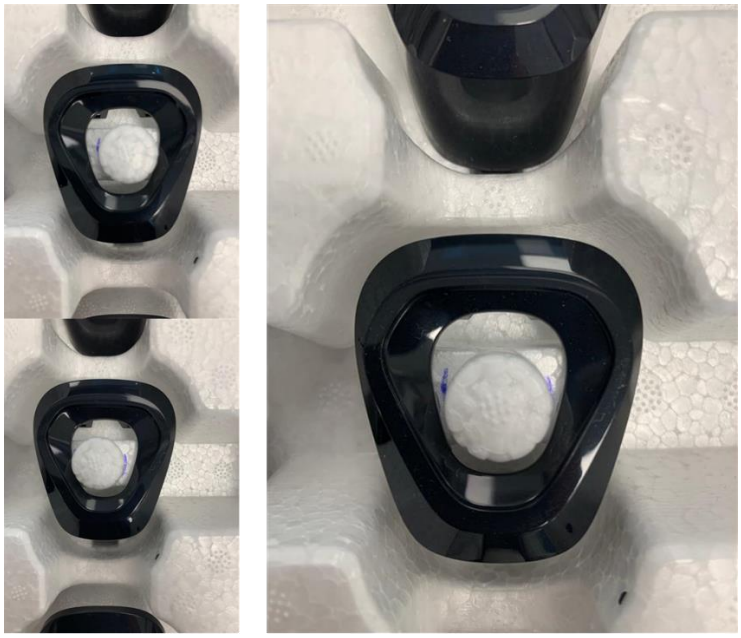

(a) (b)

Figure 56. Images showing the visibility of markers (a) before and (b) after the horizontal alignment of the Atlas chest.

Part 5 (Hera s3000 deco panel)

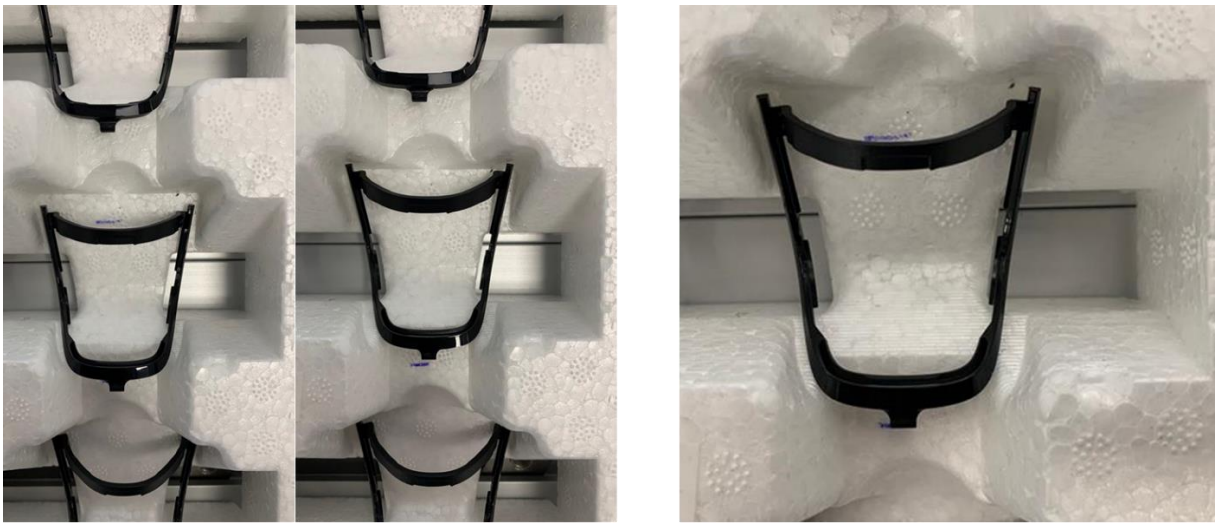

Figure 57. Images showing the visibility of markers (a) before and (b) after the horizontal alignment of Part 5.

Appendix M: Tevema D12680 compression spring specifications

Table 32. Compression spring specifications (Tevema D12680)

SKU	D12680
Price Group	C
prognosed delivery time	in consultation
material	Music wire
C (N/mm)	6.68
Nw	12.50
d	2.00
Dm	12.50
Nt	14.50
Ln	33.25
Conform with	DIN 2089-1/EN 13906-1
Axle size (mm)	10.00
outer diameter	14.50
Sn	37.75
Rod Diameter mm	15.25
L0	71.00
Fn (N)	252.00

Appendix M: Force calibration readings

Spring 1:

Table 33. Spring 1 force calibration readings

force (%) displayed in UR	Spring displacement measured as the distance between the fingers					Avg.	Std. Dev.	D_avg	F_avg
	1	2	3	4	5				
0	71	71	71	71	71	71	0	0	0
5	66,58	66,66	66,65	66,66	66,68	66,646	0,038471	4,354	29
10	65,44	65,43	65,36	65,4	65,39	65,404	0,032094	5,596	37
15	64,2	64,31	64,14	64,25	64,28	64,236	0,067305	6,764	45
20	63,4	63,06	63,04	63,08	63,21	63,158	0,150732	7,842	52
25	62,19	62,1	62,26	62,21	62,34	62,22	0,0886	8,78	59
30	61,5	61,32	61,41	61,47	61,47	61,434	0,071624	9,566	64
35	61,15	61,06	61,09	61,04	61,09	61,086	0,041593	9,914	66
40	60,24	60,09	60,2	60,15	60,2	60,176	0,057706	10,824	72
45	59,39	59,07	59,15	59,2	59,21	59,204	0,117813	11,796	79
50	58,85	58,7	58,79	58,8	58,9	58,808	0,074632	12,192	81
55	58,7	58,33	58,18	58,31	58,96	58,496	0,32362	12,504	84
60	57,89	57,87	57,9	57,97	57,88	57,902	0,039623	13,098	87
65	57,08	57,19	56,98	57,02	57,08	57,07	0,079373	13,93	93
70	56,71	56,69	56,72	56,8	56,77	56,738	0,045497	14,262	95
75	56,38	56,42	56,47	56,45	56,53	56,45	0,056125	14,55	97
80	56,06	55,96	55,89	55,87	56,06	55,968	0,090388	15,032	100
85	55,62	55,66	55,17	55,02	55,17	55,328	0,291668	15,672	105
90	55,05	54,82	54,71	54,79	54,8	54,834	0,127789	16,166	108
95	54,72	54,76	54,68	54,69	54,73	54,716	0,032094	16,284	109
100	54,55	54,45	54,5	54,44	54,52	54,492	0,046583	16,508	110

Spring 2:

Table 34. Spring 1 force calibration readings

force (%) displayed in UR	Spring displacement measured as the distance between the fingers					Avg.	Std. Dev.	D_avg	F_avg
	1	2	3	4	5				
0	71	71	71	71	71	71	0	0	0
5	66,69	66,81	66,81	66,75	66,85	66,782	0,056	4,218	28
10	65,5	65,5	65,61	65,55	65,52	65,536	0,04128	5,464	36
15	64,36	64,32	64,23	64,23	64,37	64,302	0,061123	6,698	45
20	63,19	63,23	63,26	63,25	63,26	63,238	0,026382	7,762	52
25	62,33	62,27	62,39	62,28	62,32	62,318	0,042615	8,682	58
30	61,56	61,57	61,57	61,53	61,54	61,554	0,016248	9,446	63
35	61,14	61,18	61,23	61,19	61,26	61,2	0,041473	9,8	65
40	60,17	60,12	60,28	60,21	60,2	60,196	0,052383	10,804	72
45	59,24	59,29	59,25	59,23	59,23	59,248	0,022271	11,752	79
50	58,85	58,96	58,88	58,96	58,95	58,92	0,046043	12,08	81

55	58,3	58,32	58,34	58,61	58,42	58,398	0,113561	12,602	84
60	57,96	58	58,03	58,06	57,99	58,008	0,034293	12,992	87
65	57,24	57,24	57,18	57,19	57,17	57,204	0,030067	13,796	92
70	56,64	56,72	56,73	56,72	56,6	56,682	0,052307	14,318	96
75	56,5	56,61	56,53	56,6	56	56,448	0,227807	14,552	97
80	55,97	55,93	55,88	55,88	55,83	55,898	0,047917	15,102	101
85	55,23	55,26	55,22	55,15	55,27	55,226	0,042237	15,774	105
90	54,82	54,95	54,87	54,95	54,88	54,894	0,05004	16,106	108
95	54,64	54,88	54,81	54,78	54,71	54,764	0,082608	16,236	108
100	54,54	54,58	54,49	54,57	54,61	54,558	0,040694	16,442	110

Appendix N: CAPEX breakdown

Table 35. CAPEX breakdown comparison between part-specific and flexible EOAT for the automated (un)loading process components and their quantities to meet the cycle-time requirements.

Component	Quantity (to meet cycle time requirements)		Estimated cost (in k€)	
	Part-specific EOAT	Flexible EOAT	Part-specific EOAT	Flexible EOAT
EOAT	56	5	230	35
Tool change system	7	0	30	0
Standard frame + line layout + safety guards + control cabinet	7	5	400	300
Robot arm + down-holder + servo	7	5	320	250
Tray-feeder + gripper	7	5	400	250
Engineering costs	1	1	120	65
Total estimated CAPEX			**1500**	**900**

To meet the cycle time requirements of maximum 2 seconds per part, 5 robots with a flexible EOAT - having a cycle time of about 9 seconds per part – would be required. If using a part-specific EOAT, 8 EOATs (for the current variation of 8 parts) would be required per robot along with a tool change system to switch between the EOATs. Considering a similar cycle time as the flexible EOAT, 5 robots plus an additional 2 robots to counter the changeover time, is estimated. Thus, the total number of part-specific EOATs is estimated to be 56 (8 parts x 7 robots). The other quantities are all considered per robot, with no tool change system required for the flexible EOAT, and engineering costs estimated for the whole project.

Appendix O: Allowable positional inaccuracy measurement images

Part 1 (Hera s1000 front panel)

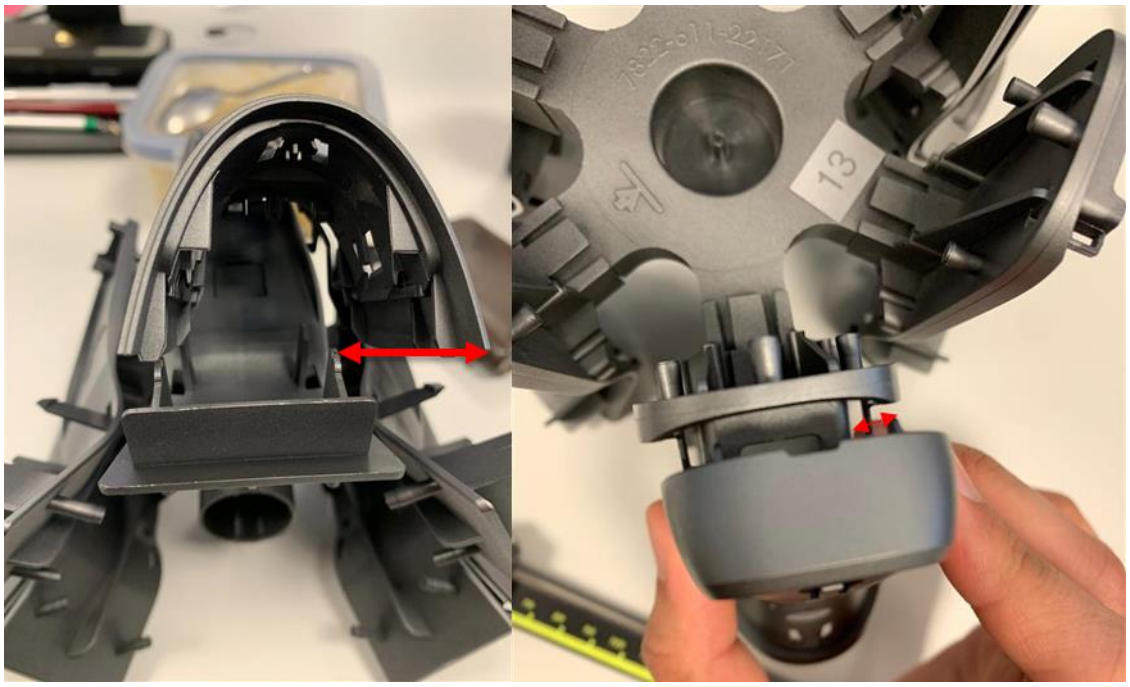

Figure 58. Distances measured for the API calculation for Part 1

Part 2 (Hera s3000 front panel)

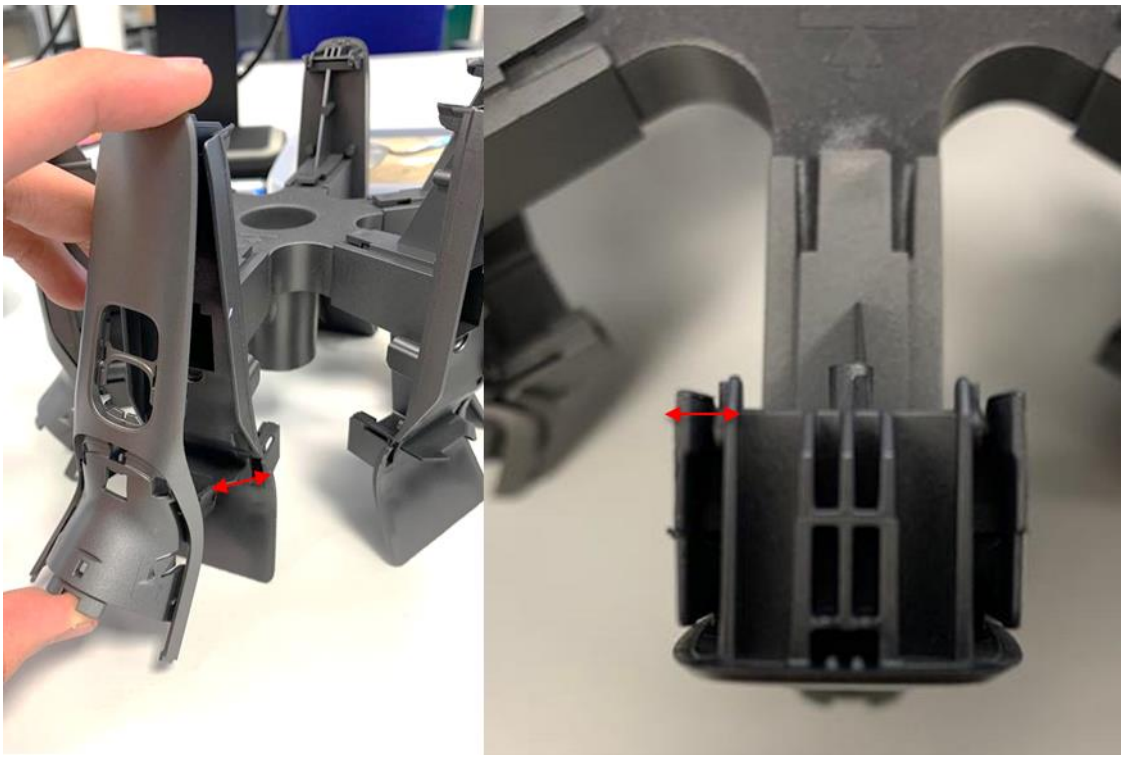

Figure 59. Distances measured for the API calculation for Part 2

Part 3 (Poseidon s7000 front panel)

Figure 60. Distances measured for the API calculation for Part 3

Part 4 (Poseidon/Atlas chest)

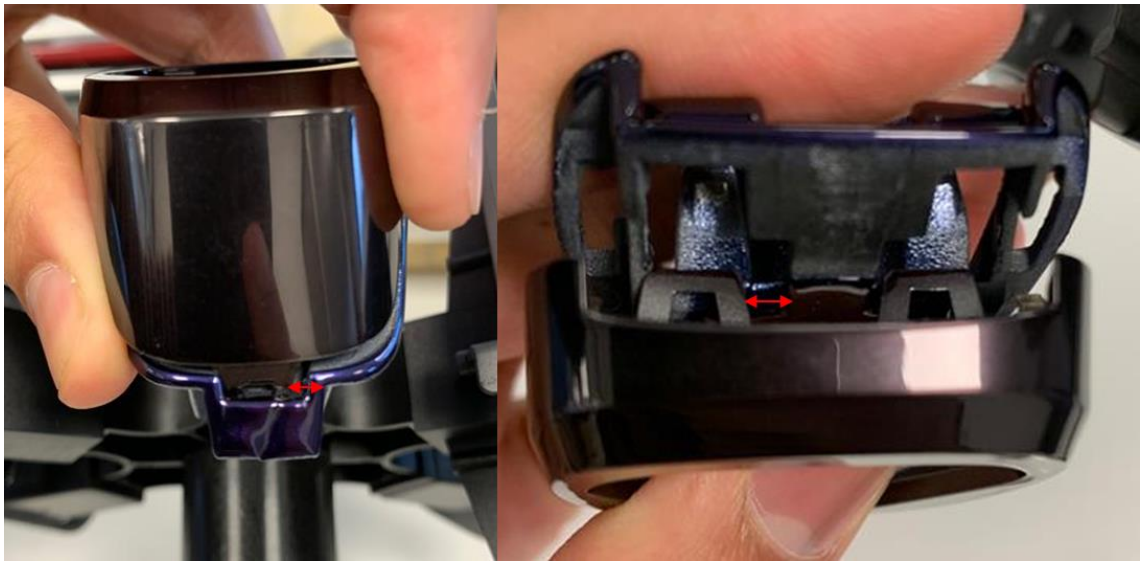

Figure 61. Distances measured for the API calculation for Part 4

Part 5 (Hera s3000 deco panel)

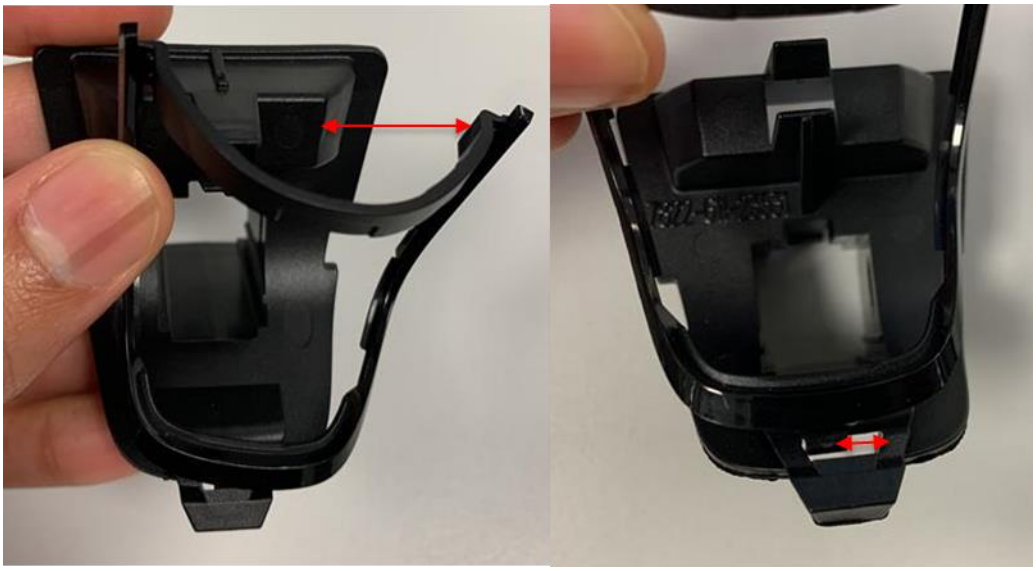

Figure 62. Distances measured for the API calculation for Part 5

Part 6 (Hera s3000 button)

Figure 63. Distances measured for the API calculation for Part 6

Appendix P: Positional variation measurements

Part 1 (Hera s1000 front panel)

Table 36. Positional variation readings for Part 1

Before				After tool translations				After tool rotations			
Top		Bottom		Top		Bottom		Top		Bottom	
Left	Right	Left	Right	Left	Right	Left	Right	Left	Right	Left	Right
26,84	27,04	18,19	17,87	26,85	27,34	18,41	17,96	26,7	27,07	18,58	17,9
				26,88	27,01	18,63	17,75	26,98	26,71	18,12	18
				26,63	26,91	18,64	17,81	26,95	27,08	18,29	18
				26,6	26,99	18,03	17,94	26,68	27,4	18,44	17,72
				26,91	27,19	17,99	17,8	26,8	27,24	18,48	17,89
				26,77	**27,09**	**18,34**	**17,85**	**26,82**	**27,10**	**18,38**	**17,90**
Positional variation (before - after)				0,07	-0,05	-0,15	0,02	0,02	-0,06	-0,19	-0,03
Total positional variation (max - min)				0,26							

Part 2 (Hera s3000 front panel)

Table 37. Positional variation readings for Part 2

Before				After tool translations				After tool rotations			
Top		Bottom		Top		Bottom		Top		Bottom	
Left	Right	Left	Right	Left	Right	Left	Right	Left	Right	Left	Right
9,5	8,94	16,1	16,17	9,36	8,82	16,15	16,15	9,7	8,85	16,21	16,16
				9,5	8,91	16,21	16,12	9,79	8,73	16,07	16,13
				9,56	9,04	16,27	16,1	9,56	8,97	16,22	15,55
				9,6	8,85	16,21	16,04	9,71	8,87	16,07	16,12
				9,62	8,88	16,02	16,11	9,49	8,98	16,03	16,14
				9,53	**8,90**	**16,17**	**16,10**	**9,65**	**8,88**	**16,12**	**16,02**
Positional variation (before - after)				-0,03	0,04	-0,07	0,07	-0,15	0,06	-0,02	0,15
Total positional variation (max - min)				0,30							

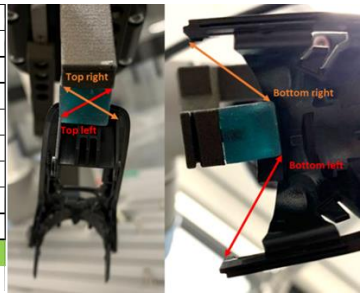

Part 3 (Poseidon s7000 front panel)

Table 38. Positional variation readings for Part 3

Before				After tool translations				After tool rotations			
Top		Bottom		Top		Bottom		Top		Bottom	
Left	Right	Left	Right	Left	Right	Left	Right	Left	Right	Left	Right
9,23	9,17	17,47	16,97	9,03	9,25	17,34	17,01	9,15	9,02	17,07	16,48
				8,94	9,12	17,47	16,74	9	9,12	17,43	16,75
				9,05	9,2	17,32	16,93	9,13	9,07	17,45	16,92
				8,98	9,12	17,39	17,09	9,06	9,06	17,29	16,9
				9,01	9,06	17,34	16,65	9,17	9,05	17,53	16,72
				9,00	**9,15**	**17,37**	**16,88**	**9,10**	**9,06**	**17,35**	**16,75**
Positional variation (before - after)				0,23	0,02	0,10	0,09	0,13	0,11	0,12	0,22
Total positional variation (max - min)				0,21							

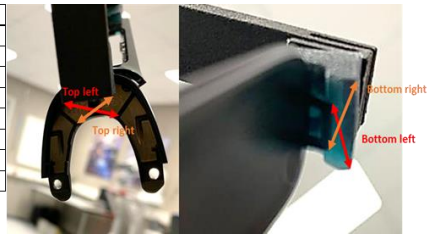

Part 4 (Poseidon/Atlas chest)

Table 39. Positional variation readings for Part 4

Before				After tool translations				After tool rotations			
Top		Bottom		Top		Bottom		Top		Bottom	
Left	Right	Left	Right	Left	Right	Left	Right	Left	Right	Left	Right
8,41	9,67	8,78	10,27	8,41	9,62	8,83	10,26	8,48	9,78	8,81	10,35
				8,42	9,67	8,74	10,32	8,31	9,65	8,78	10,29
				8,31	9,66	8,88	10,3	8,29	9,76	8,86	10,33
				8,33	9,72	8,72	10,37	8,39	9,67	8,91	10,36
				8,33	9,69	8,8	10,34	8,28	9,79	8,74	10,35
				8,36	**9,67**	**8,79**	**10,32**	**8,35**	**9,73**	**8,82**	**10,34**
Positional variation (before - after)				**0,05**	**0,00**	**-0,01**	**-0,05**	**0,06**	**-0,06**	**-0,04**	**-0,07**
Total positional variation (max - min)				**0,13**							

Part 5 (Hera s3000 deco panel)

Table 40. Positional variation readings for Part 5

Before		After tool translations		After tool rotations	
Left	Right	Left	Right	Left	Right
6,18	4,86	6,17	4,68	6,19	4,87
		6,15	4,67	6,13	4,86
		6,18	4,72	6,19	4,66
		6,13	4,65	6,19	4,71
		6,19	4,66	6,23	4,71
		6,16	**4,68**	**6,19**	**4,76**
Positional variation (before - after)		**0,02**	**0,18**	**-0,01**	**0,10**
Total positional variation (max - min)				**0,19**	

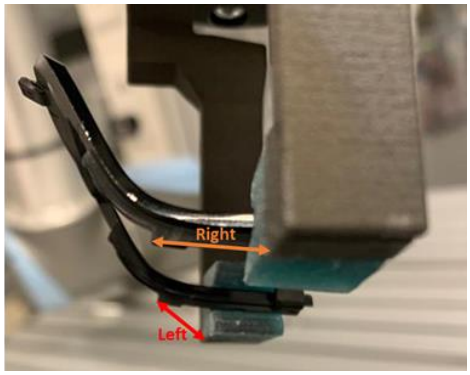

Part 6 (Hera s3000 button)

Table 41. Positional variation readings for Part 6

Before		After tool translations		After tool rotations	
Left	Right	Left	Right	Left	Right
10,29	10,69	10,16	10,38	10,06	10,41
		10,22	10,26	10,01	10,16
		10,02	10,1	10,1	10,34
		10,08	10,18	10,29	10,34
		10,39	10,5	10,43	10,54
		10,17	**10,28**	**10,18**	**10,36**
Positional variation (before - after)		**0,12**	**0,41**	**0,11**	**0,33**
Total positional variation (max - min)				**0,29**